

SSC-242

FAST FRACTURE RESISTANCE AND CRACK ARREST IN STRUCTURAL STEELS

This document has been approved
for public release and sale; its
distribution is unlimited.

SHIP STRUCTURE COMMITTEE

1973

SHIP STRUCTURE COMMITTEE

AN INTERAGENCY ADVISORY
COMMITTEE DEDICATED TO IMPROVING
THE STRUCTURE OF SHIPS

MEMBER AGENCIES:

UNITED STATES COAST GUARD
NAVAL SHIP SYSTEMS COMMAND
MILITARY SEALIFT COMMAND
MARITIME ADMINISTRATION
AMERICAN BUREAU OF SHIPPING

ADDRESS CORRESPONDENCE TO:

SECRETARY
SHIP STRUCTURE COMMITTEE
U.S. COAST GUARD HEADQUARTERS
WASHINGTON, D.C. 20590

SR 201

DEC 1973

The formation of the Ship Structure Committee resulted from an investigation into cracking in the hulls of welded ships. Today, although the incidence of hull failures from fracture has been reduced considerably, fractures do occur, and the understanding of the phenomena of crack initiation and arrest continues to be a major objective of the SSC program.

This report describes some of the analytical and experimental results obtained in an investigation of crack propagation and arrest in high strength steels.

Comments on this report would be welcomed.



W. F. REA, III
Rear Admiral, U. S. Coast Guard
Chairman, Ship Structure Committee

SSC-242

Progress Report

on

Project SR-201, "Fracture Arrest Study"

FAST FRACTURE RESISTANCE AND CRACK
ARREST IN STRUCTURAL STEELS

by

G. T. Hahn, R. G. Hoagland, M. F. Kanninen,
A. R. Rosenfield, and R. Sejnoha

Battelle Memorial Institute

under

Department of the Navy
Naval Ship Engineering Center
Contract No. N00024-72-C-5142

*This document has been approved for public release and
sale: its distribution is unlimited.*

U. S. Coast Guard Headquarters
Washington, D. C.
1973

ABSTRACT

This report presents findings of an Army Research Office supported study concerned with the response of high-strength steels to fast running cracks, and a separate Ship Structure Committee program dealing with unstable fractures in ship plates. Together, the results provide a new basis for measuring and characterizing the properties of structural alloys that control fast fracture and crack arrest.

Measurements and calculations of unstable fracture and fracture arrest in 12.7 mm- and 25.4 mm-thick, high-strength SAE4340 steel and A517F steel plates are described. The unstable fractures which propagated at steady-state velocities in the range 185 ms^{-1} to 1180 ms^{-1} , were produced in wedge-loaded DCB- (double-cantilever-beam) test specimens. The study demonstrates a new concept: the "duplex" DCB-specimen. This consists of a high-strength/low-toughness 4340 steel "starter section" which is electron beam welded to the A517F test section. The fractures are initiated in the starter section, and this makes it possible to confront test materials with a fast moving crack under controlled conditions close to the transition temperature.

A fully dynamic analysis of unstable crack propagation and arrest in the DCB-test piece is derived. The technique is based on the beam-on-elastic-foundation model of the DCB specimen used previously but with the simple beam and foundation representations replaced by a Timoshenko beam and a generalized elastic foundation. Crack speeds, energy levels, and the crack length at arrest are calculated with this model using a finite-difference method and are compared with the measurements.

The calculations and the measurements reveal that unstable propagation in the DCB-test piece proceed from the start with essentially constant, steady-state crack speeds that depend on specimen geometry and the starting conditions. The calculations also predict instances of discontinuous propagation at high speeds. The kinetic energy imparted to the test piece is recovered and contributes to the crack driving force. It follows from this that fracture arrest is controlled by the history of energy dissipation throughout the entire propagation event, rather than on K_a , a single static toughness value calculated at the arrest point. For the 4340 steel, increases in crack velocity up to 860 ms^{-1} at room temperature are accompanied by a 4-fold increase in the dynamic fracture energy (a 2-fold increase in the dynamic fracture toughness), and by increases in the size of the shear lip. Dynamic toughness values for the A517F grade at -78°C for crack speeds from 475 ms^{-1} to 780 ms^{-1} were also about 2 times the reported K_{IC} -value.

CONTENTS

| | <u>PAGE</u> |
|--|-------------|
| INTRODUCTION | 1 |
| NEW CONCEPTS | 3 |
| REFERENCES | 5 |
| SECTION 1. RAPID CRACK PROPAGATION IN A HIGH STRENGTH STEEL | |
| ABSTRACT | 6 |
| I. INTRODUCTION | 7 |
| II. EXPERIMENTAL PROCEDURES | 8 |
| III. RESULTS | 13 |
| IV. DISCUSSION | 15 |
| V. CONCLUSIONS | 20 |
| VI. REFERENCES | 21 |
| APPENDIX 1-A - VELOCITY MEASURING PROCEDURE | 23 |
| SECTION 2. THE CHARACTERIZATION OF FRACTURE ARREST IN A STRUCTURAL STEEL | |
| ABSTRACT | 25 |
| I. INTRODUCTION | 26 |
| II. EXPERIMENTAL PROCEDURES | 28 |
| III. ANALYSIS | 30 |
| IV. RESULTS AND DISCUSSION | 32 |
| V. CONCLUSIONS | 40 |
| VI. REFERENCES | 41 |
| APPENDIX 2-A - SUPPLEMENTARY ILLUSTRATIONS | 43 |
| SECTION 3. DYNAMIC ANALYSIS OF CRACK PROPAGATION IN THE DCB TEST SPECIMEN | |
| ABSTRACT | 55 |
| I. INTRODUCTION | 56 |
| II. SUMMARY OF PREVIOUS WORK | 56 |
| III. A MODEL OF THE DCB SPECIMEN USING A TIMOSHENKO BEAM ON A GENERALIZED ELASTIC FOUNDATION | 60 |
| IV. RESULTS AND CONCLUSIONS ON DYNAMIC CRACK PROPAGATION | 69 |
| V. REFERENCES | 76 |
| APPENDIX 3-A - DERIVATION OF THE GOVERNING EQUATIONS FOR THE TIMOSHENKO BEAM-GENERALIZED ELASTIC FOUNDATION MODEL OF THE DCB SPECIMEN | 77 |

CONTENTS (Cont'd)

| | PAGE |
|--|------|
| APPENDIX 3-B - DERIVATION OF THE COMPONENTS OF ENERGY AND THE CRACK EXTENSION CRITERION FOR THE TIMOSHENKO BEAM-GENERALIZED ELASTIC FOUNDATION DCB MODEL | 82 |
| APPENDIX 3-C - SOLUTION FOR INITIAL CRACK EXTENSION IN THE TIMOSHENKO BEAM-GENERALIZED ELASTIC FOUNDATION DCB MODEL | 87 |
| APPENDIX 3-D - FINITE-DIFFERENCE APPROXIMATION TO EQUATIONS FOR DYNAMIC-CRACK PROPAGA- TION IN THE TIMOSHENKO BEAM- GENERALIZED ELASTIC FOUNDATION DCB MODEL | 94 |
| APPENDIX 3-E - COMPUTER PLOTS OF RESULTS FOR DYNAMIC CRACK PROPAGATION IN STEEL DCB TEST SPECIMENS | 98 |
| ACKNOWLEDGMENTS | 98 |

LIST OF FIGURES

| <u>Figure</u> | | <u>PAGE</u> |
|-------------------------|--|-------------|
| 1 | WEDGE-LOADING ARRANGEMENT FOR DCB-SPECIMEN SHOWING THE VELOCITY MEASURING CONDUCTING STRIPS | 2 |
| 2 | THE DUPLEX DCB-TEST PIECE | 2 |
| 3 | BEAM-ON-ELASTIC-FOUNDATION MODEL AT DCB-SPECIMEN | 2 |
| 4 | APPLICATION OF THE R-CURVE CONCEPT TO A CRACK ARRESTOR .. | 4 |
| Section 1 | | |
| 1 | SCHEMATIC DRAWING OF DOUBLE-CANTILEVER-BEAM SPECIMEN | 9 |
| 2 | VARIATION OF STRESS INTENSITY AT THE ONSET OF FAST FRACTURE WITH ROOT RADIUS OF THE STARTING NOTCH | 9 |
| 3 | SCHEMATIC OF PLATE CROSS SECTION FOR A TUNNELING FLAT FRACTURE AND A SHEAR FRACTURE THAT LAGS BEHIND | 10 |
| 4 | THEORETICAL CALCULATIONS OF CRACK PROPAGATION AND ARREST USING THE TIMOSHENKO BEAM WITH A GENERALIZED FOUNDATION MODEL | 12 |
| 5 | VELOCITY AND SURFACE PROFILE MEASUREMENT ON SAE4340 STEEL .. | 13 |
| 6 | FRACTURE SURFACES OF TEST SPECIMENS | 14 |
| 7 | RELATION BETWEEN DYNAMIC FRACTURE TOUGHNESS AND CRACK VELOCITY FOR SAE4340 STEEL | 15 |
| 8 | STRESS INTENSITY AT CRACK ARREST OF SAE4340 STEEL | 16 |
| 9 | RELATIONS AMONG VARIOUS SHEAR LIP DIMENSIONS | 16 |
| 10 | VARIATION OF FRACTURE ENERGY WITH SPECIMEN TOUGHNESS IN SAE 4340 STEEL TESTED UNDER STATIC CONDITIONS AT ROOM TEMPERATURE | 19 |
| 11 | COMPARISON BETWEEN THEORETICAL PREDICTIONS AND EXPERIMENTAL MEASUREMENTS OF THE RELATION BETWEEN CRACK VELOCITY AND CRACK TRAVEL | 19 |
| <u>APPENDIX 1-A</u> | | |
| A-1 | RESISTANCE-TIME RECORDING OF THE RUPTURE OF CONDUCTING STRIPS IN 2 ADJACENT GRIDS (ABSCISSA $16 \mu \text{ sec/cm}$, ORDINATE 0.5 volts/cm) DURING A CRACK PROPAGATION EVENT | 24 |
| Section 2 | | |
| 1 | SCHEMATIC REPRESENTATION OF THE ENERGETICS OF FRACTURE ARREST IN THE DCB-TEST PIECE, ILLUSTRATING (a) THE ARREST TOUGHNESS CONCEPT, (b) THE R-CURVE CONCEPT, AND (c) THE CONCEPT OF A DYNAMIC STRAIN ENERGY RELEASE RATE | 27 |
| 2 | DIMENSIONS OF DUPLEX TEST PIECES | 29 |
| 3 | THEORETICAL CALCULATIONS OF CRACK PROPAGATION AND ARREST IN TIMOSHENKO BEAM-ON-ELASTIC-FOUNDATION MODELS OF AN ORDINARY AND A DUPLEX DCB-SPECIMEN | 33 |

LIST OF FIGURES (Cont'd)

| <u>Figure</u> | | <u>PAGE</u> |
|---------------------|---|-------------|
| 4 | DUPLEX DCB SPECIMENS TESTED AT DIFFERENT TEMPERATURES | 36 |
| 5 | EXAMPLES OF VELOCITY (CRACK LENGTH VS. TIME) MEASUREMENTS DERIVED FROM THE CONDUCTING STRIPS | 36 |
| 6 | COMPARISON OF THE VELOCITY DEPENDENCE OF K_d -VALUES FROM DIFFERENT INVESTIGATIONS (14, 15, 25-29) | 38 |
| 7 | COMPARISON OF THE CHARPY AND FRACTURE TOUGHNESS VALUES FOR A517F OBTAINED IN THIS INVESTIGATION, AND THOSE REPORTED BY BARSON AND ROLFE ⁽³⁰⁾ AND HOAGLAND, ET AL. ⁽⁹⁾ | 38 |
| <u>APPENDIX 2-A</u> | | |
| A-1 | DUPLEX DCB SPECIMEN BLANKS | 43 |
| A-2 | MICROGRAPH OF ELECTRON BEAM WELD AND HEAT AFFECTED ZONE OF SPECIMEN 3VY-10 TAKEN ON PLATE MIDPLANE | 44 |
| A-3 | MICROGRAPH OF ELECTRON BEAM WELD AND HEAT AFFECTED ZONE OF SPECIMEN 3VY-11 TAKEN ON PLATE MIDPLANE | 44 |
| A-4 | ORDINARY 4340 STEEL DCB SPECIMEN 3V40 (12.7 mm-THICK, TESTED AT 0°C, $K_q/K_d = 1.57$) | 45 |
| A-5 | ORDINARY 4340 STEEL DCB SPECIMEN 3V44 (12.7 mm-THICK, TESTED AT -78°C, $K_q/K_d = 1.88$) | 45 |
| A-6 | DUPLEX 4340/A517F DCB TEST PIECE 3VY1 (12.7 mm-THICK, TESTED AT 0°C) | 45 |
| A-7 | DUPLEX 4340/A517F DCB TEST PIECE 3VY3 (25.4 mm-THICK, TESTED AT -78°C) | 46 |
| A-8 | DUPLEX 4340/A517F DCB TEST PIECE 3VY-4 (25.4 mm-THICK, TESTED AT -78°C) | 46 |
| A-9 | DUPLEX 4340/A517F DCB TEST PIECE 3VY10 (12.7 mm-THICK, TESTED AT -78°C) | 46 |
| A-10 | DUPLEX 4340/A517F DCB TEST PIECE 3VY11 (12.7 mm-THICK, TESTED AT 0°C) | 47 |
| A-11 | DUPLEX 4340/A517F DCB TEST PIECE 3VY12 (12.7 mm-THICK, TESTED AT -78°C) | 47 |
| A-12 | DUPLEX 4340/A517F DCB TEST PIECE 3VY13 (12.7 mm-THICK, TESTED AT -78°C) | 47 |
| A-13 | DUPLEX 4340/A517F DCB TEST PIECE 3VY22 (25.4 mm-THICK, TESTED AT -78°C) | 48 |
| A-14 | DUPLEX 4340/A517F DCB TEST PIECE 3VY23 (25.4 mm-THICK, TESTED AT -78°C) | 48 |
| A-15 | DUPLEX 4340/A517F DCB TEST PIECE 3VY24 (25.4 mm-THICK, TESTED AT 0°C) | 49 |
| A-16 | DUPLEX 4340/A517F DCB TEST PIECE 3VY28 (25.4 mm-THICK, TESTED AT -78°C) | 49 |
| A-17 | CRACK VELOCITY MEASUREMENTS DERIVED FROM THE CONDUCTING STRIPS | 50 |
| A-18 | EXTENT OF FRACTURE PROPAGATION IN THE DUPLEX 4340/A517F DCB TEST PIECE 3VY10 | 52 |

| <u>Figure</u> | LIST OF FIGURES (Cont'd) | <u>PAGE</u> |
|---------------------|---|-------------|
| A-19 | EXTENT OF FRACTURE PROPAGATION IN THE DUPLEX 4340/A517F DCB TEST PIECE 3VY11 | 53 |
| A-20 | PROFILE OF THE ARRESTED CRACK IN THE A517F STEEL TEST SECTION OF SPECIMEN 3VY-10 (12.7 mm-THICK, TESTED AT -78°C) | 54 |
| Section 3 | | |
| 1 | THE DOUBLE CANTILEVER BEAM (DCB) TEST SPECIMEN AND THE BEAM-ON-ELASTIC FOUNDATION MODEL | 58 |
| 2 | COMPARISON BETWEEN STRESS INTENSITY FACTORS FOR THE DCB SPECIMEN CALCULATED USING TWO DIMENSIONAL ELASTICITY THEORY WITH THOSE FROM VARIOUS DIFFERENT BEAM-ON-ELASTIC FOUNDATION MODELS | 65 |
| 3 | SPECIMEN A, $K_q/K_d = 2$ | 70 |
| 4 | SPECIMEN A, $K_q/K_d = 2$ | 71 |
| 5 | SPECIMEN B, $(K_q/K_d)_S = 3.0$, $(K_q/K_d) = 2.0$ | 74 |
| 6 | SPECIMEN B, $(K_q/K_d)_S = 3.0$, $(K_q/K_d)_T = 2.0$ | 74 |
| <u>APPENDIX 3-E</u> | | |
| E-1 - E-30 | COMPUTER PRINTOUTS | 99-113 |

LIST OF TABLES

| <u>TABLE</u> | <u>PAGE</u> |
|---------------------|--|
| <u>Section 1</u> | |
| I | MEASUREMENTS OF FRACTURE FEATURES IN SAE4340 STEEL QUENCHED AND TEMPERED AT 205°C 16 |
| II | DYNAMIC FRACTURE ENERGY AND TOUGHNESS VALUES FOR UNSTABLE CRACKS IN 4340 STEEL INCLUDING VALUES FOR THE SHEAR LIP AND FLAT PORTIONS OF THE FRACTURE 17 |
| <u>Section 2</u> | |
| I | DUPLEX SPECIMEN TEST RESULTS 37 |
| <u>Section 3</u> | |
| I | DIMENSIONS OF DCB SPECIMENS USED IN THE COMPUTATIONS 70 |
| II | COMPUTATIONAL RESULTS FOR SINGLE-SECTION DCB SPECIMENS 72 |
| III | COMPUTATIONAL RESULTS FOR DUPLEX DCB SPECIMENS 72 |
| IV | COMPUTATIONAL RESULTS SHOWING THE RFLATIVE EFFECTS OF VARYING THE MASS OF THE LOAD PINS 75 |
| <u>APPENDIX 3-C</u> | |
| I | COEFFICIENTS IN THE RELATION FOR THE COMPLIANCE OF THE DCB SPECIMEN AS GIVEN BY VARIOUS DIFFERENT ANALYTICAL MODELS .. 93 |
| <u>APPENDIX 3-D</u> | |
| I | COMPARISON OF CRACK LENGTH VS TIME RESULTS COMPUTED USING DIFFERENT FINITE DIFFERENCE STEP SIZES 97 |
| II | COMPARISON OF COMPUTATIONAL RESULTS USING DIFFERENT FINITE DIFFERENCE STEP SIZES 97 |

NOMENCLATURE

| | | |
|-------------|---|---|
| A | = | area of surface depression associated with shear lip <u>or</u> cross-sectional area of beam (=bh) |
| D | = | pin diameter |
| E | = | Young's modulus |
| ϵ | = | total energy of specimen |
| F | = | compressive force parallel to crack plane introduced by action of wedge on pins |
| G | = | strain energy release rate <u>or</u> shear modulus |
| G_c | = | critical strain energy release rate |
| G_d | = | strain energy release rate at onset of crack extension on blunt-notch DCB specimen |
| H | = | instantaneous value of specimen kinetic energy |
| H* | = | modified Heaviside step function |
| I | = | moment of inertia (= $bh^3/12$) |
| K | = | stress intensity |
| K_a | = | stress intensity at crack arrest |
| K_d | = | dynamic fracture toughness |
| \bar{K}_d | = | average value of K_d in duplex test specimen |
| K_{Ic} | = | static plane strain fracture toughness |
| K_{Ic}^* | = | stress intensity required to reinitiate arrested crack |
| K_q | = | stress intensity at crack initiation in blunt-notch DCB specimen |
| L | = | Specimen length |
| L_1 | = | length of "starter section" in duplex test piece |
| L_2 | = | length of "test section" in duplex test piece |
| L_3 | = | total length of duplex test piece |
| M | = | couple initially applied to beam in analytical model |
| P | = | load |
| Q | = | pinching force initially applied to beam in analytical model |
| R | = | dynamic fracture energy |

R_f = flat fracture component of R
 R_{SL} = shear lip component of R
 T = kinetic energy
 U = strain energy content of specimen
 U_{SL} = shear lip energy per unit volume
 V = crack velocity
 W = plastic work dissipated in the formation of one shear lip or work done on specimen during crack propagation (= 0 for these experiments) or w/w_c = dimensionless displacement
 Y = $\frac{h}{w_c} \Psi$ = dimensionless rotation
 a = crack length
 a_a = crack length at arrest
 a_r = crack length at arrest
 a_o = initial crack length
 a_l = crack length at point where crack enters test section in duplex specimen
 b = specimen thickness
 c = $L-a-e$ = uncracked length of specimen
 c_o = $\sqrt{E/\rho}$ = bar wave speed (5120 m/s)
 d = distance by which flat portion of crack in interior of specimen leads crack on surface during propagation
 e = distance from center of pinhole to end of specimen
 f = distance from the center of a loading pin to the crack plane or width of flat fracture surface
 h = height of arm of DCB specimen
 k_e = extensional stiffness of the foundation in the beam model
 k_r = rotational stiffness of the foundation in the beam model
 l = width of surface depression associated with shear lip or pin length
 s = width of shear lip
 t = time
 u_z = local value of beam displacement
 w = average deflection of the cross section in the beam model

- w_c = critical spring deflection in beam-on-elastic foundation model
 x = length coordinate on crack propagation direction
 y = length coordinate parallel to thickness direction
 z = length coordinate parallel to displacement direction
 K = shear deflection coefficient of the beam, $K = E/3G$
 Ψ = mean angle of rotation of the cross section about the neutral axis in the beam model
 δ = displacement of one arm of DCB specimen
 δ_T = crack-tip opening displacement
 $\dot{\epsilon}$ = strain rate
 θ = crack-extension parameter, $\theta = k_e w^2 + k_r \Psi^2$
 θ_c = critical value of the crack-extension parameter, $\theta_c = bR$
 $\hat{\theta}$ = θ/θ_c = dimensionless crack-extension parameter
 ν = Poisson's Ratio
 ξ = x/h = dimensionless length
 ρ = specific gravity
 $\bar{\sigma}$ = flow stress
 σ_i = local value of tensile stress
 σ_y = nominal yield stress
 τ = $\left(\frac{E}{12\rho}\right)^{1/2} \frac{t}{h}$ = dimensionless time
 τ_y = local value of shear stress

CONVERSION OF SI UNITS TO ENGLISH UNITS

| <u>Quantity</u> | <u>SI Unit</u> | | | | <u>English Unit</u> |
|--------------------|---------------------|---|-------|---|------------------------|
| Velocity | m/s | X | 3.281 | = | ft/sec |
| Velocity | m/s | X | 2.237 | = | mph |
| Stress | MN/m ² | X | 0.145 | = | Ksi |
| Fracture energy | KJ/m ² | X | 5.71 | = | lb/in |
| Fracture toughness | MN/m ^{3/2} | X | 0.91 | = | Ksi $\sqrt{\text{in}}$ |

SHIP STRUCTURE COMMITTEE

The SHIP STRUCTURE COMMITTEE is constituted to prosecute a research program to improve the hull structure of ships by an extension of knowledge pertaining to design, materials and methods of fabrication.

RADM W. F. Rea, III, USCG, Chairman
Chief, Office of Merchant Marine Safety
U.S. Coast Guard Headquarters

CAPT J. E. Rasmussen, USN
Head, Ship Systems Engineering
and Design Department
Naval Ship Engineering Center
Naval Ship Systems Command

Mr. M. Pitkin
Asst. Administrator for
Commercial Development
Maritime Administration

Mr. K. Morland
Vice President
American Bureau of Shipping

CAPT L. L. Jackson, USN
Maintenance and Repair Officer
Military Sealift Command

SHIP STRUCTURE SUBCOMMITTEE

The SHIP STRUCTURE SUBCOMMITTEE acts for the Ship Structure Committee on technical matters by providing technical coordination for the determination of goals and objectives of the program, and by evaluating and interpreting the results in Terms of ship structural design, construction and operation.

NAVAL SHIP SYSTEMS COMMAND

Mr. P. M. Palermo - Chairman
Mr. J. B. O'Brien - Contract Administrator
Mr. G. Sorkin - Member
Mr. C. H. Pohler - Member

U. S. COAST GUARD

CDR C. S. Loosmore - Secretary
CAPT D. J. Linde - Member
CDR E. L. Jones - Member
CDR W. M. Devlin - Member

MARITIME ADMINISTRATION

Mr. J. J. Nachtsheim - Member
Mr. F. Dashnaw - Member
Mr. F. Seibold

MILITARY SEALIFT COMMAND

Mr. R. R. Askren - Member
Mr. T. W. Chapman - Member
CDR A. McPherson, USN - Member
Mr. A. B. Stavovy - Member

AMERICAN BUREAU OF SHIPPING

Mr. S. Stiansen - Member
Mr. I. L. Stern - Member

NATIONAL ACADEMY OF SCIENCES Ship Research Committee

Mr. R. W. Rumke - Liaison
Prof. J. E. Goldberg - Liaison

SOCIETY OF NAVAL ARCHITECTS & MARINE ENGINEERS

Mr. T. M. Buermann - Liaison

BRITISH NAVY STAFF

CDR P. C. Bryan, RCNC - Liaison

WELDING RESEARCH COUNCIL

Mr. K. H. Koopman - Liaison

INTERNATIONAL SHIP STRUCTURE CONGRESS

Prof. J. H. Evans - Liaison

INTRODUCTION

The goal of the research described in this report is to characterize the fast fracture resistance and the fracture arrest capabilities of steels. The report contains the results of two separate studies. One is supported by ARO and is concerned with the response of high-strength steels to fast running cracks. The second study, sponsored by the Ship Structure Committee, seeks to establish material properties and criteria for stopping unstable fractures in ship hulls. The results are presented under one cover because the same concepts and material properties apply to fast fracture and to fracture arrest. For this reason, too, the findings of these two studies are closely related. The ARO funded measurements of fast fracture in SAE-4340 steel, presented in Section I, support the theoretical analysis conducted for SSC and described in Section III. This analysis, together with measurements performed on A517F steel (Section II), establish the valid criterion for fracture arrest. It should be noted that the approach described herein is sufficiently general that it can be used to characterize both ferrous and nonferrous alloys. It has already been applied successfully to a glassy polymer^(1,2).

The studies described in this report make use of a new testing procedure for producing unstable fracture and fracture arrest in the laboratory under controlled conditions. This procedure was described in an earlier report, SSC-219⁽³⁾, and is illustrated in Figure 1. The test piece is in the form of a double-cantilever-beam (DCB) specimen, with a blunt starting slot. The specimen is slowly loaded in an ordinary testing machine (operating in the compression mode) by forcing dual wedges between the pins. This arrangement offers several unique features:

- The blunt notch permits the specimen to sustain stress intensity values that are greater than K_{Ic} . Consequently, as soon as a sharp crack emerges from the blunt notch, the crack immediately becomes unstable and propagates rapidly.
- Since wedge loading is inherently "stiff", crack propagation proceeds with essentially constant displacement at the load point. Under these conditions the strain energy release rate diminishes as the crack grows and this ultimately causes the crack to arrest within the confines of the test piece, provided it is long enough.
- Little energy is exchanged between the wedge-loaded DCB-specimen and the testing machine during the propagation event. For this reason, the results can be expected to be relatively insensitive to the character of the testing machine.
- The wedge introduces a modest compressive stress parallel to the crack plane, typically 2 to 15% of the yield strength, which tends to stabilize the crack path. Hence, the side grooves ordinarily required to keep the crack from turning can be eliminated. This makes it possible to reproduce the shear lips obtained in practice, and simplifies the task of measuring the fracture velocity.
- The measurements and analysis described in this report also show that the unstable fractures generated in this way propagate at an essentially constant velocity, which can be controlled by altering the bluntness of the starting slot. In this way fractures traveling at constant speeds

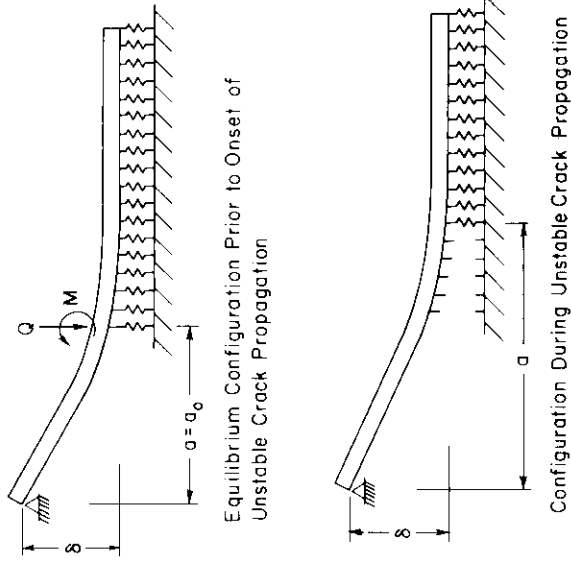


FIGURE 3. BEAM-ON-ELASTIC-FOUNDATION MODEL AT DCB-SPECIMEN. δ is the wedge-opening displacement at the onset of unstable propagation. The force Q and couple M are used in the initial configuration to simulate the blunt starting slot

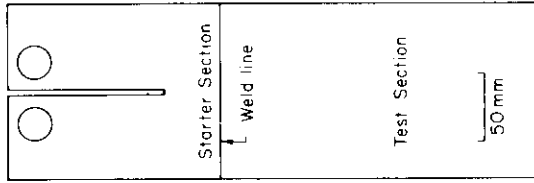


FIGURE 2. THE DUPLEX DCB-TEST PIECE.

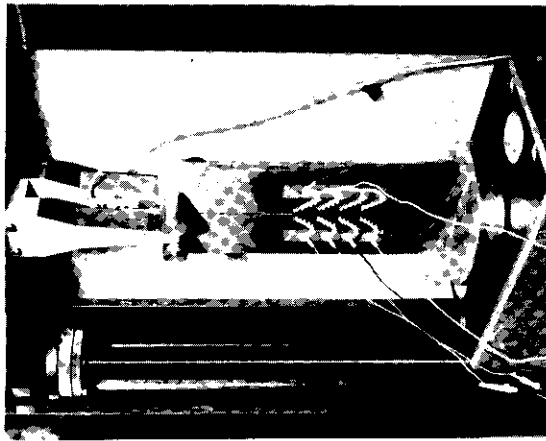


FIGURE 1. WEDGE-LOADING ARRANGEMENT FOR DCB-SPECIMEN SHOWING THE VELOCITY MEASURING CONDUCTING STRIPS.

of from 200 ms⁻¹ to 1100 ms⁻¹ have been produced in 4340 steel test pieces with modest dimensions, e.g., 120 mm wide by 300 mm long.

NEW CONCEPTS

This report presents, in detail, experimental and analytical studies carried out during the past 15 months. The following new concepts are discussed.

(1) The Duplex DCB Test Piece. The "duplex" DCB-test specimen was developed to facilitate the production of fast propagating cracks close to the transition temperature. The specimen is illustrated in Figure 2, and discussed more fully in Section II. It consists of a high-strength/low-toughness 4340 steel "starter section" electron beam welded to the "test section". Unstable fractures have been initiated in a 4340 steel starter section at ambient as well as at low temperatures, and directed at high speed into an A517F steel test section. The high-strength starter section also reduces the specimen size required for measuring a given toughness level.

(2) A Fully Dynamic Analysis of Crack Propagation in the DCB Specimen. A fully dynamic analysis of unstable crack propagation in the beam-on-elastic foundation model of a DCB specimen (shown in Figure 3) has been carried out. The model treats the arms of the DCB-specimen as Timoshenko beams with lateral and rotational inertia. To simulate a moving crack each spring in the elastic foundation is systematically removed when a critical deflection corresponding to the dynamic toughness is exceeded (for duplex specimens, 2 spring deflections are employed). The treatment given in Section III supersedes a primitive version reported earlier⁽⁴⁾. The analysis makes it possible to extract dynamic fracture energy or toughness values independently from two measurements: The fracture velocity and the crack length at arrest.

(3) Fracture Velocity Measurements. An experimental procedure for measuring the fracture velocity was devised. The method, which employs a grid of conducting strips, insulated from the specimen by a thin epoxy layer, is described in Section I, Appendix A. Actual velocity measurements described in Sections I and II reveal that unstable fractures in the DCB-specimen propagate at essentially constant velocity, in agreement with the theoretical analysis in Section III.

(4) Energy Conservation and the Criterion for Fracture Arrest. The theoretical calculations in Section III show that as much as 85% of the kinetic energy imparted to the DCB-specimen by the growing crack is recovered to drive the crack in the latter stages of the propagation event. At the same time, values of the dynamic fracture energy (or toughness) deduced from velocity measurements and, independently, from the length of the crack at arrest are in close agreement (Sections I and II). These agreements represent a critical test of the theory that the kinetic energy is substantially conserved. It follows that arrest is controlled by the history of energy dissipation throughout the entire propagation event rather than by K_a , the arrest toughness value.

(5) Origins of Dynamic Toughness. The dynamic toughness values associated with 900 ms⁻¹ fractures in SAE-4340 steel at room temperature, and with 500 to 800 ms⁻¹ fractures in A517F steel at -78°C are roughly twice as large as the static K_{IC} -values reported at these temperatures. The higher dynamic toughness for the

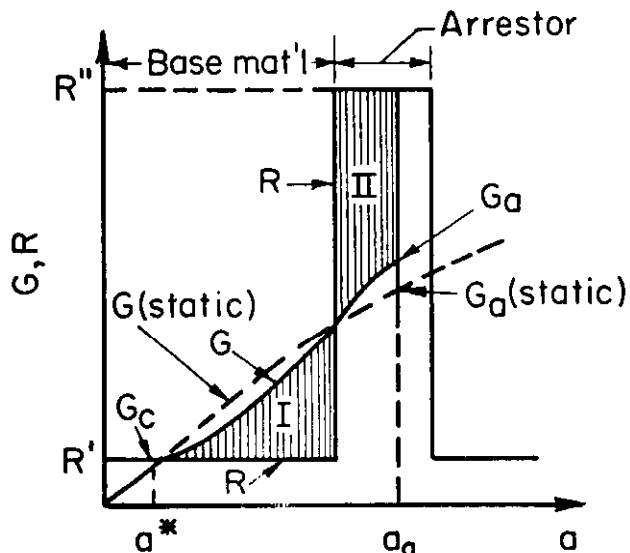


FIGURE 4. APPLICATION OF THE R-CURVE CONCEPT TO A CRACK ARRESTOR. R' is the dynamic fracture energy of the base material; R'' is the dynamic fracture energy of the arrestor. G is the strain energy release rate; G_c and G_a and a^* and a_a are the strain energy release rates and crack lengths corresponding to the onset of unstable fracture and to fracture arrest, respectively. The shaded areas I and II represent the amount of kinetic energy imparted to the structure, and the amount recovered in the form of fracture energy prior to arrest.

4340 steel, which displayed ductile (dimpled) fractures, could be correlated with an increase in the size of the shear lips; the specific shear lip and flat fracture energies are relatively constant. The higher dynamic toughness of the A517F grade, which involves cleavage, cannot be attributed to shear lips, but may be connected to the ductile ligaments left behind by the crack front⁽³⁾.

The material property that emerges from these studies as the most significant measure of both the fast fracture resistance and the fracture arrest capability is R , the dynamic fracture energy (or K_d , the corresponding dynamic toughness.[†]) This quantity and its variation with velocity, together with G , the strain energy release rate (which depends on the inertia of the structure), determines the arrest condition. This is shown schematically in Figure 4 for a plate (low energy, R') fitted with arrestor (high energy, R''). The problem of calculating the minimum width of the arrestor might be simplified: (1) by relying on the static strain energy release curve and (2) by assuming all of the kinetic energy is conserved--approximations that are likely to be conservative. However, more work is needed to test this concept, and to provide a sound basis for selecting R -values appropriate for base materials and arrestors.

[†] $K_d \equiv \sqrt{\frac{ER}{1-\nu^2}}$, where E is the elastic modulus and ν is Poisson's ratio.

References

1. M. F. Kanninen, A. R. Rosenfield, and R. G. Hoagland, "Fast Fracture In PMMA", Deformation and Fracture of High Polymers, H. Kausch, et al, eds. (to be published by Plenum Press).
2. A. R. Rosenfield and M. F. Kanninen, "The Fracture Mechanics of Glassy Polymers", J. Macro Molecular Science (in press).
3. G. T. Hahn, R. G. Hoagland, P. N. Mincer, A. R. Rosenfield, and M. Sarrate, "Crack Propagation and Arrest In Ship and Other Steels", Final Report SSC-219, Naval Ship Eng. Center, 1971. See also:
 - (a) G. T. Hahn, M. Sarrate, and A. R. Rosenfield, "Plastic Zones in Fe-3Si Steel Double-Cantilever-Beam Specimens", Int. J. Fract. Mechs., 7, p. 435, 1971.
 - (b) G. T. Hahn, A. R. Rosenfield, and M. Sarrate, "Observations of Yielding Accompanying Crack Growth", Inelastic Behavior of Solids, McGraw-Hill, New York, p. 673, 1970.
 - (c) R. G. Hoagland, A. R. Rosenfield, and G. T. Hahn, "Mechanisms of Fast Fracture and Arrest in Steels", Met. Trans., 3, p. 123, 1972.
4. G. T. Hahn, R. G. Hoagland, M. F. Kanninen, and A. R. Rosenfield, "A Preliminary Study of Fast Fracture and Arrest in the DCB-Test Specimen", Int. Conf. on Dynamic Crack Propagation, Lehigh University, 1972, to be published.

SECTION 1

RAPID CRACK PROPAGATION IN A HIGH STRENGTH STEEL

by

G. T. Hahn, R. G. Hoagland, A. R. Rosenfield, and R. Sejnoha

ABSTRACT

The relation between fracture velocity and the energy dissipated by unstable fractures in high strength 12.7 mm-thick plates of SAE4340 steel has been measured using the wedge-loaded double-cantilever-beam (DCB) specimen. The experiments are analyzed using the dynamic beam-on-elastic-foundation model. In agreement with the model, steady-state crack velocities are attained. In addition, the theoretical velocity-arrest length relation is closely obeyed. Increases in crack velocity up to $\sim 860 \text{ ms}^{-1}$ are accompanied by a 2-fold increase in the dynamic toughness (a 4-fold increase in the dynamic fracture energy) and by corresponding increases in the size of the shear lips. Measurements of the plastic work associated with the shear lips show that the per-unit-volume shear lip fracture energy, $U_{SL} = 0.21 \text{ J/mm}^3$, is essentially constant over this range of velocity. The fracture energies derived from the model are in good agreement with those derived by assuming that all of the strain energy released during crack propagation is converted into fracture energy.

RAPID CRACK PROPAGATION IN A HIGH-STRENGTH STEEL

I. INTRODUCTION

The behavior of unstable cracks in engineering structures is not well understood. Such features as the crack velocity, the tendency for crack branching and fragmentation, and the process of crack arrest have been measured in isolated cases, but few generalizations are established. The main difficulties are the need for simple laboratory tests and for suitable dynamic analyses that can distinguish the contributions of inertia, kinetic energy, and velocity dependent toughness values.(1,2) In addition, there have been only a few attempts to relate R or K_d^\dagger , the dynamic fracture energy or fracture toughness of a fast running crack to the underlying fracture processes. The situation is clearest for the glassy polymer, PMMA. In this case the dynamic fracture energy and the nature of the dissipative process have been related to the density of small (~ 0.1 mm) parabolas on the fracture surface(3,4).

Cleavage fractures in steels have received attention, but here it is not yet clear how the dynamic toughness varies with crack velocity(2,5-11). For example Eftis and Krafft(5) and others(2,7,10,11) find as much as a 5-fold increase in the dynamic toughness with increasing crack velocity in the range 100 to 1400 ms^{-1} . At the same time, Bilek and Burns(9) and Fitzpatrick, et al(8) present evidence favoring a decrease in toughness with crack speeds in the range 50 to 700 ms^{-1} . Several authors(10,12,13) report evidence that the major contribution to the toughness arises from the ductile rupture of unbroken ligaments left behind by the cleavage crack front. These ligaments could account for either an increase or a decrease in toughness depending on whether the number of ligaments generated and the work of rupturing them increases or decreases with crack velocity.

Unstable ductile fractures have been studied in thin metal foils. In these cases the fracture surface is composed entirely of shear lip and it appears that the toughness increases with the crack speed consistent with the increased resistance to plastic flow with strain rate within the crack tip plastic zone(14,15). However, there have been no systematic studies of unstable propagation in thicker sections of high-strength structural alloys with the characteristic flat, dimpled fracture surfaces. A single determination reported by the authors(1) for a 500 ms^{-1} fracture in SAE4340 steel at the 1380 MNm^{-2} (200 ksi) yield strength level gave a dynamic toughness about twice the static K_{Ic} -value.

The present paper extends the measurements of unstable propagation and arrest in 4340 steel DCB-test pieces to a range of fracture velocities from 180 ms^{-1} to 860 ms^{-1} . A systematic increase in the dynamic toughness is observed and this is correlated with increases in the width of the shear lip. The measured values of crack velocity and the length of the crack at arrest are found to be in excellent accord with an improved dynamic analysis of crack propagation in the DCB-test piece. The agreement implies that kinetic energy imparted to the DCB-test piece by the propagating crack is substantially recovered and used to drive the crack in the latter stages of the propagation event.

$\dagger K_d \equiv \sqrt{\frac{ER}{1-\nu^2}}$, where E is Young's modulus, and ν is Poisson's ratio.

II. EXPERIMENTAL PROCEDURES

Measurements of fast fracture and arrest were performed on 12.7 mm-thick, quenched and tempered (1 hr. at 205°C) SAE4340 steel plates at room temperature[†]. The procedures used have been reported earlier⁽¹³⁾ and are described here briefly.

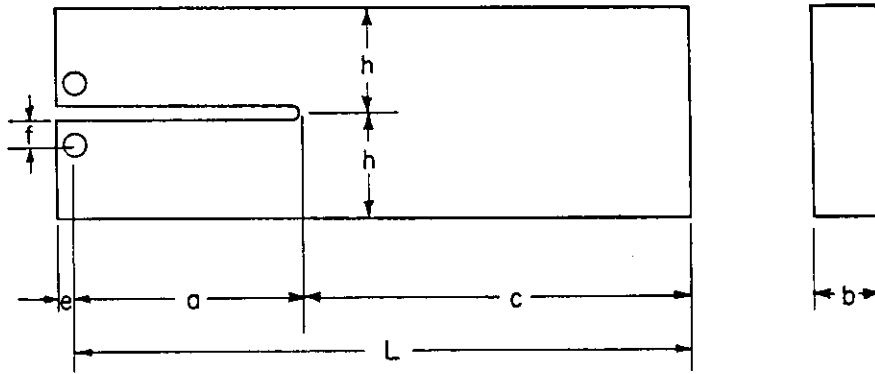
The Wedge-Loaded DCB-Test. Unstable fractures were produced by wedge loading double-cantilever-beam (DCB) specimens as shown in Figure 1 of the General Introduction. Dimensions of the test pieces are given in Figure 1. The sample contains a blunted starting slot which allows it to sustain a stress intensity, K_q , which can be as much as 3 to 4 times K_{Ic} . Consequently, as soon as a sharp crack emerges from the blunt notch, the crack immediately becomes unstable and propagates rapidly. The loading arrangement is stiff allowing the crack to propagate under essentially fixed-grip conditions. Under these conditions the strain energy release rate decreases as the crack grows, and this ultimately causes the crack to arrest within the confines of the test piece provided it is long enough. The wedge also induces a compressive load parallel to the direction of crack propagation, eliminating the need for side grooves to promote a straight-line crack path and facilitating the measurement of velocity.

The value of K_q was derived from the opening displacement measured with a clip gage mounted to the end of the specimen^{††}. Crack velocities were measured using an electric-resistance grid technique described in Appendix A. Earlier results on PMMA⁽³⁾ and the previously reported test in this series⁽¹⁾ show that unstable cracks in the wedge-loaded DCB test piece propagate from the start with a steady-state speed which is maintained until shortly before arrest. This speed depends on K_q , and can therefore be varied by changing the root radius of the starting slot. The root radius was formed by spark machining a hole in the specimen ahead of a saw-cut and then extending the saw-cut. There was some scatter in the value of stress intensity required to initiate a fast moving fracture (K_q) as shown in Figure 2. Late in this series of experiments the notch roots were smoothed by electropolishing. This tended to eliminate very low K_q values in subsequent tests. Figure 2 shows that K_q varies as (root radius)^{1/2}, as has been observed for cleavage crack extension⁽¹⁷⁾; while this simplifies the problem of selecting the root radius needed to produce a given crack velocity, it is immaterial for the subsequent analysis whether a particular K_q versus root radius relation is obeyed.

Shear Lip Measurements. Profiles of specimen surfaces in the vicinity of the crack line--the "necking-in" associated with the shear lips--were measured using a Talysurf machine to determine the depression width ℓ and area Δ which are illustrated in Figure 3. These quantities, can be related to $R_{SL} \equiv \frac{dW}{sda}$ and

† The composition of the 4340 steel is given in Reference 1. Tensile properties are as follows: yield strength = 1380 MNm⁻² (200 ksi), ultimate strength = 1940 MNm⁻² (282 ksi), reduction in area = 50%.

†† The corresponding displacement of the load points was calculated using the expression derived by Kanninen⁽¹⁶⁾.



$a_o = 2.670$ in. (67.8 mm) $f = 0.80$ in. (20.3 mm)
 $b = 0.500$ in. (12.7 mm) $h = 2.500$ in. (63.5 mm)
 $c = 0.63$ in. (16.0 mm) $L = 11.36$ in. (305.0 mm)
Pin Diameter 1.00 in. (25.4 mm)

FIGURE 1. SCHEMATIC DRAWING OF DOUBLE-CANTILEVER-BEAM SPECIMEN.

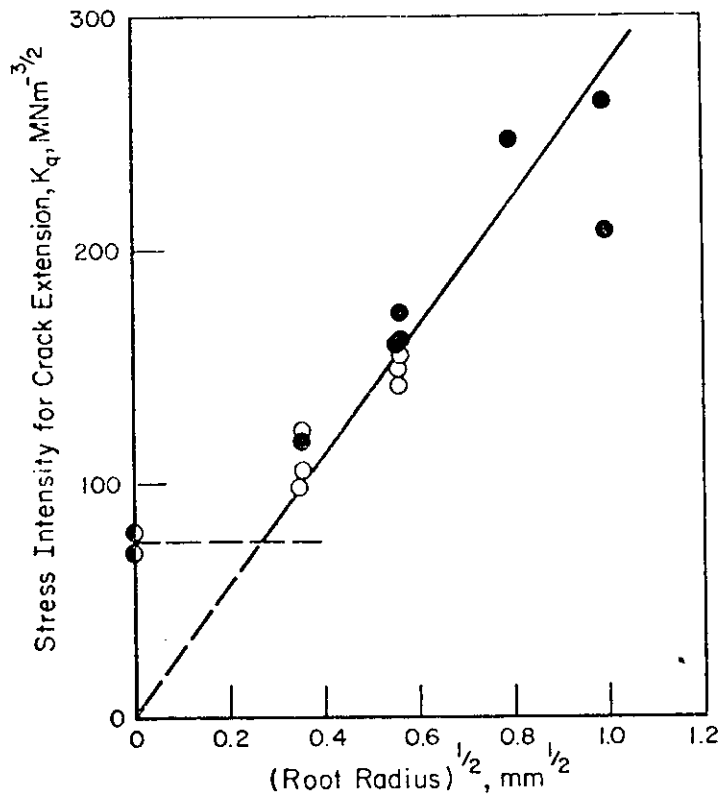


FIGURE 2. VARIATION OF STRESS-INTENSITY AT THE ONSET OF FAST FRACTURE WITH ROOT RADIUS OF THE STARTING NOTCH. Closed points refer to specimens where velocity was measured. Half closed points refer to reinitiation of an arrested crack.

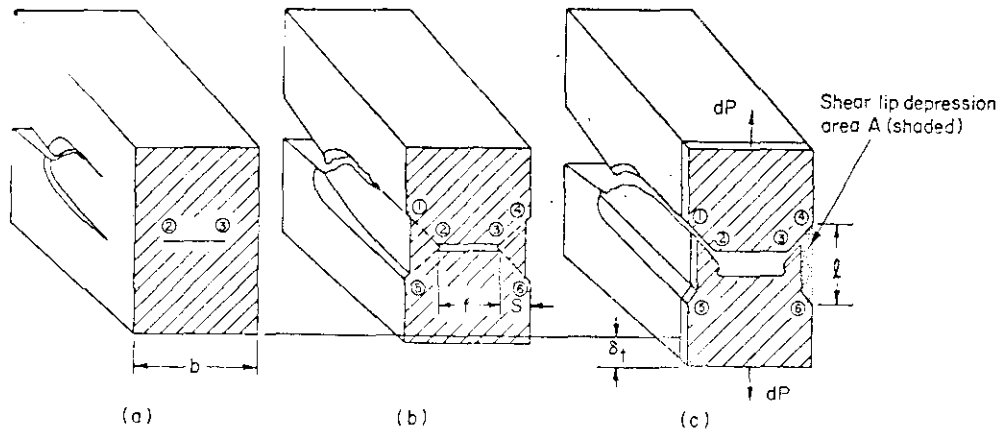


FIGURE 3. SCHEMATIC OF PLATE CROSS SECTION FOR A TUNNELING FLAT FRACTURE AND A SHEAR FRACTURE THAT LAGS BEHIND: (a) flat fracture in region 2-3 arrives at cross section, (b) flat fracture opens by plastic deformation in regions 1-2, and 3-6 (dashed lines), between the ends of the flat fracture and the surface producing depressions on the surface in regions 1-5 and 4-6 and (c) complete fracture at section by rupture in regions of intense shear 1-2 and 3-4, producing the characteristic shear lips.

$U_{SL} = \frac{2dW}{s\ell da}$, where R_{SL} and U_{SL} are the per-unit-area and per-unit-volume fracture energies of the shear lip, respectively, $2W$ is the plastic work dissipated in the shear lips, a is the crack length, and s is the shear lip width[†]:

$$R_{SL} = \frac{\bar{\sigma}A}{s} \quad (1)$$

$$U_{SL} = \frac{2\bar{\sigma}A}{s\ell} \quad (2)$$

These quantities, together with R_F , the per-unit-area fracture energy of the flat portion of the fracture, make up the total or averaged fracture energy R :

$$R = \left(\frac{2s}{b}\right) R_{SL} + \left(\frac{f}{b}\right) R_F, \text{ or} \quad (3a)$$

$$R = \left(\frac{\ell s}{b}\right) U_{SL} + \left(\frac{f}{b}\right) R_F \quad (3b)$$

where b is the plate thickness and f is the width of the flat portion. Equations (3a) and (3b) are analogous to the expression derived by Bluhm(18).

[†] The differential plastic work, dW can be expressed in terms of dP , the differential force, and δ_t , a displacement: $dW = \delta_t \cdot dP$, where $dP = \bar{\sigma} \cdot s \cdot da$, $\bar{\sigma}$ is the average flow stress, and a is the crack length. The quantity $\delta_t = A \cdot s^{-1}$ by virtue of volume conservation provided deformation of the shear lip in the direction of crack propagation is negligible. The shear lip volume-per-unit length of crack extension (for the 2 shear lips on either side) is arbitrarily defined $\delta(\text{volume})/da = s \cdot \ell$.

Analysis of Unstable Propagation. The analysis of crack propagation in the DCB test piece is derived from the beam-on-elastic foundation model illustrated in Figure 3 of the General Introduction to this report. A simplified treatment of this model which employs Euler-Bernoulli-beam theory and accounts for the lateral inertia of the beam has already been described(1). The present study employs a more complete analysis which accounts for both translational and rotational inertia of the test piece. The analysis, based on Timoshenko beam theory, is described in detail in Section III.(19)

The elastic foundation, representing the material in the path of the advancing crack, consists of a line of springs. In the dynamic calculation the breaking of successive springs simulates crack advance and it is specified that a spring will break when it reaches a critical displacement. Because the springs are linear elastic this corresponds to either a critical crack-tip-opening displacement (COD), a critical strain energy release rate (G_c), or a critical dynamic toughness (K_d). At the same time, it should be noted that the breaking of springs, i.e., the dissipation of fracture energy at the crack tip, is the only energy dissipation mechanism provided for.

The analysis describes the crack length, crack velocity, time-variation of the displacements of the arms of the DCB specimen and the length of the crack at arrest as a function: (a) R or K_d , (b) the specimen dimensions, (c) density, (d) elastic moduli, and (e) K_q (the bluntness of the starting notch). Examples of such calculations are given in Figure 4 for the specimen configuration employed in this study. Figure 4a illustrates that the analysis reproduces the constant velocity propagation that is observed experimentally†. Figure 4b shows that kinetic energy T is first imparted to the beams; of the maximum amount imparted, 5% is recovered during the latter 2/3 of the growth increment, with less than 10% of the total strain energy released remaining as unrecovered kinetic energy in this case.

Figure 4c illustrates that both the steady-state velocity V and the arrest length a_a are single valued functions of $\frac{K_q}{K_d}$ for a given material and specimen configuration. This means that K_d can be obtained independently from measurements of either: (i) K_q and a_a , or (ii) K_q and V , and the appropriate functional relations derived from the theoretical model. Alternatively, the arrest length can be interpreted without resorting to the detailed analysis by way of the relation(13):

$$K_d = \left[K_q \cdot K_{a(\text{static})} \right]^{1/2} \quad (4)$$

Equation (4) is a close approximation when all of the kinetic energy is recovered at arrest, and is approximate when the unrecovered kinetic energy is a small fraction of the total strain energy released. Figure 4c shows that Equation (4) represents a close approximation of the detailed analysis consistent with the calculated result that the kinetic energy in the beam-on-elastic-foundation model is substantially recovered.

† It should be noted that the crack length versus time curves in Figure 4a contain small sinusoidal fluctuations which are accompanied by 180° out-of-phase fluctuations in the strain energy and kinetic energy (see Figure 4b). These fluctuations, which appear to be connected with stress waves traveling in the arms of the beam, became more intense as the ratio K_q/K_d is increased, ultimately producing a discontinuous propagation when $K_q/K_d \gtrsim 2.5$. Additional information is reported in Section III.

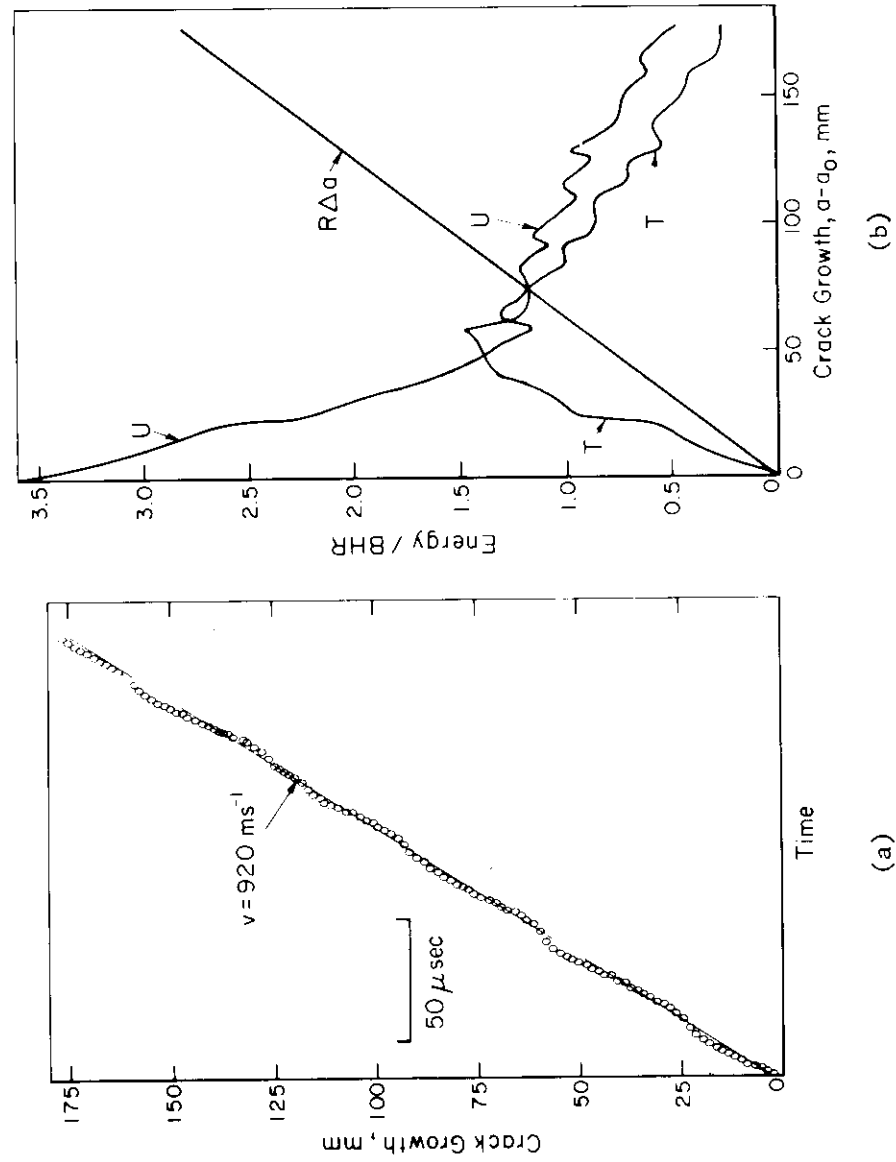


FIGURE 4. THEORETICAL CALCULATIONS OF CRACK PROPAGATION AND ARREST USING THE TIMOSHENKO BEAM WITH A GENERALIZED FOUNDATION MODEL: (a) typical velocity profile, (b) variation of the energy distribution with crack length; U = strain energy, T = kinetic energy, and R = fracture energy. (c) Influence of the ratio of stress intensity at crack initiation to dynamic toughness on average crack velocity and length of crack propagation.

III. RESULTS.

All specimens exhibited an extended region of constant velocity propagation followed by rapid deceleration and arrest, as typified by Figure 5. At the same time, the cross sectional area of the surface depression associated with the shear lips attains a plateau value within a distance from the starting notch about equal to the specimen thickness. The larger contractions closer to the starting notch are probably associated with the plastic zone generated in the vicinity of the blunted notch during static loading. As the crack decelerates and arrests, the depression decreases accordingly. In addition, the plateau value of the shear lip width increased systematically with increasing crack speed, the extremes being shown in Figure 6. The flat fracture surfaces also become noticeably rougher (see Figure 6). As reported earlier⁽¹⁾ at higher magnifications, both the flat and shear portions of the fracture display the dimples characteristic of ductile, fibrous mode of extension.

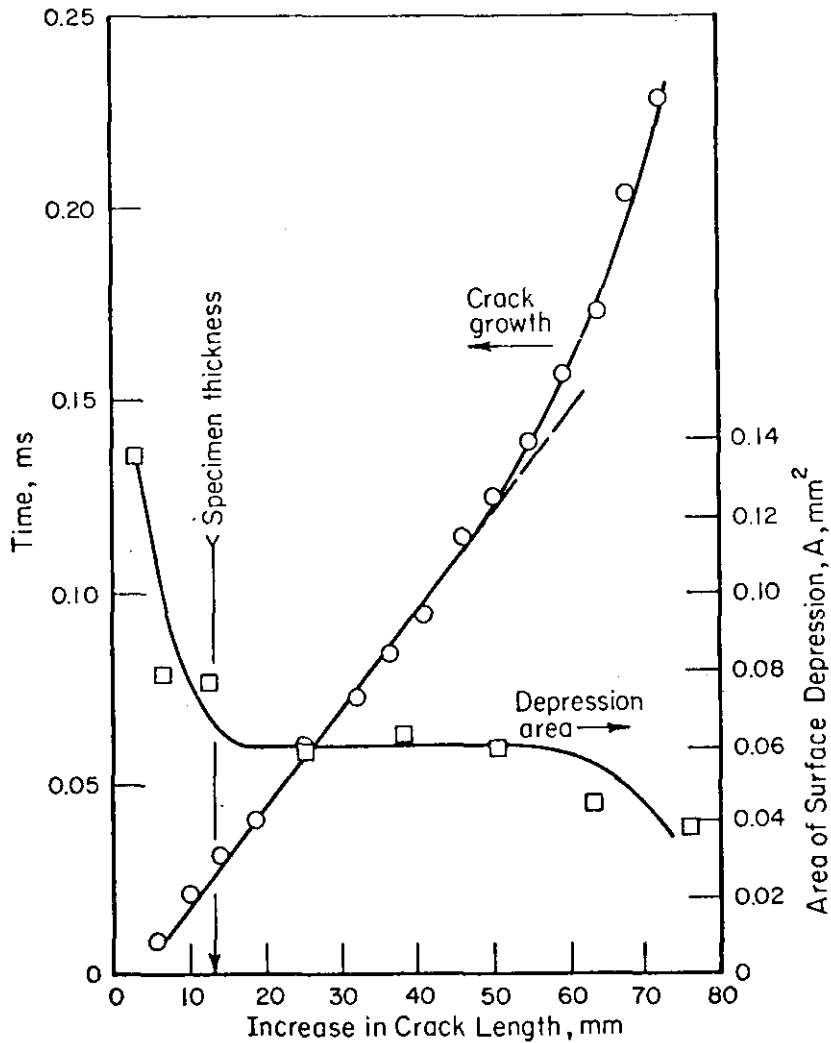


FIGURE 5. VELOCITY AND SURFACE PROFILE MEASUREMENT ON SAE4340 STEEL (SAMPLE No. 33).

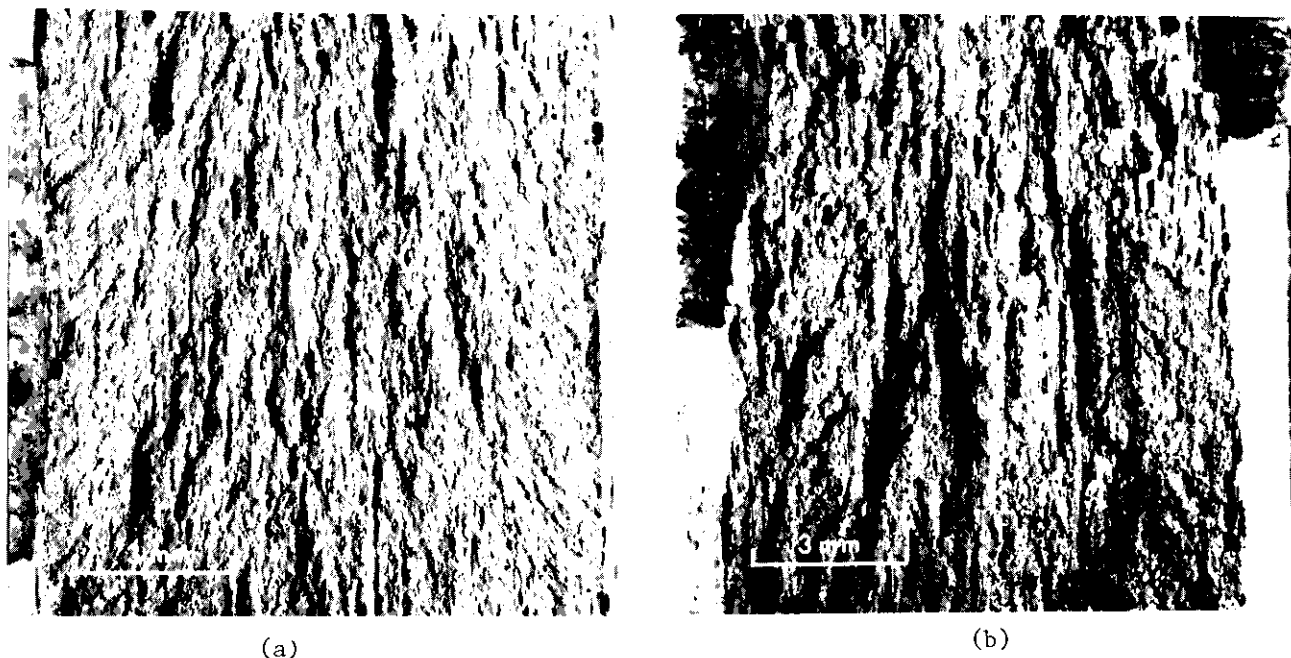


FIGURE 6. FRACTURE SURFACES OF TEST SPECIMENS: (a) crack velocity = 185 m/s per second and (b) crack velocity = 869 m/s per second.

Two separate evaluations were made of the dynamic fracture energy: (a) from the measured velocity (see top of Figure 4c) and (b) from the crack length measured at arrest (Equation (4)). As shown in Figure 7, these two essentially independent determinations of R or K_d are in close agreement. The one point that departs from this pattern was determined from velocity data and appears to be $\sim 30\%$ too high. Overall, the data show that the toughness almost doubles between the static value and the highest velocity attained ($\sim 17\%$ of the bar wave speed).

In contrast to the dynamic toughness, K_a , the stress intensity at crack arrest (derived from the static analysis), increased slightly with K_d (and, in turn, with crack velocity in the range 0 to 200 ms^{-1}) then remained about at the level required to reinitiate an arrested crack, K_{IC} , as shown in Figure 8.

The measurements of surface profile are given in Table 1. Note that the various measures of distortion are closely related to one another. Two examples are given in Figure 9 where it is shown that the width of the depression is proportional to the shear lip width and that the area of the depression is proportional to the area of the shear lip. The shear lip fracture energies, R_{SL} and U_{SL} , were calculated with Equations (1) and (2) from the measurements of the surface depression using the flow stress value[†]: $\bar{\sigma} = 1700 \text{ MNm}^{-2}$, and are listed in Table 2.

† The plastic strain rate in the shear lips: $\dot{\epsilon} \sim \frac{A}{2s} \cdot \frac{V}{d}$, where V is the fracture velocity and $d \sim 5 \text{ mm}$ is the distance by which flat fracture in the interior leads the shear fracture on the surface. For the values in Table 1, $\dot{\epsilon} \sim 10^4 \text{ sec}^{-1}$. While the dynamic flow stress of 1400 MNm^{-2} yield strength steels at this rate is not established, the dynamic flow stress values are expected to be close to the static values at 10^4 sec^{-1} on the basis of measurements on lower strength materials by Harding⁽²⁰⁾ and other considerations. For strain rates $> 10^4 \text{ sec}^{-1}$, rate sensitivity could be expected, and this is important since strain rates associated with the flat fracture are probably 2 to 4 orders of magnitude larger.

Values of the flat fracture energy, R_F were then obtained from Equation (3a). Table 2 shows that R_{SL} , the per-unit-area fracture energy, increases with shear lip width, while U_{SL} , the energy per unit volume is essentially constant. The average value, $U_{SL} \approx 0.21 \text{ J/mm}^3$, corresponds to a local temperature rise of $\sim 30^\circ\text{C}$.^{††} A measure of the temperature rise on the surface of Specimen 33 was obtained by using a series of Tempilsticks which responded to temperatures of 45°C to 73°C . A surface temperature rise in excess of 22°C and 50°C were detected out to $\sim 0.8 \text{ mm}$ and $\sim 0.25 \text{ mm}$ on either side of the crack line, respectively. The 22°C rise corresponds closely to the shear lip height, l , and while this suggests that the calculated value of U_{SL} is reasonable, it does not provide an exact check.

IV. DISCUSSION

The measurements described here show that the dynamic fracture energy for crack propagation in 4340 steel experiences a 4-fold increase with crack speed in the velocity range 0 to 860 ms^{-1} . The increase in energy, equivalent to a ~ 2 -fold increase in K_d , arises mainly from a systematic increase in the proportion of shear to flat fracture. However, there is room for a modest contribution arising from an increase in the specific flat fracture energy with speed (see Table 2) consistent with the observed roughening of the surface. While the change in the fracture surface occupied by shear lip is relatively modest, increasing from $\sim 0\%$ to 15% at the highest velocity, the effect on R is dramatic, because R_{SL} , the shear fracture energy is 5 times to 10 times the R_F , the flat fracture energy.

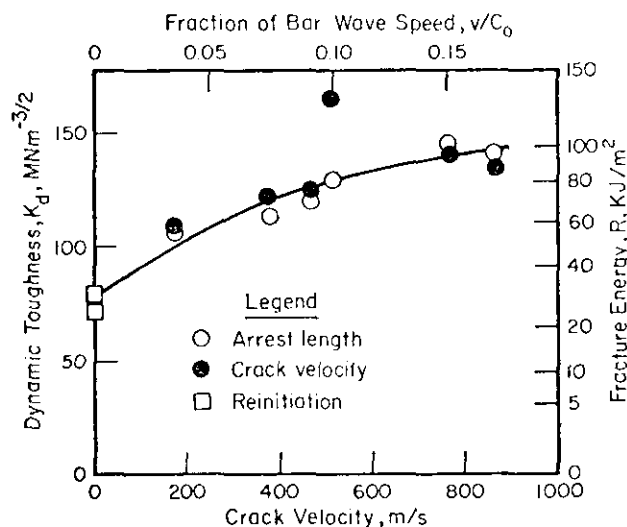


FIGURE 7. RELATION BETWEEN DYNAMIC FRACTURE TOUGHNESS AND CRACK VELOCITY FOR SAE4340 STEEL (Q & T 1 HR. AT 205°C , $b = 12.7 \text{ mm}$). Tested at room temperature.

^{††} The temperature rise is calculated assuming the heat generated by the plastic work accompanying the intense shearing of regions 2-3 and 2-4 in Figure 3 is confined to the area $l \cdot s$ outlined by the dashed lines.

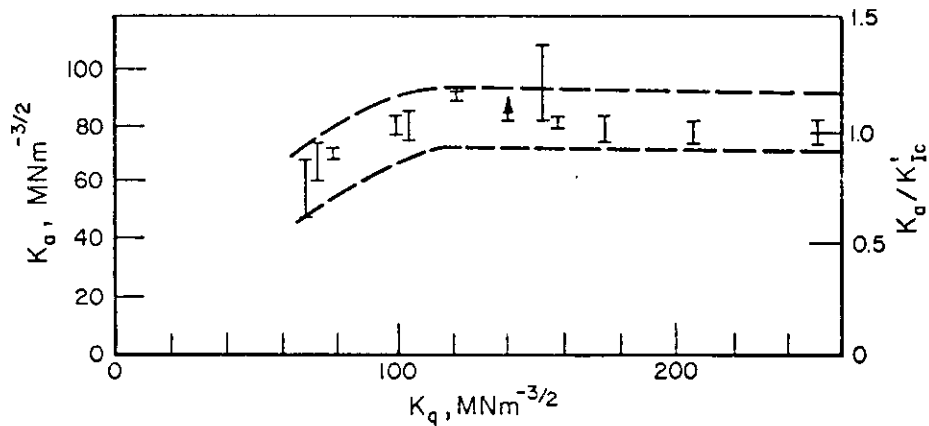


FIGURE 8. STRESS INTENSITY AT CRACK ARREST OF SAE4340 STEEL.

TABLE I. MEASUREMENTS OF FRACTURE FEATURES IN SAE4340 STEEL QUENCHED AND TEMPERED AT 205°C

| Sample No. | Steady-state crack speed V, m/s | Depression area, A, 10 ⁻³ mm ² | Depression height, λ, mm | Shear lip width, s, mm | Flat fracture width, f, mm |
|------------|---------------------------------|--|--------------------------|------------------------|----------------------------|
| 30B | 0 | ~ 0 | ~ 0 | ~ 0 | 12.7 |
| 32 | 0 | ~ 0 | ~ 0 | ~ 0 | 12.7 |
| 30D | 185 | 50 | 2.0 | 0.47 | 11.06 |
| 33 | 381 | 63 | 1.75 | 0.51 | 10.98 |
| 34 | 472 | - | - | - | - |
| 31 | 513 | 100 | 2.6 | 0.63 | 10.74 |
| 35 | 772 | - | - | - | - |
| 37 | 869 | 200 | 3.5 | 0.91 | 10.18 |

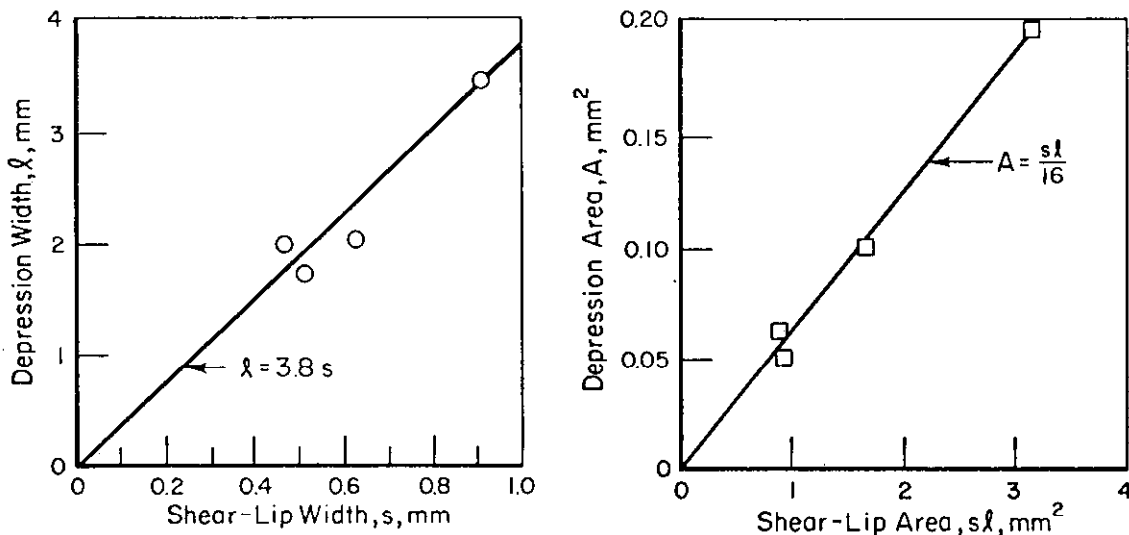


FIGURE 9. RELATIONS AMONG VARIOUS SHEAR LIP DIMENSIONS.

TABLE II. DYNAMIC FRACTURE ENERGY AND TOUGHNESS VALUES FOR UNSTABLE CRACKS IN 4340 STEEL INCLUDING VALUES FOR THE SHEAR LIP AND FLAT PORTIONS OF THE FRACTURE

| SAMPLE NO. | CRACK VELOCITY ms ⁻¹ | DYNAMIC FRACTURE ENERGY AND TOUGHNESS VALUES | | | | | | | |
|------------|------------------------------------|--|--|---------------------------------------|---|---|--|--|---|
| | | K _d ^(a) (MNm ^{-3/2}) | K _d ^(b) (MNm ^{-3/2}) | R ^(d) (KJm ⁻²) | R _{SL} ^(e) (KJm ⁻²) | V _{SL} ^(f) (J/mm ³) | K _{d(SL)} ^(c) (MNm ^{-3/2}) | R _F ^(g) (KJm ⁻²) | K _{d(F)} ^(c) (MNm ^{-3/2}) |
| 30B | ~ 0 | 73 | - | 27 | - | - | - | ~ 27 | 73 |
| 32 | ~ 0 | 76 | - | 29 | - | - | - | 29 | 76 |
| 30D | 185 | 105 | 108 | 54 | 180 | 0.18 | 190 | 42 | 92 |
| 33 | 381 | 115 | 121 | 64 | 210 | 0.24 | 205 | 47 | 97 |
| 34 | 472 | 121 | 124 | 71 | - | - | - | - | - |
| 31 | 513 | 130 | 166 | 82 | 270 | 0.21 | 232 | 55 | 105 |
| 35 | 772 | 144 | 141 | 101 | - | - | - | - | - |
| 37 | 869 | 142 | 136 | 98 | 370 | 0.21 | 272 | 40 | 89 |

(a) From Equation (4).

(b) From Figure 4c.

(c) K_{d(SL)} and K_{d(F)} are toughnesses derived from the corresponding fracture energies: $K_{d(SL)} = \sqrt{\frac{ER_{SL}}{1-\nu^2}}$, $K_d = \sqrt{\frac{ER_F}{1-\nu^2}}$

The measurements of the surface depression show that R_{SL} increases with the size of the shear lip, while the per-unit-volume shear fracture energy, $U_{SL} = 0.21 \text{ J/mm}^3$ remains essentially constant. These results are very similar to those which can be derived from the data of Steigerwald⁽²¹⁾ who examined the variation of K_{IC} with specimen thickness, also for a 4340 steel in a quenched and 205°C-tempered condition. The shear lip width did not vary systematically with thickness in these experiments, $s \sim 0.5 \text{ mm}$, while the proportion of shear to flat fracture increased as the specimen thickness was reduced. Figure 10 shows that Steigerwald's results[†] can be represented by Equation (3b). The quantity $U_{SL} \approx 0.20 \text{ J/mm}^3$ is derived from the slope of the straight line, assuming that the relation between l and s of Figure 9a holds in this case. Another estimate $U_{SL} \approx 0.19 \text{ J/mm}^3$ can be obtained from Equation (2), by assuming that $A/l_s = 1/16$ as before, and by using the measured yield strength⁽²¹⁾ of 1500 MN/m^2 , again in good agreement with the value obtained here. The relative constancy of U_{SL} -values derived from these 2 investigations suggests that R-values can be predicted once the relative amounts of flat and shear fracture are known. The factors governing the size of the shear lip are not clearly resolved but this may be connected with R_F since R_F and the dimensions l and s tended to increase with crack speed.

Perhaps the most important findings of this study are the agreements between theory and experiment. The Timoshenko beam theory/beam-on-elastic foundation analysis makes the following predictions about crack propagation in the DCB-test piece:

- (1) The crack propagates at an essentially constant, steady-state velocity from the start. This is confirmed by the velocity measurements (compare Figures 4a and 5).
- (2) The steady-state velocity is not an invariant, but depends on the initial conditions, i.e., the bluntness of the starting slot. This is confirmed by the measurements (see Figure 7).
- (3) For a given DCB-configuration, material density and modulus, the crack velocity and arrest length are separate, single-valued functions of R or K_d (see Figure 4c). This means that R - or K_d -value can be inferred independently from the velocity and from the arrest length. The fact that values obtained in these two ways agree closely (see Figure 7) can be regarded as a critical test of the theory.
- (4) Alternatively, the theory predicts a unique relation between crack velocity and the length of the crack at arrest, that is independent of the dynamic toughness of the material. This relation is compared in Figure 11 with the predictions of quasi-static analyses and with the measurements. Since the quasi-static analyses^(16,22) do not all predict a constant velocity, peak velocities are plotted. Furthermore, the curves will shift with changes in the test piece geometry. The data points also do not all represent the identical geometry since different initial crack lengths were used in some cases. Despite this, it is clear from the figure that the present fully dynamic analysis provides, by far, the best description of the relation between the velocity and crack length at arrest, two quantities that can be measured directly.

† Steigerwald's K_C -values have been converted to G_C which approximates the value of R at zero velocity.

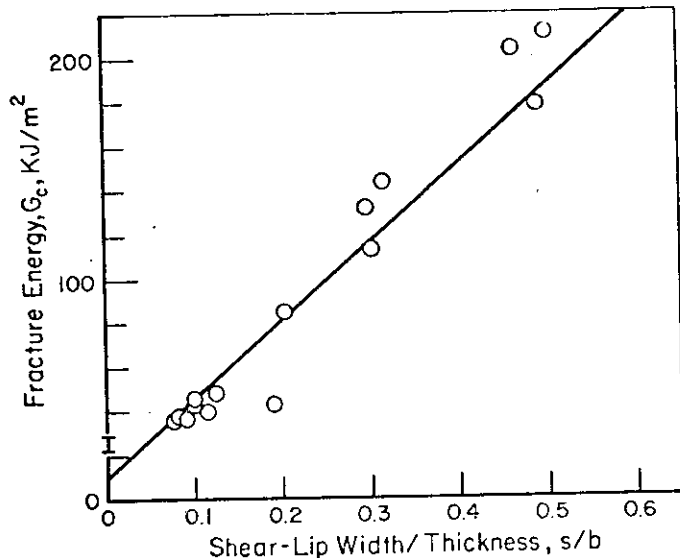


FIGURE 10. VARIATION OF FRACTURE ENERGY WITH SPECIMEN TOUGHNESS IN SAE 4340 STEEL TESTED UNDER STATIC CONDITIONS AT ROOM TEMPERATURE. Data of Steigerwald(21)

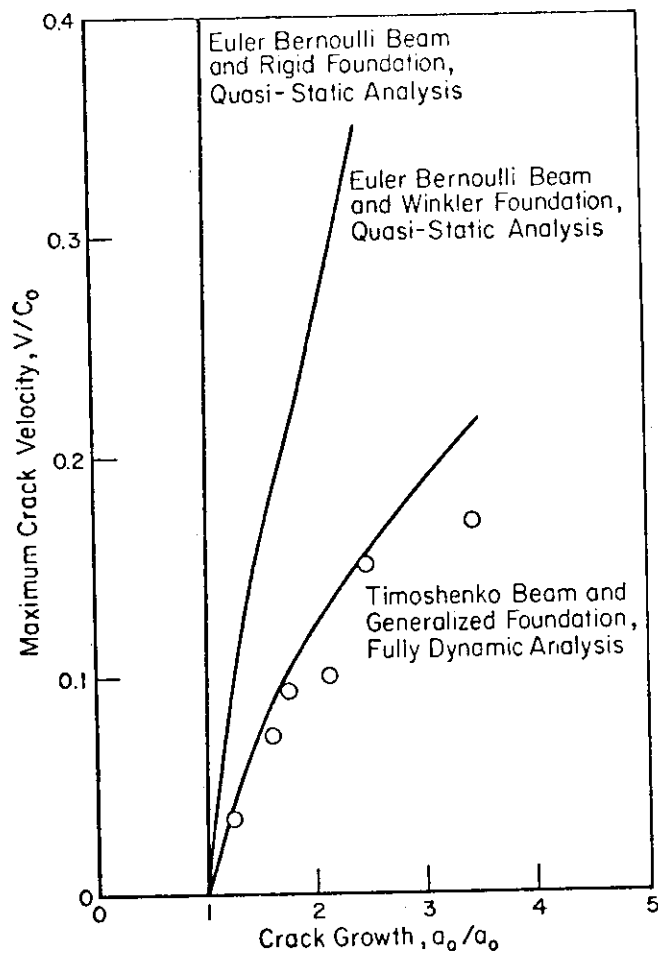


FIGURE 11. COMPARISON BETWEEN THEORETICAL PREDICTIONS AND EXPERIMENTAL MEASUREMENTS OF THE RELATION BETWEEN CRACK VELOCITY AND CRACK TRAVEL.

These agreements are important for two reasons. By validating the analysis, they confirm that a large part of the kinetic energy imparted to the DCB-test piece by the unstable crack is recovered and used to drive the crack. This conclusion has implications for fracture arrest which are discussed in Section II. One of these is that K_a , the stress intensity at arrest calculated from static considerations, is not a materials property. The relative constancy of the K_a -values reported in Figure 8 is fortuitous--a consequence of the increase of K_d with velocity ($K_d \propto \sqrt{K_q}$, see Figure 7) together with Equation (4)--and not a sign that K_a is an invariant. Additional evidence that K_a depends on specimen geometry has been reported by Kanazawa(23).

The agreements cited are also important because they provide the basis for a convenient laboratory test procedure for measuring crack propagation. The wedge-loaded DCB test makes it possible to control the velocity and energy dissipation rate of unstable cracks and to extract dynamic fracture energy and toughness values from the measurements. The method has already been extended to tougher steels by facilitating fracture initiation. This is accomplished with a "duplex"/DCB specimen consisting of high-strength/low-toughness SAE4340 "starter" welded to the test section.(2) The fracture is initiated from a slot in the starter section in the manner described here and enters the test section at high velocity. In this way R and K_d values can be measured close to the transition temperature. The technique is also being used to study crack arrestors.

V. CONCLUSIONS

1. Unstable fractures in high-strength 4340 steel, wedge-loaded DCB-test pieces propagate at essentially constant velocities. The existence of steady-state velocities, their variation with the initial conditions, and the relation between steady-state velocity and arrest length are all in close agreement with the dynamic beam-on-elastic-foundation analysis. The measurements represent a critical test of this theory. These results confirm that the kinetic energy imparted to the wedge-loaded DCB test piece is substantially converted into fracture energy during the latter stages of a propagation event.
2. The dynamic toughness of the 4340 steel increases systematically with crack speed in the range 0 to 860 ms^{-1} from 75 $\text{MNm}^{-3/2}$ to 140 $\text{MNm}^{-3/2}$, reflecting a ~ 4 -fold increase in the dynamic fracture energy R .
3. The per-unit-volume shear lip fracture energy, $U_{SL} = 0.21 \text{ J/mm}^3$ appears to be essentially independent of shear lip size and crack speed over the ranges observed. The temperature rise detected on the surface in the vicinity of the crack is consistent with the U_{SL} -value derived from measurements of shear lip geometry.
4. Both the size of the shear lips and R_{SL} , the per-unit-area fracture energy dissipated within the shear lips, increase with crack speed. The increase in toughness with speed is observed mainly because the quantity R_{SL} is 5 to 10 times R_F , the flat fracture energy.
5. The flat fracture energy also appears to increase with crack speed consistent with noticeable increases in the roughness of the fracture surface.

VI. REFERENCES

1. G. T. Hahn, R. G. Hoagland, M. F. Kanninen, and A. R. Rosenfield, "A Preliminary Study of Fast Fracture and Arrest in the DCB-Test Specimen", Dynamic Crack Propagation Conference, Lehigh University, 1972.
2. G. T. Hahn, R. G. Hoagland, M. F. Kanninen, and A. R. Rosenfield, "The Characterization of Fracture Arrest in a Structural Steel", This Report, Section II.
3. M. F. Kanninen, A. R. Rosenfield, and R. G. Hoagland, "Fast Fracture in PMMA", Deformation and Fracture of High Polymers, H. Kausch, et al., eds. (in press).
4. A. R. Rosenfield and M. F. Kanninen, "The Fracture Mechanics of Glassy Polymers", J. Macro-Molecular Sci. (in press).
5. J. Eftis and J. M. Krafft, "A Comparison of the Initiation With the Rapid Propagation of a Crack in A Mild Steel Plate", Trans. ASME, Vol. 87D, p. 916, 1965.
6. F. W. Barton and W. J. Hall, "Brittle-Fracture Tests of Six-Foot Wide Prestressed Steel Plates", Weld. J. Res. Supp., Vol. 39, p. 379s, 1960.
7. T.A.C. Stock, "Stress Field Intensity Factors for Propagating Brittle Cracks", Int. J. Fract. Mech., Vol. 3, p. 121, 1967.
8. N. P. Fitzpatrick, P. L. Pratt, and T.A.C. Stock, "Fracture in Structural Alloys", J. Austr. Inst. Met., Vol. 13, p. 243, 1968.
9. S. J. Burns and Z. J. Bilek, "The Dependence of the Fracture Toughness of Mild Steel on Temperature and Crack Velocity", Report NYO-2394-42, Div. of Engg., Brown University, 1971.
10. G. J. Dvorak, "A Model of Brittle Fracture Propagation Part I: Continuum Aspects", Engg. Fract. Mech., Vol. 3, p. 351, 1971.
11. H. Kihara and K. Ikeda, "A Proposal on Evaluation of Brittle Crack Initiation and Arresting Temperatures and Their Application to Design of Welded Structures", Papers of the Ship Research Institute, No. 14, Tokyo, April, 1966.
12. J. M. Krafft, "Correlation of Plane-Strain Toughness with Strain Hardening Characteristics of a Low, a Medium and a High Strength Steel", Applied Materials Research, Vol. 3, p. 88, 1964.
13. R. G. Hoagland, A. R. Rosenfield, and G. T. Hahn, "Mechanisms of Fast Fracture and Arrest in Steels", Met. Trans., Vol. 3, p. 123, 1972.
14. G. T. Hahn, M. F. Kanninen, and A. R. Rosenfield, "Ductile Crack Extension and Propagation in Steel Foil", Fracture 1969, P. L. Pratt, et al, eds., Chapman and Hall (London, 1969), p. 58.
15. A. J. Carlsson, L. Dahlberg, and F. Nilsson, "Experimental Studies of the Unstable Phase of Crack Propagation in Metals and Polymers", Dynamic Crack Propagation Conference, Lehigh University, 1972.
16. M. F. Kanninen, "An Augmented Double Cantilever Beam Model for Studying Crack Propagation and Arrest", Int. J. Fract. Mech., Vol. 9, p. 83, 1973.

17. J. Malkin and A. S. Tetelman, "Relation Between K_{Ic} and Microscopic Strength of Low Alloy Sheets", Engg. Fract. Mech., Vol. 3, p. 151, 1971.
18. J. I. Bluhm, "A Model for the Effect of Thickness on Fracture Toughness", ASTM Proc., Vol. 61, p. 1324, 1961.
19. M. F. Kanninen, "Dynamic Analysis of Crack Propagation in the DCB Test Specimen" This Report, Section III.
20. J. Harding, "Effect of High Strain Rate on the Room-Temperature strength and Ductility of Five Alloy Steels", J. Iron Steel Inst., Vol. 210, p. 425, 1972.
21. E. A. Steigerwald and G. L. Hanna, "Influence of Work-Hardening Exponent on the Fracture Toughness of High-Strength Materials", Trans. AIME, Vol. 242, p. 320, 1968.
22. J. P. Berry, "Some Kinetic Considerations of the Griffith Criterion for Fracture": Part I - Equations of Motion at Constant Force, Vol. 8, p. 194, 1960; Part II - Equations of Motion at Constant Displacement", Vol. 8, p. 207, 1960, J. Mech. Phys., Solids.
23. T. Kanazawa, "Recent Studies on Brittle Crack Propagation in Japan", Dynamic Crack Propagation Conference, Lehigh University, 1972.

APPENDIX 1-A

VELOCITY MEASURING PROCEDURE

The velocity of crack propagation was measured from the change in the resistance of grids as the advancing crack severed successive strips of the grid. This grid was deposited on top of an epoxy† film coated on the steel specimen to serve as an insulator.

The epoxy was mixed 1 part activator to 1 part resin. Then a bead of epoxy about 1/4" in diameter was placed across the width of the specimen. Following this, the specimen and the epoxy bead were covered with a 5 mil sheet of mylar. Using a straight edge, the epoxy was "squeegeed" to an almost (3 to 4 mils) uniform thickness covering the specimen. After an overnight "set", the mylar was stripped from the specimen leaving behind a glass-smooth bubble-free epoxy coating on the specimen surface.

As additional preparation, the conducting grid was deposited through a mylar mask prepared for the specimen. This mask had an array of four grids, each consisting of 5 parallel strips 1-1/4 mm wide and spaced 5 mm apart, 15 to 40 mm long, in the form of a trapezoid, cut out with a razor blade (see Figure 1 of the introduction).

After the mask was taped to the specimen surface, the specimen was placed in a vacuum evaporation unit and the system was evacuated to $< 2 \times 10^{-5}$ torr. Using a platinum carbon composite as a source, $\sim 1,000 \text{ \AA}$ of material was deposited perpendicular to the specimen surface, through the mask.

Upon removal from the evaporator, each line was checked for continuity with a volt ohm-meter. Typical values for the lines ranged from 30 to 50 K ohms. The ends of the lines were then joined with conductive paint resulting in four separate parallel circuits with resistance values ranging from 7,500 to 12,500 ohms.

The four individual trapezoidal arrays were connected in parallel circuit. Each leg of the circuit contained not only a trapezoid but also a single channel of a high-speed tape recorder and a variable resistor. A voltage (12 V d.c.) is imposed on the total circuit. An oscilloscope trace of the output of two individual channels of the tape recorder is shown in Figure A-1. The velocity measurements were made from such traces displayed two at a time so that the time interval between grids could be measured.

Since the tape recorder speed was 3 m/sec and the reel contained about 2-1/2 km of tape, it had a recording time of almost 15 minutes. Thus, the tape recorder could be started well before the crack began to propagate with assurance that the resistance changes would be captured. Triggering problems were accordingly eliminated. At the speeds employed, signal changes 5μ sec apart could be distinguished and velocities as high as 1000 m/sec could thus be measured for a conducting strip spacing of 5 mm. Larger velocities could be detected by increasing the strip spacing.

† Duro E-Pox-E, No. EPX1, Woodhill Chemical Sales, Cleveland, Ohio.

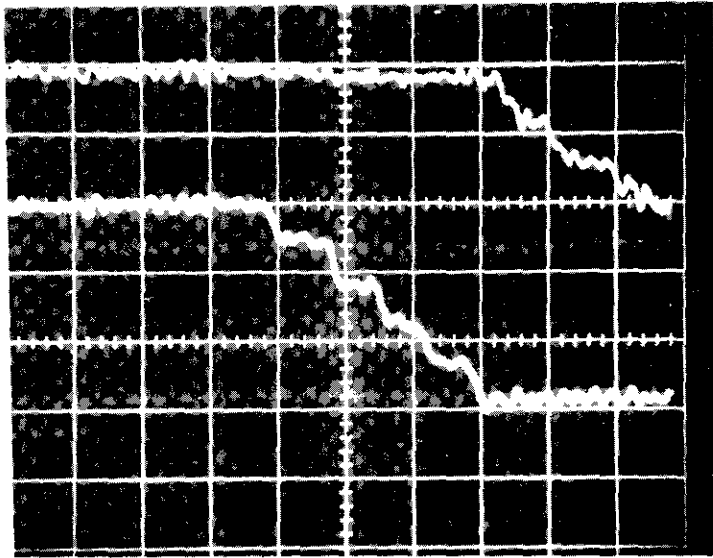


FIGURE A-1. RESISTANCE-TIME RECORDING OF THE RUPTURE OF CONDUCTING STRIPS IN 2 ADJACENT GRIDS (ABSCISSA $16 \mu \text{ sec/cm}$, ORDINATE 0.5 volts/cm) DURING A CRACK PROPAGATION EVENT.

SECTION 2

THE CHARACTERIZATION OF FRACTURE ARREST IN A STRUCTURAL STEEL

by

G. T. Hahn, R. G. Hoagland, M. F. Kanninen, and A. R. Rosenfield

ABSTRACT

A new method of characterizing the fracture arrest capabilities of structural steels is described. The method employs wedge-loaded "duplex" double-cantilever-beam (DCB) specimens and a fully dynamic analysis of crack propagation in the test piece. In this way (1) unstable fractures can be initiated and arrested over a wide range of temperature encompassing the transition temperature, (2) the speed of unstable fracture in the test piece can be controlled, and (3) R or K_d , the dynamic fracture energy or dynamic toughness of the material, can be evaluated. Results for fractures propagating at 600 ms^{-1} to 1100 ms^{-1} in 12.7 mm- and 25.4 mm-thick plates of A517F steel and SAE 4340 steel at 0°C and -78°C , are described. The analysis of the test data lends support to the view that kinetic energy contributes to the crack driving force, and that K_a , the static stress intensity at arrest is not a material property.

THE CHARACTERIZATION OF FRACTURE ARREST IN A STRUCTURAL STEEL

I. INTRODUCTION

The risk of catastrophic fracture can be reduced by endowing pressure vessels and other monolithic structures with a predetermined fracture arrest capability. This can be done by selecting base materials with specified toughness levels or by installing tough crack arrestors in strategic locations. A number of methods of characterizing the arrest capabilities of steels have been devised including Robertson's arrest temperature⁽¹⁾, Pellini's FAD⁽²⁾, and the arrest toughness, K_a ⁽³⁻⁶⁾.

The arrest toughness concept has features of a quantitative methodology comparable to crack extension fracture mechanics, but it involves several arbitrary and questionable assumptions about the energetics of fracture arrest. A tacit assumption is that the kinetic energy imparted to a structure by an unstable crack is not converted into fracture energy and is not a source of crack driving force. In contrast, Berry⁽⁷⁾, Romualdi and Sanders⁽⁸⁾, and the present authors^(9,10) adopt the position that the kinetic energy is substantially conserved and that it contributes to the crack driving force. Another assumption implicit in the analyses of Irwin and Wells⁽³⁾, Kanazawa⁽⁴⁾, and Crosley and Ripling^(5,6) is that the strain energy release rate of the propagating crack can be approximated by values derived from static considerations. However, analyses by Broberg⁽¹¹⁾ and Eshelby⁽¹²⁾, as well as the interpretation of fracture velocity measurements⁽¹⁰⁾, suggest that the inertia of structural members influences the strain distribution and G-values in a significant way. These assumptions are important because they affect the interpretation of test data, and this is illustrated in Figure 1 for the DCB (double-cantilever-beam) test piece which is used to measure K_a :

• The arrest toughness concept presupposes that G, the strain energy release rate, is the only contribution to the crack driving force[†], and that the crack arrests when $G < R$, where R is the energy that must be supplied to the crack-tip region to produce crack extension (the dynamic fracture energy of the material). In contrast, kinetic energy utilization implies arrest when $(G + H) < R$ ($G \equiv -\frac{\delta U}{\delta a}$, $H \equiv -\frac{\delta T}{\delta a}$ is the kinetic energy release rate, and U and T are the strain energy and kinetic energy of the system).

• When G is the sole driving force, G_a , the value of G at arrest, must always lie on the R curve, and can therefore be regarded as the controlling material property (see Figure 1a). The corresponding stress intensity value, $K_a \equiv \sqrt{\frac{EG_a}{1-\nu^2}}$ is the arrest toughness, where E is Young's

† The statements in this and the following paragraph presuppose fixed grip conditions; otherwise the rate of external work input, $-\frac{\delta W}{\delta a}$, is an additional driving force.

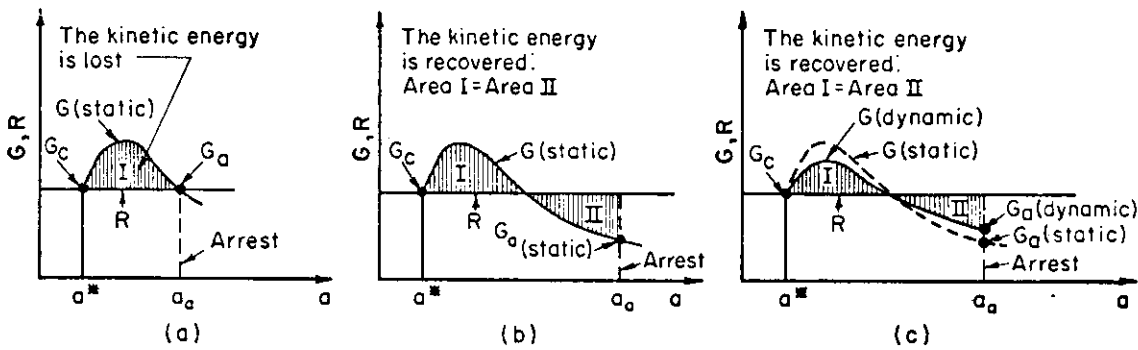


FIGURE 1. SCHEMATIC REPRESENTATION OF THE ENERGETICS OF FRACTURE ARREST IN THE DCB-TEST PIECE, ILLUSTRATING (a) THE ARREST TOUGHNESS CONCEPT, (b) THE R-CURVE CONCEPT, AND (c) THE CONCEPT OF A DYNAMIC STRAIN ENERGY RELEASE RATE. The quantities G_c , a^* , G_a , and a_a are the critical strain energy release rates and crack lengths corresponding to the onset of unstable fracture and to fracture arrest, respectively. The shaded areas I and II represent the amount of kinetic energy imparted to the structure, and the amount recovered in the form of fracture energy prior to arrest. The drawings reflect the simplifying assumption that there is no external work exchanged between the test piece and the loading system during unstable fracture.

modulus and ν is Poissons ratio. When kinetic energy is conserved, G does not lie on the R curve, and neither G_a nor K_a can be interpreted^a as material properties (see Figure 1b). In this case, the quantity R , or an equivalent (apparent) dynamic stress intensity $K_d \equiv \sqrt{\frac{ER}{1-\nu^2}}$ are the appropriate material parameters for defining the arrest capability of a structural material.

- Figure 1c illustrates the concept of a dynamic G -curve that departs from static values. The departures influence the kinetic energy in the system and the crack speed. This is important in situations where R (and K_d) vary with V , the fracture velocity⁽¹³⁻¹⁵⁾. In this case $R(V)$ and $K_d(V)$ must be introduced to predict the instantaneous velocity and the point of arrest.

These assumptions also have a bearing on the design of arrestors. For example, the K_a -approach implies that arrest is instantaneous when $G < R$. Accordingly, a strip of tough material ($R > G$) just wide enough to contain the heavily strained region adjacent to the crack tip is adequate to stop a propagating crack if the K_a -approach is valid. The R -curve concept implies that the arrestor must be wide enough to absorb the kinetic energy stored in the structure.

This paper describes a new testing procedure and an appropriate dynamic analysis which help to distinguish between the K_a - and R -curve approach to fracture arrest. The procedure provides a wide range of constant fracture velocities and thereby affords opportunities for measuring the variation of R with crack speed. A preliminary description of the method, which utilizes wedge-loaded DCB-test pieces with blunt starting slots, is contained in an earlier report.⁽⁹⁾ The present paper describes the use of "duplex" DBC-test pieces which make it possible to initiate fractures at temperatures close to (or even above) the transition temperature and to direct unstable, high speed

cracks into the test material under controlled conditions. Results for 4340 and A517F steel at 0°C and -78°C are presented. A more comprehensive study of the 4340 steel appears in Section I and a more complete description of the analysis is given in Section III. The results obtained favor the idea that kinetic energy can contribute to the crack driving force, necessitating an R-curve- rather than a K_a -approach to fracture arrest.

II. EXPERIMENTAL PROCEDURES.

Measurements of fast fracture and arrest were performed on material from a 25.4 mm-thick plate of A517F steel[†], at 0°C and -78°C. Plate specimens, machined to a thickness of 12.7 and 24.5 mm, were wedge-loaded as shown in Figure 1 of the General Introduction. Dimensions of the DCB-test pieces are given in Figure 2 (The longitudinal axis of the test piece is parallel to the rolling direction.). The configuration, instrumentation, and analysis differ in 4 essential respects from those employed by Hoagland⁽¹³⁾, Ripling and coworkers^(5,6), Burns and Bilek⁽¹⁵⁾ and others who have used the DCB-specimen to study propagation and arrest:

(1) Blunting Starting Slot. The fracture is initiated with the aid of a blunt slot rather than a sharp crack. The blunted notch permits the specimen to sustain a stress intensity, K_q , which is typically 3 to 4 times as large as K_{Ic} . Consequently, as soon as a sharp crack emerges from the blunt notch, the crack immediately becomes unstable and propagates rapidly. The K_q -value can be systematically altered by varying the slot root radius (See Section I, Figure 2). Results reported here were obtained with a root radius of about 0.7 mm, prepared by spark machining followed by electropolishing to make the crack initiation conditions more reproducible.

(2) Wedge Loading. The specimen is slowly loaded in an ordinary testing machine (operating in the compression mode) by forcing a split wedge

[†] The composition of the A517F steel is: C-0.18, Mn-0.93, Ni-0.85, MO-0.42, Cr-0.54, V-0.038, Cu-0.3. Tensile properties are as follows:

| | <u>Yield Strength</u> | <u>Ultimate Strength</u> | <u>RA%</u> |
|-------|---------------------------------|---------------------------------|------------|
| RT | 763 MNm ⁻² (111 Ksi) | 823 MNm ⁻² (119 Ksi) | 70 |
| -78°C | 810 MNm ⁻² (118 Ksi) | 886 MNm ⁻² (129 Ksi) | 69 |

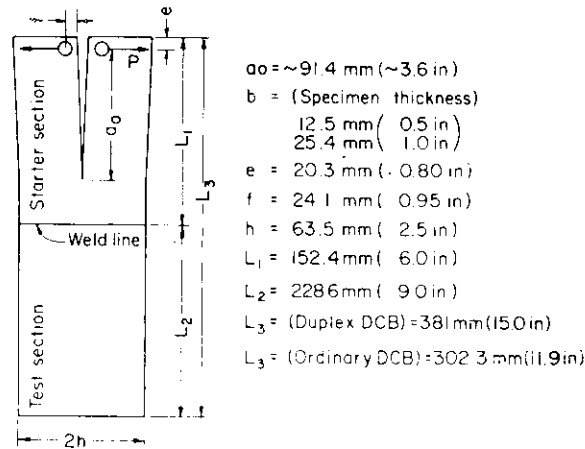


FIGURE 2. DIMENSIONS OF DUPLEX TEST PIECES

between the pins. Since the wedge loading is inherently "stiff", crack propagation proceeds with essentially constant displacement at the load point[†]. Under these conditions G decreases as the crack grows, and this ultimately causes the crack to arrest within the confines of the specimen provided the test piece is long enough⁽¹⁶⁾. Wedge loading has two other virtues. Since little energy is exchanged between the DCB-specimen and the testing machine during the propagation event, the results are expected to be relatively insensitive to the character of the testing machine. The friction between the wedge and the pins introduces a modest compressive stress parallel to the crack plane, typically 2 to 15% of the yield strength, which tends to stabilize the crack path⁽¹⁷⁾. Hence, the side grooves ordinarily required to keep the crack from turning are not needed. This simplifies the measurement of velocity and makes the test a closer replica of service conditions.

(3) The Duplex Specimen. To facilitate the production of fast propagating cracks at temperatures close to the transition temperature, "duplex-DCB test specimens" were employed. These consisted of a high-strength/low-toughness 4340 steel^{††} "starter section" electron beam welded^{†††} to the A517F

† The dynamic analysis given in the next section indicates that the displacement of the load points remains fixed during the first part of the propagation event and then experiences a series of oscillations.

†† The composition of the 4340 steel is given in Reference 9. Tensile properties are as follows:

| | <u>Yield Strength</u> | <u>Ultimate Strength</u> | <u>RA%</u> |
|---|----------------------------------|----------------------------------|------------|
| Quenched and Tempered 1 hr. at 200°C, Tested at RT | 1380 MNm ⁻² (200 Ksi) | 1940 MNm ⁻² (282 Ksi) | 50 |
| Tested at -78°C | 1600 MNm ⁻² (232 Ksi) | 2010 MNm ⁻² (292 Ksi) | 50 |
| As-Quenched, Tested at -78°C | 1670 MNm ⁻² (242 Ksi) | 2260 MNm ⁻² (328 Ksi) | 29 |

††† Electron beam welding produced a sound and relatively narrow fusion and heat-affected zone about 3 mm wide.

steel "test section", as shown in Figure 2 and in the Appendix to this section, Figures A-1 - A-3. The fracture is initiated from the slot in the starter section, and directed at high speed into the test section. The high-strength starter section also makes it possible to attain higher K_q -values without exceeding the limitation on yielding imposed by linear elastic fracture mechanics theory[†]. This is important because the maximum fracture velocities that can be produced in the test piece, and the maximum values of R and K_d that can be measured in a particular specimen vary directly with K_q . The requirements are less stringent once the crack is propagating since the higher dynamic yield strength corresponding to crack tip strain rates $\sim 10^4$ to 10^7 sec⁻¹ is then appropriate⁽¹⁸⁾.

(4) Analysis of Measurements. The analysis described in the next section makes it possible to extract R - (or K_d -) values from K_q and K_a (static), the stress intensity at initiation and arrest which are measured with a standard displacement gage mounted to the end of the DCB specimen.^{††} Alternatively R or K_d can be evaluated independently from K_q and V , the fracture velocity in the test section. The velocity measuring system consisted principally of a grid of conducting strips whose resistance is monitored during the propagation event. A description of the grid, the method of preparation, and the recording technique are given in the Appendix to Section 1.

III. ANALYSIS

The analysis of crack propagation in ordinary and duplex DCB-test pieces, is derived from the beam-on-elastic-foundation model. Kanninen⁽²⁰⁾ has shown that a static analysis of the model employing a Euler-Bernoulli beam and a Winkler layer provides a description of the stress intensity factor for the DCB-specimen which is in excellent agreement with two-dimensional analyses and

† The maximum value of $K_q \lesssim 0.9 \sigma_Y \sqrt{h}$, where h is the beam height and σ_Y is the yield stress⁽¹⁹⁾. Thus the maximum value of K_q that can be generated at room temperature in the present duplex sample ($h = 63.5$ mm, $\sigma_Y (4340) = 1380$ MNm⁻²) is ~ 310 MN/m^{-3/2}. However comparison of the results in Specimens 3V44 and 3VY10 (see Table I), p. 37) suggests that this might be sufficiently conservative.

†† The quantity K_q is calculated for the wedge opening and a crack length a_0 equal to the initial slot length. The quantity K_a (static) is calculated for the wedge opening and crack length a_a measured after arrest from purely static considerations. It does not account for the kinetic energy distribution in the arms of the DCB-specimen at the instant of arrest. For this reason, K_a is not necessarily a precise measure of the stress intensity at instant of crack arrest. Both of these calculations are based on displacement measurements made with a gage attached at a distance $e = 1.65$ mm from the center of the pins (see Figure 2), and corrected by using an expression derived by Kanninen⁽²⁰⁾.

with experimental results.[†] This model was initially adapted to unstable crack-
ing by⁽¹⁰⁾: (1) introducing a force Q to allow for the larger deflection of the
specimen at the load point which is permitted by the blunt starting slot (see
Section 3), (2) incorporating lateral inertia forces into the equations govern-
ing the beam deflection, and (3) systematically removing the springs comprising
the foundation when the critical spring deflection $w_c = \left(\frac{hR}{2E}\right)^{1/2}$,
corresponding to the dynamic fracture energy R, is exceeded. This model
gives a good representation of the constant speed propagation observed in the
DCB-test piece, and much better estimates of the crack speed than quasistatic
treatments that ignore inertia.⁽¹⁰⁾ However, the calculated speeds still exceed
the experimental values by about a factor of two.⁽¹⁰⁾

This analysis has now been substantially refined. Timoshenko's beam
equations^(21,22) and a model having a generalized elastic foundation with exten-
sional and rotational stiffness⁽²³⁾ have been introduced. This makes it possible
to account for lateral and rotational inertia. The governing equations for this
model, derived in Section 3, starting from the equations of three-dimensional elas-
ticity, and adapting the method given by Cowper,⁽²⁴⁾ thus gives the relations

$$EI \frac{\partial^2 \Psi}{\partial x^2} + \kappa GA \left(\frac{\partial w}{\partial x} - \Psi \right) - k_r H^*(\theta_c - \theta) \Psi = \rho I \frac{\partial^2 \Psi}{\partial t^2} \quad (2a)$$

$$\kappa GA \left(\frac{\partial^2 w}{\partial x^2} - \frac{\partial \Psi}{\partial x} \right) - k_e H^*(\theta_c - \theta) w = \rho A \frac{\partial^2 w}{\partial t^2} \quad (2b)$$

where

| | |
|---|---|
| w = average deflection of the cross section | A = cross sectional area of beam (=bh) |
| Ψ = mean angle of rotation of the cross section about the neutral axis | k_e = extensional stiffness of the foundation |
| E = elastic modulus | k_r = rotational stiffness of the foundation |
| I = moment of inertia (= $bh^3/12$) | κ = shear deflection coefficient of the beam, $\kappa = E/3G$ |
| G = shear modulus | θ = crack extension parameter, $\theta = k_e w^2 + k_r \Psi^2$ |
| ρ = density | θ_c = critical value of the crack extension parameter, $\theta_c = bR$ |

[†] When the "uncracked length" of the beam is $> 2h$ and $\frac{h}{a} \lesssim 1$, the expression derived for K reduces to:

$$K = 2 \sqrt{3} \frac{Pa}{bh^{3/2}} \left[1 + \alpha \frac{h}{a} \right] \quad (1)$$

where K is the stress intensity factor, P is the load applied at the end of the specimen, a is the crack length, 2h is the height of the specimen, b is the thickness of the specimen, and $\alpha = (6)^{-1/4} = 0.64$.

and $H^*(x)$ is the ordinary Heaviside step function modified such that a spring once broken always remains broken. The crack extension parameter can be evaluated by considering the energy components of the system, as described below.

The boundary conditions to be imposed are those which correspond to a minimum displacement δ of the load pins with no applied torque at the cracked end of the specimen ($x = 0$) and stress-free conditions on the uncracked end ($x = L$). Using the equations derived in Section 3, these are

$$\begin{aligned} w(0,t) &\geq \delta, \quad \Psi'(0,t) = 0 \\ w'(L,t) - \Psi(L,t) &= 0 \\ \Psi'(L,t) &= 0 \end{aligned} \quad (3)$$

where the prime notation indicates differentiation with respect to x . The initial conditions are obtained by finding the static solution that satisfies the above boundary conditions and has, in addition, a force Q acting at $x = \alpha_0$ such that $\theta(\alpha_0, 0) = \theta_c$ (for duplex specimens, 2 θ_c -values are introduced: one for the starter section and one for the test section). This static solution has been obtained in closed form, while the dynamic equations (2a and 2b) are evaluated by finite difference techniques.

IV. RESULTS AND DISCUSSION

Theoretical Analysis

Calculations of the speed, extent and energetics of unstable fracture, employing the Timoshenko-beam-on-elastic-foundation model, were carried out for the DCB configuration employed in this study. The main features of the results are contained in Figure 3 and may be summarized as follows:

(1) Crack Velocity Characteristics. Crack propagation under wedge loading tends to proceed at constant velocity. Figure 3a illustrates that the crack assumes the steady-state velocity immediately, and maintains this velocity until shortly before arrest. The magnitude of this speed depends on several factors: (i) the specimen configuration, (ii) the elastic modulus and density (or equivalently, on C_0 , the bar wave speed), (iii) K_q , and, consequently, the bluntness of the starting notch, and (iv) the dynamic toughness R (or K_d), with (iii) and (iv) entering as the dimensionless ratio K_q/K_d (see Figure 3d). Figure 3a shows that a crack propagating in a duplex specimen begins by propagation at the speed consistent with the ratio K_q/K_d (starter section) and then assumes a second velocity characteristic of K_q/K_d (test section). Since the velocity in both the starter and the test section obey essentially the same K_q/K_d -dependence (see Figure 3d), it appears that the velocity in the test section is independent of the speed in the starter section. Finally, it should be noted that the crack length versus time curves in Figure 3a contain small sinusoidal fluctuations which are accompanied by 180° out-of-phase fluctuations in the strain energy and kinetic energy (see Figure 3b). These fluctuations, which appear to be connected with stress waves traveling in the arms of the beam, became more intense as the ratio K_q/K_d is increased, ultimately producing a discontinuous propagation when $\frac{K_q}{K_d} \gtrsim 2.5$. Additional information is reported in Section 3.

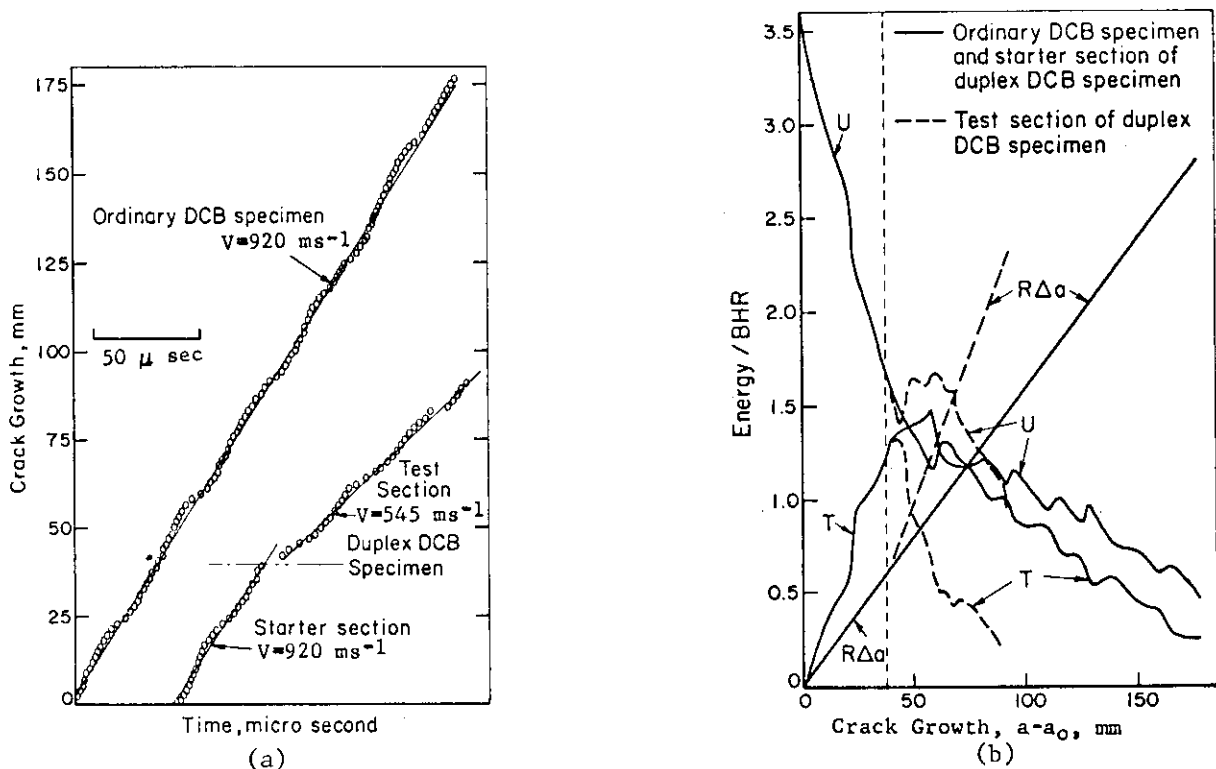
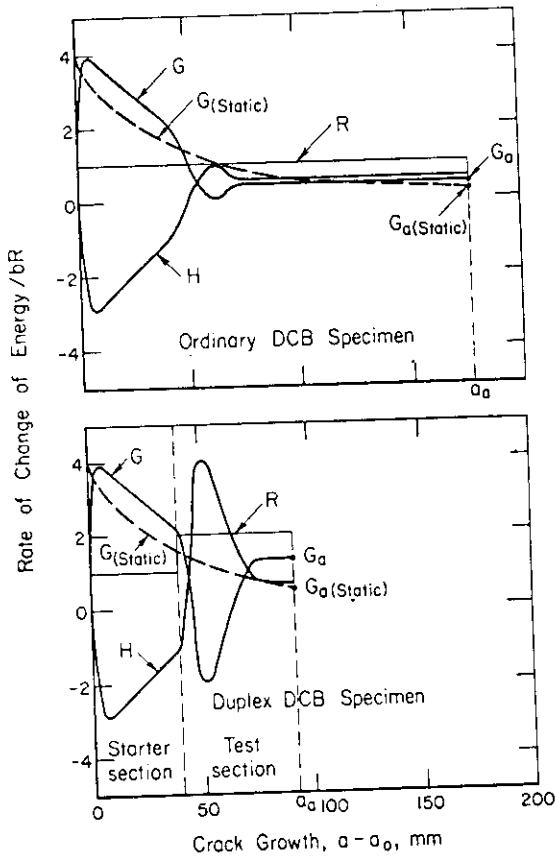


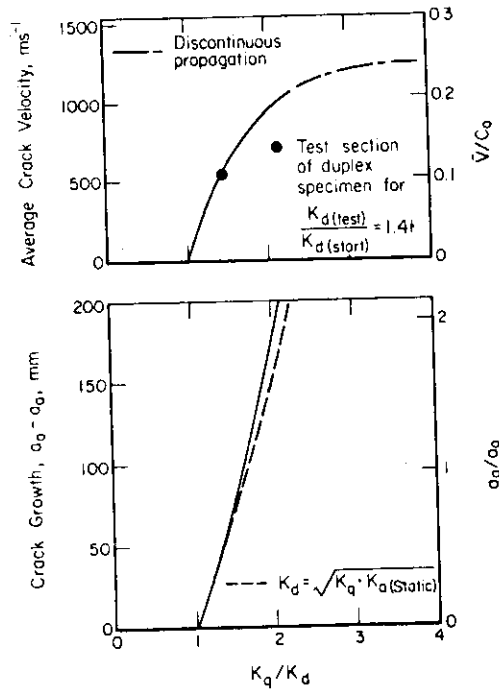
FIGURE 3. THEORETICAL CALCULATIONS OF CRACK PROPAGATION AND ARREST IN TIMOSHENKO BEAM-ON-ELASTIC-FOUNDATION MODELS OF AN ORDINARY AND A DUPLEX DCB-SPECIMEN ($K_q/K_d(\text{starter section})=2$, $K_d(\text{test section})/K_d(\text{starter section})=1.4$): (a) velocity profiles, (b) energy changes, (c) G , H , and R , and (d) the influence of K_q/K_d on velocity and arrest length. The quantities G and H in Figure 3(c) do not reflect the small fluctuations evident in the variation of U and T with crack length in Figure 3(b).

(2) Energetics. The energetics of crack propagation in the theoretical model are described in Figures 3b and 3c. Figure 3b illustrates that kinetic energy is first imparted to the beam and then recovered during the latter 2/3 of the growth increment; with about 85% of the kinetic energy recovered prior to arrest, and less than 10% of the total strain energy released remaining as unrecovered kinetic energy in these two cases. Figure 3c shows that H , the kinetic energy release rate, is comparable to and in some places an even larger part of the crack driving force than G , the strain energy release rate. The true, dynamic values of G depart substantially from the $G_{(\text{static})}$, the values derived from static consideration, except at the point of arrest. The relatively small discrepancy between the real G_a and $G_{a(\text{static})}$ arises because there is relatively little kinetic energy trapped in the specimen at arrest. However, this should not be interpreted as evidence that $G_{a(\text{static})}$ or $K_{a(\text{static})}$ are closely related to the fracture energy or toughness of the material at arrest. This is clearly revealed in Figure 3c which shows that neither G_a nor $G_{a(\text{static})}$ correspond with R .

(3) Evaluation of R (or K_d). Figure 3d illustrates that both the steady state velocity V and the arrest length a_a are single-valued functions of $\frac{K_q}{K_d}$ for a given material and specimen configuration. This means that K_d can be



(c)



(d)

FIGURE 3 (CONTINUED)

obtained independently from measurements of either: (i) K_q and a_a , or (ii) K_q and V , and the appropriate functional relations derived from the theoretical model. Alternatively, the arrest length can be interpreted without resorting to the detailed analysis by way of the relation⁽⁹⁾:

$$K_d = K_q \cdot K_{a(\text{static})}^{1/2} \quad (4)$$

Equation (4) is a close approximation when all of the kinetic energy is recovered at arrest, and is approximate when the unrecovered kinetic energy is a small fraction of the total strain energy released. For example, for the ordinary DCB-specimen and test conditions described in Figures 3a-3c, Equation (4) yields a value of K_d that is only 6% smaller than given by the detailed analysis (see Figure 3d). The K_d -value for the test section of a duplex specimen can be inferred from measurements of K_q , V (the crack velocity in the test section), and the functional relation in Figure 3d, independent of the value of K_d for the starter section. The analysis can also be used to derive the K_d -value for the test section from the arrest length, K_q , and $K_d(\text{starter section})$ by calculating a curve analogous to the one in Figure 3d. Similarly, Equation (4) can be

incorporated into an energy balance for duplex specimens after K_d for the material on the starter section has been derived from the test of an ordinary DCB-specimen. Since the energy consumed in the starter section is $R\Delta a = K_d^2 \Delta a/E$:

$$K_{d(\text{test section})} = \left[\frac{K_q K_a(\text{static}) (a_a - a_o) - K_{d(\text{starter section})}^2 (a_1 - a_o)}{(a_a - a_1)} \right]^{1/2} \quad (4a)$$

where a_a , a_o , and a_1 are the arrest length, initial length, and the length of the crack when it first enters the test section, all for the duplex test piece.

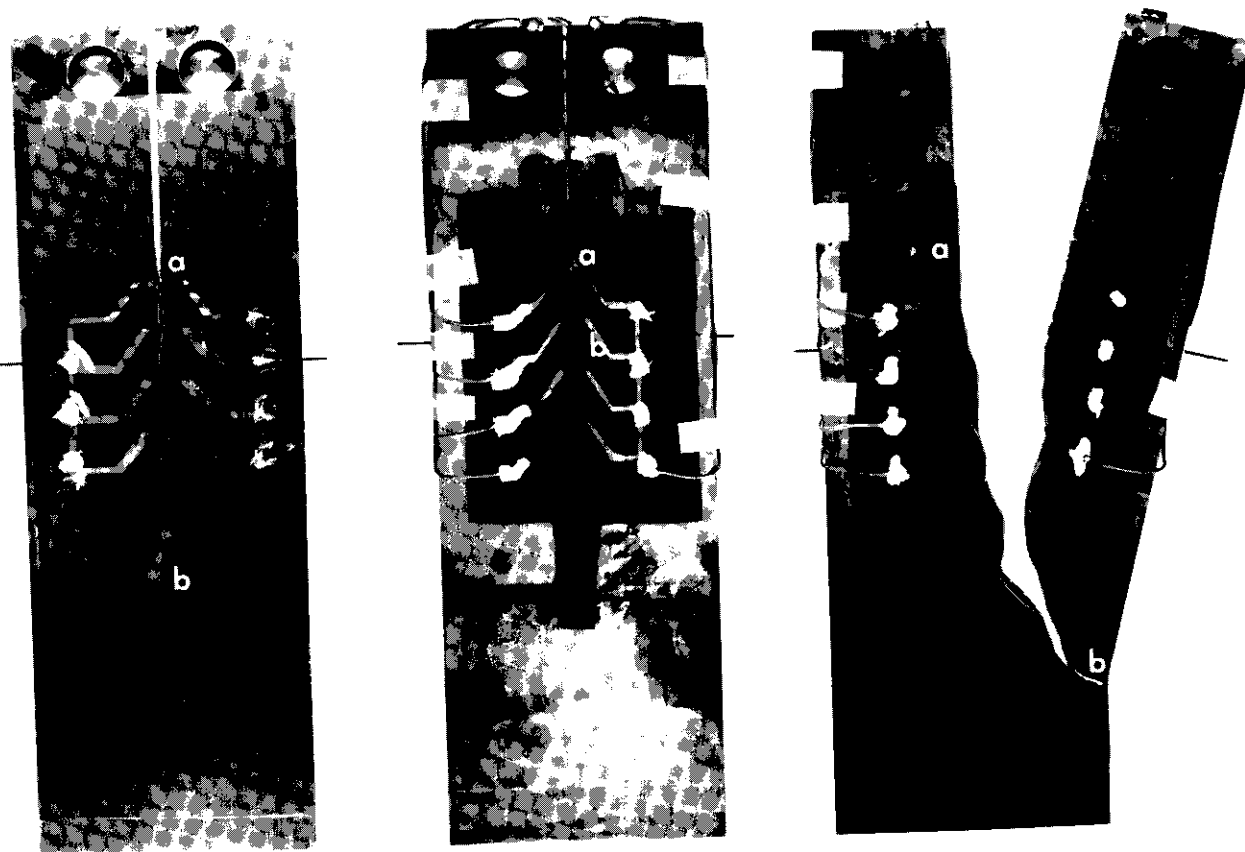
Experimental Results

Examples of the extent of propagation in duplex specimens and typical fracture velocity measurements are shown in Figures 4 and 5 and the test results are presented in Table 1. Additional illustrations and velocity records are given in the Appendix to this section, Figures A-4 - A-18. Figures A-14 and A-15 show that the behavior of the DCB-test pieces is quite reproducible. The fractures propagate at 800 to 1100 ms^{-1} in the 4340 starter section and penetrate the test section at this speed. At -78°C the fractures continue to propagate in the A517F for some distance (Figures 4b and 4c), while at 0°C , the fractures were stopped by the A517F steel close to the weld line (Figure 4a).

The fractures propagated further in the center of the plate than on the surface, and this is illustrated in the Appendix to this section by Figures A-18 and A-19. These figures show the morphology of the fracture after arrest and it is not clear to what extent the crack was tunneling during rapid propagation. The crack length at arrest was identified with the distance propagated in the center of the plate, i.e., the point of furthest propagation. At 0°C where the extent of the unbroken shear lips represent a large fraction of the arrest length, the calculated K_d -values underestimate the real values and are regarded as lower limits.

Figure 6 compares the K_d -values for the A517F steel with existing measurements for other steels. With two exceptions, the results of Fitzpatrick, et al⁽²⁷⁾ and Bilek and Burns⁽¹⁵⁾, a trend toward higher K_d -values with increasing fracture velocity is apparent. However, the exact form of the dependence is not well defined for any of the steels that have been studied. The K_d -values for the A517F do not display a clear-cut velocity dependence in the 475 ms^{-1} to 780 ms^{-1} range examined here, but the existence of one should not be ruled out.

Perhaps the most striking feature of the results is the large difference at -78°C between the K_d -values measured for a propagating crack, and the dynamic initiation K_{Id} -values reported by Barsom and Rolfe⁽³⁰⁾ for a rapidly loaded, but stationary crack. It has generally been thought that K_{Id} -values approximate the toughness of propagating cracks. Figure 7 shows that this could be true at -196°C . However at -78°C the K_{Id} -values fall below the K_{Ic} -curve, while the K_d -values obtained here are 4 times larger than K_{Id} and fall well above the K_{Ic} -curve. These differences cannot be attributed to differences in chemistry or to a heat-to-heat variation in the transition temperature. The present material has virtually the same composition and tensile properties as the heat studied by Barsom and Rolfe⁽³⁰⁾. Furthermore, the Charpy transition of the present heat was about 25°C higher than the one tested



(a) 12.7 mm, 0°C

(b) 12.7 mm, -78°C

(c) 25.4 mm, -78°C

FIGURE 4. DUPLEX DCB SPECIMENS TESTED AT DIFFERENT TEMPERATURES: (a) 3VY11, (b) 3VY13, and (c) 3VY23. The letters a and b identify the points of initiation and arrest; the horizontal line marks the weld line.

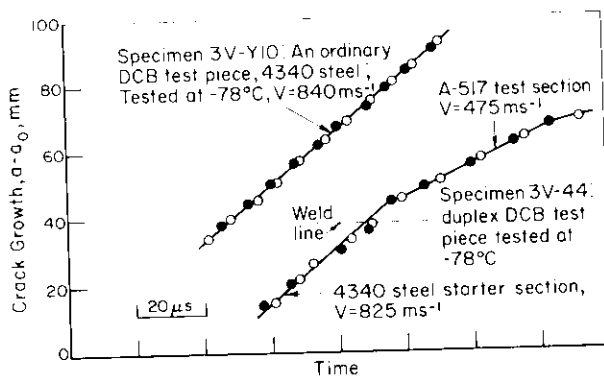


FIGURE 5. EXAMPLES OF VELOCITY (CRACK LENGTH VS. TIME) MEASUREMENTS DERIVED FROM THE CONDUCTING STRIPS.

TABLE 1 - DUPLEX SPECIMEN TEST RESULTS

| Specimen No. (a) | Critical Displacement (d) (mm) | K_q (MNm ^{-3/2}) | K_a (Static) (MNm ^{-3/2}) | \bar{K}_d (e) (MNm ^{-3/2}) | 4340 STEEL STARTER SECTION | | | A517 STEEL TEST SECTION | | | |
|---|--------------------------------|------------------------------|---------------------------------------|--|----------------------------|--------------------|----------------------------------|-------------------------|------------------------|----------------------------------|----------------------------------|
| | | | | | V (m/s) | $(a_1 - a_0)$ (mm) | K_d (f) (MNm ^{-3/2}) | V (m/s) | $(a_a - a_1)$ (mm) | K_d (g) (MNm ^{-3/2}) | K_d (h) (MNm ^{-3/2}) |
| <u>Plate Thickness = 12.7 mm, T = 0°C</u> | | | | | | | | | | | |
| 3V40(b) | 2.02 | 178 | - | 113 | - | 84.1 | 113 ^(e) | - | - | - | - |
| 3VY1 | 2.45 | 229 | 119 | 165 | - | 40 | - | - | ~ 7.6 | > 360 ^(k) | - |
| 3VY11(b) | 3.25 | 210 | 114 | 166 | 645 | 40 | 133 | - | 6 | > 305 | - |
| <u>Plate Thickness = 12.7 mm, T = -78°C</u> | | | | | | | | | | | |
| 3V44(b) | 2.20 | 314 | (i) | - | 840 | (i) | 167 | - | - | - | - |
| 3VY2 | 2.64 | 229 | 60.5 | 118 | - | 40 | - | - | 86.4 | 109 ^(k) | - |
| 3VY10(b) | 3.87 | 250 | 114 | 169 | 825 | 38.8 | 135 | 475 | 32.9 | 202 | 180 |
| 3VY12 | 3.66 | 234 | 102 | 155 | 940 | 39.8 | 111 | 560 | 42.9 | 184 | 159 |
| 3VY13(c) | 4.16 | 266 | 68 | 134 | 1080 | 39.9 | 106 | 625 | 106.0 | 143 | 170 |
| <u>Plate Thickness = 25.4 mm, T = 0°C</u> | | | | | | | | | | | |
| 3VY24(c) | 4.80 | 308 | 198 | 247 | 910 | 38.7 | 154 | ~ 240 | 23.6 | > 380 ^(k) | ~ 270 |
| <u>Plate Thickness = 25.4 mm, T = -78°C</u> | | | | | | | | | | | |
| 3VY3 | 1.63 | 154 | 77 | 109 | - | 40 | - | - | 20.3 | > 115 ^(k) | - |
| 3VY4 | 2.20 | 198 | (j) | - | - | (i) | - | - | - | - | - |
| 3VY22(b) | 4.01 | 243 | (j) | - | 860 | (i) | 127 | - | - | - | - |
| 3VY23 | 4.19 | 272 | ~ 73 ⁽¹⁾ | ~ 141 | 1125 | 40 | 101 | 740 | > 112 ⁽¹⁾ | ~ 152 | 159 |
| 3VY28(c) | 4.60 | 291 | ~ 78 ⁽¹⁾ | ~ 151 | 1180 | 38.6 | ~ 106 | 780 | > 101.4 ⁽¹⁾ | ~ 165 | 164 |

(a) Series 3V-specimens are ordinary 4340 steel DCB-test pieces; series 3VY are 4340/A517 duplex DCB specimens. Except where noted, the 4340 steel was in the quenched and tempered 1 hr. at 200°C, and the wedge angle was 11°.

(b) 4340 steel tested in the as-quenched condition.

(c) 30° wedge angle employed.

(d) Displacement measurement at the onset of fast fracture by the displacement gage mounted 1.65 mm from the end of the specimen, i.e., 21.97 mm from the point of load application.

(e) \bar{K}_d is the average value of K_d for the crack path (starter- and test-section) calculated from the critical displacement and the arrest length by way of Equation (3).

(f) This is the K_q -value for the 4340 steel that is obtained from K_q and the fracture velocity in the starter section using the relation between these quantities derived from the Timoshenko analysis as shown in Figure 8a unless otherwise noted.

(g) \bar{K}_d is the average value of K_d for the A517 steel calculated from the arrest length by way of Equation (4a).

(h) This is the K_d -value for the A517 test section obtained from K_q and the fracture velocity in the test section as described in (f).

(i) Fracture did not arrest.

(j) Fracture did not penetrate weld but propagated along weld line.

(k) Calculated assuming $K_d(4340) = 106 \text{ MNm}^{-3/2}$.

(1) In these cases, where the crack path veered from the specimen center line during the latter stages of propagation, the arrest length is defined as the length corresponding to the point where the path deviates 20% from the plate center line.

a_0 - Initial slot length.

a_1 - The length of the crack when it enters the A517 steel test section.

a_a - Crack length at arrest.

V - Measured fracture velocity.

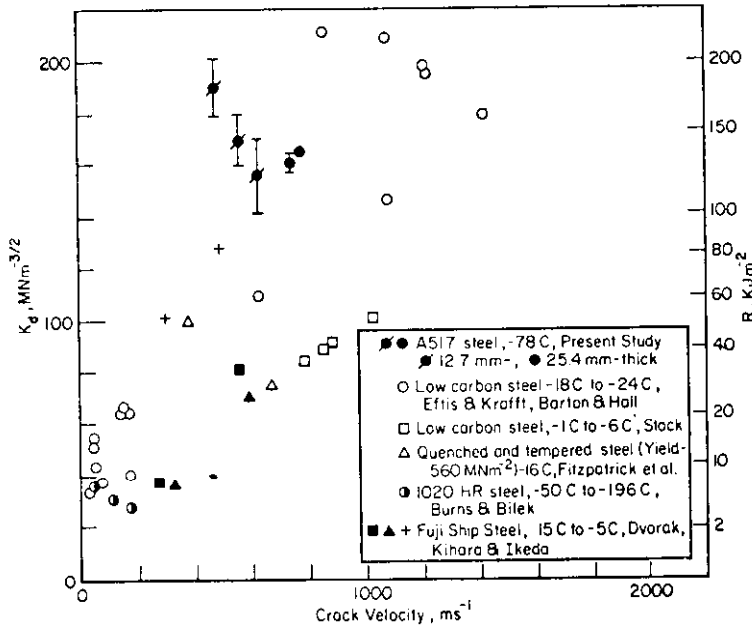


FIGURE 6. COMPARISON OF THE VELOCITY DEPENDENCE OF K_d -VALUES FROM DIFFERENT INVESTIGATIONS (14,15,25-29)

by Barsom and Rolfe (see Figure 7), and in the wrong direction to explain the higher K_d -values at -78°C . The discrepancy between K_d and K_{Ic} and K_{Id} could be connected with the relaxation of constraint (the ASTM E 399-72 thickness requirement for plane strain is not satisfied for the static yield and K_d -values measured at -78°C), but this is unlikely for several reasons. For one thing, the dynamic yield strength appropriate to the extremely high-strain rates produced in the crack tip plastic zone, could be large enough to provide for plane strain in a 25.4 mm-thick section. In line with this, the 25.4 mm

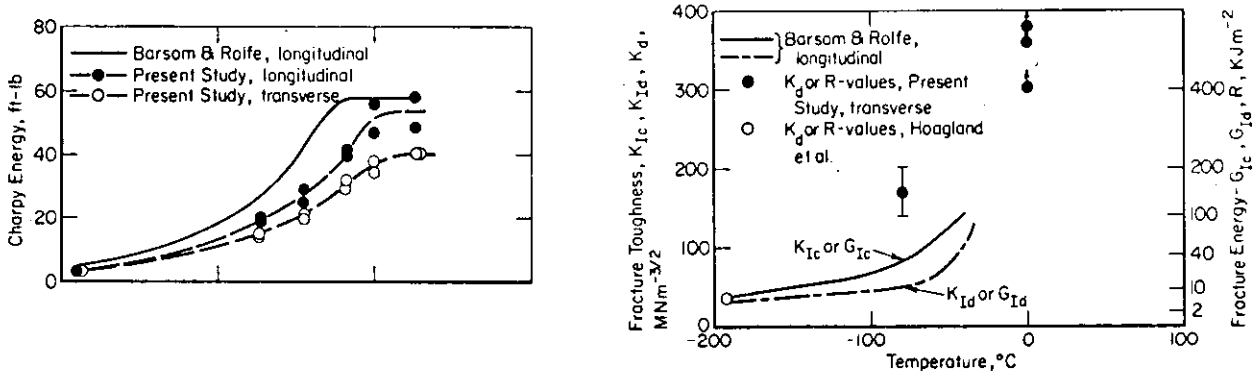


FIGURE 7. COMPARISON OF THE CHARPY AND FRACTURE TOUGHNESS VALUES FOR A517F OBTAINED IN THIS INVESTIGATION, AND THOSE REPORTED BY BARSOM AND ROLFE (30) AND HOAGLAND, ET AL (9)

A517F test pieces displayed flat fractures with virtually no shear lip and no measurable reduction in thickness. In addition, the K_d -values for the 25.4 mm 4340 steel starter sections which do satisfy plane-strain requirements also appear to be much greater than K_{Ic} at -78°C .^{(31)†}

Perhaps the main findings of this study relate to the agreements between theory and experiment. The theoretical velocity profiles are surprisingly close representations of the measurements (compare Figures 3a and 5). Values of K_d deduced from the fracture velocity measurements (Figure 3a) and those derived independently from the measured arrest lengths (Figure 3b), are in close agreement (see last two columns of Table 1). This type of agreement is also demonstrated in Section I for fracture arrest in 4340 steel at room temperature where the theoretical crack velocity-arrest length relation is closely obeyed.

These agreements represent a critical test of the theory that the kinetic energy imparted to the wedge-loaded DCB test piece is substantially conserved and converted into fracture energy during the latter stages of the propagation event. It follows that arrest is controlled by the history of energy dissipation throughout the entire propagation event (the R-curve) rather than by K_a . The results also demonstrate the power of the beam-on-elastic-foundation model to provide a realistic description of crack propagation and arrest. In view of the agreements between theory and experiment, and the evidence that plane strain conditions were maintained ahead of the propagating cracks, it seems likely that K_d (or R) is a unique property which cannot always be inferred from measurement on stationary cracks. The difference between K_d and the dynamic initiation K_{Id} -results may be connected with the contribution of ductile ligaments which has been discussed in Reference 9. Examples of the ligaments observed in the A517F sheet at -78°C are shown in the Appendix to this section, Figure A-20. It was shown that the deformation and rupture of these ligaments during rapid propagation can account for a large fraction of the energy dissipated by a cleavage fracture. The flat fracture energy of 4340 steel, which consists of nothing but ligaments, doubles in the range $0 - 860 \text{ ms}^{-1}$, showing that ligament formation can be sensitive to the crack velocity. Finally, such ligaments would be expected to be less prevalent at -196°C , and initially absent at the onset of fracture in specimens containing a starter crack prepared by fatiguing.

Finally, some comments about the significance of the wedge-loaded duplex DCB-test are in order. The test is comparable to a fracture-toughness evaluation, in that it provides an absolute value of the dynamic fracture energy or toughness for full-thickness plates, which can be used to predict the likelihood of crack arrest and to design crack arrestors. Unlike the Charpy, the drop weight or explosive-bulge tests, the R or K_d -values derived from the duplex test do not require full-scale service experience to make them useful. As with other fracture-mechanics tests, the magnitude of the toughness that can be measured is limited by the test-piece dimensions, but not as severely,

† It should be noted that the existence or nonexistence of plane-strain conditions is not a main issue here since the objective of the present study is to characterize the fracture of 12.7 mm- and 25.4 mm-thick plates, rather than the behavior of cracks under plane-strain conditions. However, it does have a bearing on the applicability of the results to even heavier sections.

because extremely high-strain rates and high dynamic yield stress values are involved. The present configuration, with overall dimensions of 127 mm by 381 mm is capable of measuring dynamic-toughness values up to $\sim 200 \text{ MNm}^{-3/2}$. More energy can be stored in the test piece relative to the fracture energy by doubling the height dimension, increasing the strength of the starter section or undercutting along the crack line. Such changes might make it possible to measure toughness values in the range 300 to 400 $\text{MNm}^{-3/2}$ or even higher. The requirements for an electron-beam weld and spark machining and grinding to size the hardened 4340 starter section add to the cost and detract from the convenience of the test. These are partly compensated by the fact that fatigue precracking is not required, and that the test can be performed on an ordinary tensile testing machine. Crack-velocity measurements are also not required. The test results quoted here and in Section I show that K_{Id} (or R) and the velocity can be inferred simply from the displacement-gage readings at the onset of fast fracture and a measurement of the length of the crack at arrest.

V. CONCLUSIONS

1. The concept of a "duplex" DCB-test piece in which an unstable crack is initiated in a high-strength/low-toughness "starter section" which is electron-beam welded to the "test section" has been successfully demonstrated. In this way, the response of A517F steel test sections to 1000 ms^{-1} fractures has been studied at -78°C , and also at 0°C which is close to the full-shear end of the ductile-to-brittle transition.
2. The Timoshenko beam theory/beam-on-elastic-foundation analysis has been extended to duplex test pieces. The theoretically derived velocity profiles are in excellent agreement with the actual velocity measurements. The analysis makes it possible to derive dynamic fracture energy or fracture-toughness values either from the velocity of the crack in the test section or the length of the crack at arrest. Values obtained independently from these two measurements are in close agreement, and this represents a critical test of the theory.
3. The analysis and the agreements with experiment show that the kinetic energy imparted to the wedge-loaded DCB-test piece is substantially converted into fracture energy during the latter stages of a propagation event. It follows that fracture arrest is controlled by the history of energy dissipation throughout the entire propagation event (the R-curve) rather than by K_a , a critical toughness at the point of arrest.
4. The dynamic fracture toughness values measured at -78°C for 12.7 mm- and 25.4 mm-thick plates of A517F steel, $K_{Id} = 143 \text{ MNm}^{-3/2} - 202 \text{ MNm}^{-3/2}$ are 2-times and 3-times K_{Ic} , and K_{Id} , the values for static and dynamic initiation from stationary cracks. It appears that K_{Id} does not always reflect the behavior of fast propagating cracks. At 0°C , $K_d > 300 \text{ MNm}^{-3/2}$ for this steel.

VI. REFERENCES

1. T. S. Robertson, "Propagation of Brittle Fracture in Steel", J. Iron and Steel Inst., Vol. 175, p. 361, 1953.
2. W. S. Pellini and P. P. Puzak, "Fracture Analysis Diagram Procedures for the Fracture-Safe Engineering Design of Steel Structures", NRL Report 5920, U. S. Naval Research Laboratory, March 15, 1963.
3. G. R. Irwin and A. A. Wells, "A Continuum Mechanics View of Crack Propagation", Met. Reviews, Vol. 10, p. 223, 1965.
4. T. Kanazawa, "Recent Studies of Brittle Crack Propagation in Japan", International Conference on Dynamic Crack Propagation, Lehigh University, 1972.
5. P. B. Crosley and E. J. Ripling, "Dynamic Fracture Toughness of A533 Steel", Trans. ASME, Vol. 91, Series D, p. 525, 1969.
6. P. B. Crosley and E. J. Ripling, "Crack Arrest Fracture Toughness of A533 Grade B Class 1 Pressure Vessel Steel", Materials Research Laboratory Report, Glenwood, Illinois, 1970.
7. J. P. Berry, "Some Kinetic Considerations of the Griffith Criterion for Fracture": Part I - Equations of Motion at Constant Force, Vol. 8, p. 194, 1960; Part II - Equations of Motion at Constant Displacement", Vol. 8, p. 207, 1960, J. Mech. Phys., Solids.
8. J. P. Romualdi and P. H. Sanders, "Fracture Arrest by Riveted Stiffeners", Carnegie Institute of Technology Report, Pittsburgh, Pennsylvania, 1960.
9. R. G. Hoagland, A. R. Rosenfield, and G. T. Hahn, "Mechanisms of Fast Fracture and Arrest in Steels", Vol. 3, p. 123, 1972.
10. G. T. Hahn, R. G. Hoagland, M. F. Kanninen, and A. R. Rosenfield, "A Preliminary Study of Fast Fracture and Arrest in the DCB-Test Specimen", Dynamic Crack Propagation Conference, Lehigh University, 1972.
11. K. B. Broberg, "The Propagation of a Brittle Crack", Arkiv Fys., Vol. 18, p. 159, 1960.
12. J. D. Eshelby, "Energy Relations and The Energy-Momentum Tensor in Continuum Mechanics", Inelastic Behavior of Solids, Kanninen, et al., eds., McGraw-Hill, New York, p. 77, 1970.
13. R. G. Hoagland, "On the Use of the Double-Cantilever Beam Specimen for Determining the Plane Strain Fracture Toughness of Metals", Trans ASME, Vol. 89, Series D, p. 525, 1967.
14. J. Eftis and J. M. Krafft, "A Comparison of the Initiation with the Rapid Propagation of a Crack in a Mild Steel Plate", Trans ASME, Vol. 87, Series D, p. 257, 1965.
15. S. J. Burns and Z. J. Bilek, "The Dependence of the Fracture Toughness of Mild Steel on Temperature and Crack Velocity", Report NYO-2394-42, Div. of Engg., Brown U., 1971.
16. M. F. Kanninen, A. R. Rosenfield, and R. G. Hoagland, "Fast Fracture in PMMA", Deformation and Fracture of High Polymers, H. Kausch, et al., eds. (in press).

17. J. J. Benbow and F. C. Roesler, "Experiments on Controlled Fractures", Proc. Phys. Soc. (London), Vol. B70, p. 201, 1957.
18. J. Harding, "Effect of High Strain Rate on the Room-Temperature Strength and Ductility of Fine Alloy Sheets", J. Iron and Steel Inst., Vol. 210, p. 425, 1972.
19. G. T. Hahn, M. Sarrate, and A. R. Rosenfield, "Plastic Zones in Fe-3Si Steel Double-Cantilever-Beam Specimens", Vol. 7, p. 435, 1971.
20. M. F. Kanninen, "An Augmented Double Cantilever Beam Model for Studying Crack Propagation and Arrest", Int. J. Fract. Mech., Vol. 9, p. 83, 1973.
21. S. P. Timoshenko, "On the Correction for Shear of the Differential Equation for Transverse Vibrations of Prismatic Bars", Phil. Mag., Vol. 41, p. 744, 1921.
22. S. P. Timoshenko, "On the Transverse Vibrations of Bars of Uniform Cross-Section", Phil. Mag., Vol. 43, p. 125, 1922.
23. A. D. Kerr, "Elastic and Viscoelastic Foundation Models", J. Appl. Mech., Vol. 31, p. 491, 1964.
24. G. R. Cowper, "The Shear Coefficient in Timoshenko's Beam Theory", J. Appl. Mech., Vol. 33, p. 335, 1966.
25. F. W. Barton and W. J. Hall, "Brittle-Fracture Tests of Six-Foot Wide Pre-stressed Steel Plates", Weld. J. Res. Supp., Vol. 39, p. 379s, 1960.
26. T.A.C. Stock, "Stress Field Intensity Factors for Propagating Brittle Cracks", Int. J. Fract. Mech., Vol. 3, p. 121, 1967.
27. N. P. Fitzpatrick, P. L. Pratt, and T.A.C. Stock, "Fracture in Structural Alloys", J. Austr. Inst. Met., Vol. 13, p. 243, 1968.
28. G. J. Dvorak, "A Model of Brittle Fracture Propagation - Part I: Continuum Aspects", Engg. Fract. Mech., Vol. 3, p. 351, 1971.
29. H. Kihara and K. Ikeda, "A Proposal on Evaluation of Brittle Crack Initiation and Arresting Temperatures and Their Application to Design of Welded Structures", Papers of the Ship Ship Research Institute, No. 14, Tokyo, April, 1966.
30. J. M. Barsom and S. T. Rolfe, " K_{Ic} Transition-Temperature Behavior of A517-F Steel", Engg. Fract. Mech., Vol. 2, p. 341, 1971.
31. E. A. Steigerwald, "Crack Toughness Measurements of High-Strength Steels", ASTM STP 463, p. 102, 1970.

APPENDIX 2-A

SUPPLEMENTARY ILLUSTRATIONS

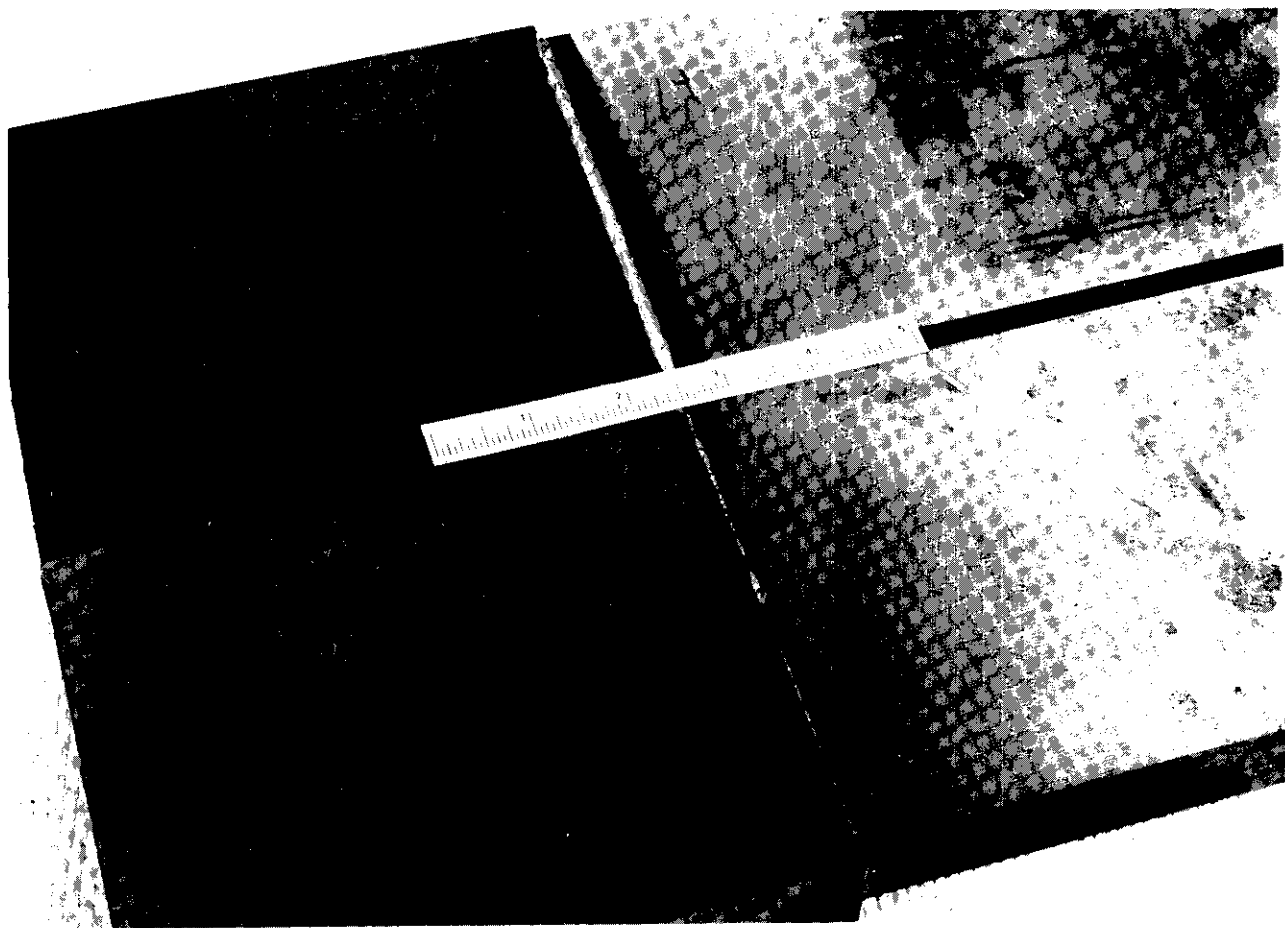


FIGURE A-1. DUPLEX DCB SPECIMEN BLANKS. The photograph shows the single pass electron beam weld which joins the 25.4 mm-thick 4340 steel starter and A517F test section; top: near side relative to beam; bottom: far side

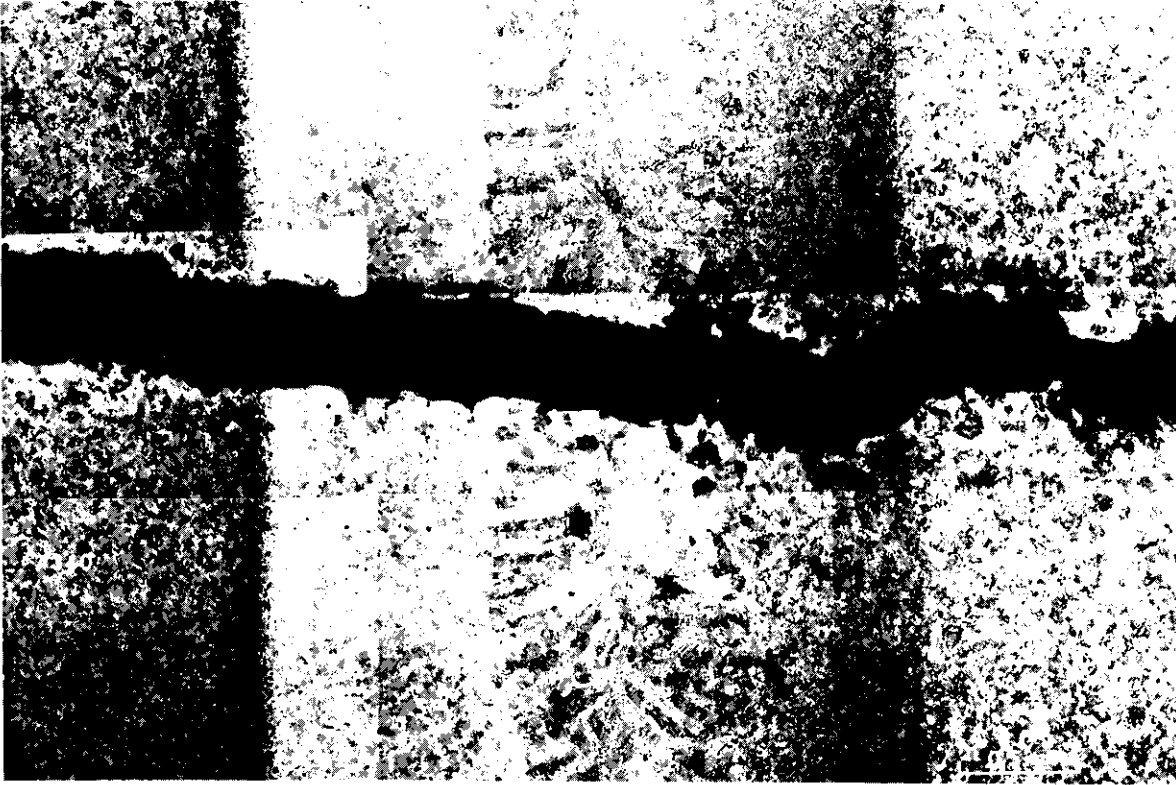


FIGURE A-2. MICROGRAPH OF ELECTRON BEAM WELD AND HEAT AFFECTED ZONE OF SPECIMEN 3VY-10 TAKEN ON PLATE MIDPLANE. The fracture propagated from left to right

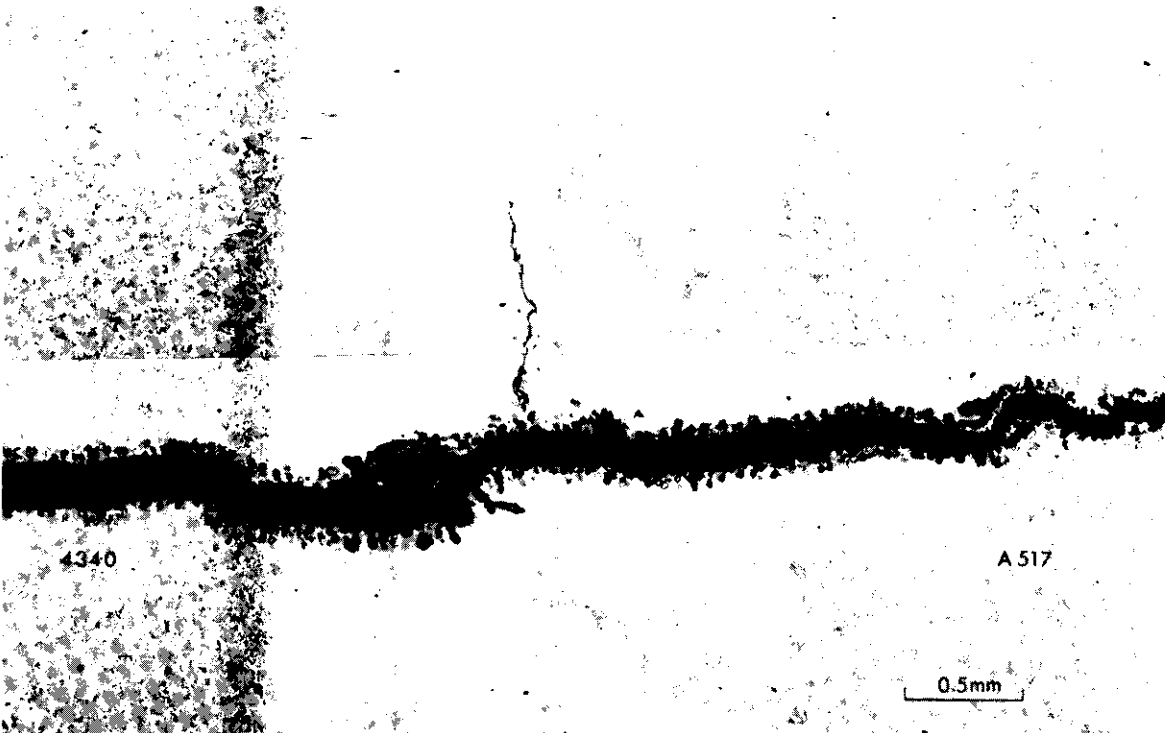


FIGURE A-3. MICROGRAPH OF ELECTRON BEAM WELD AND HEAT AFFECTED ZONE OF SPECIMEN 3VY-11 TAKEN ON PLATE MIDPLANE. The fracture propagated from left to right. A small transverse crack was observed close to the fusion zone at (a)

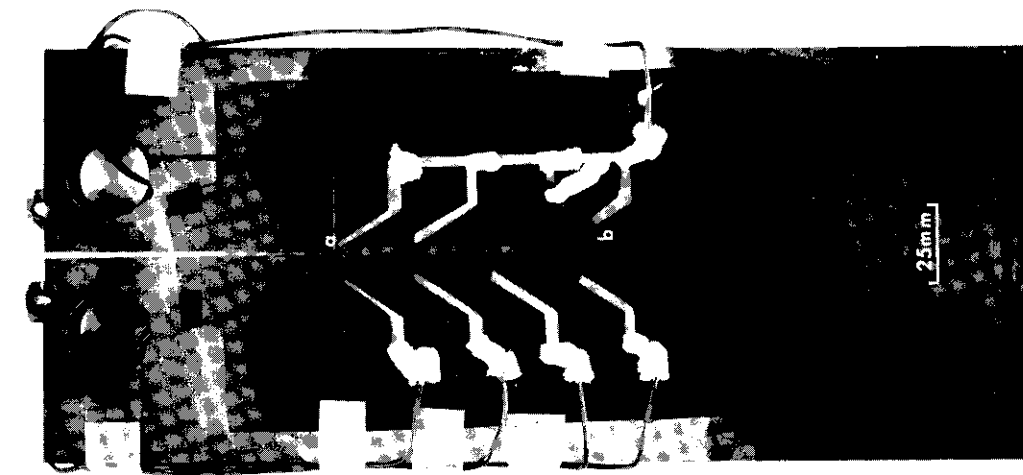


FIG. A-4. ORDINARY 4340 STEEL DCB SPECIMEN 3V40 (12.7 mm-THICK, TESTED AT 0°C, $K/K_d = 1.57$). Fracture initiated at a and arrested at b

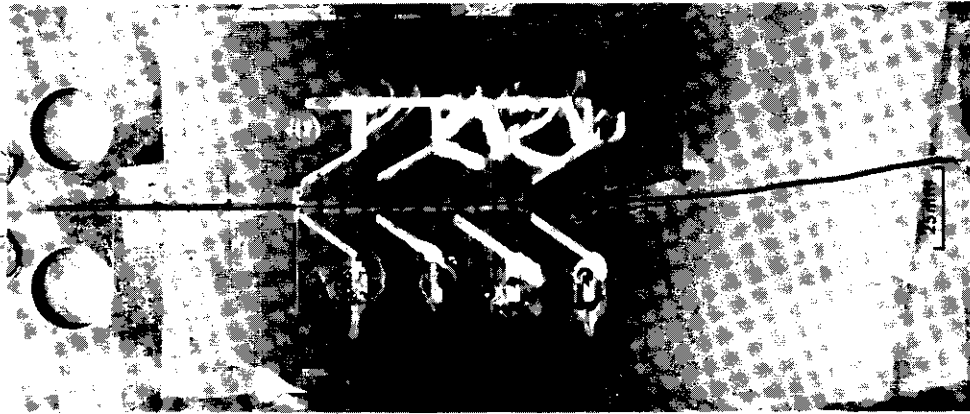


FIG. A-5. ORDINARY 4340 STEEL DCB SPECIMEN 3V44 (12.7 mm-THICK, TESTED AT -78°C, $K/K_d = 1.88$). Fracture initiated at a and failed to arrest

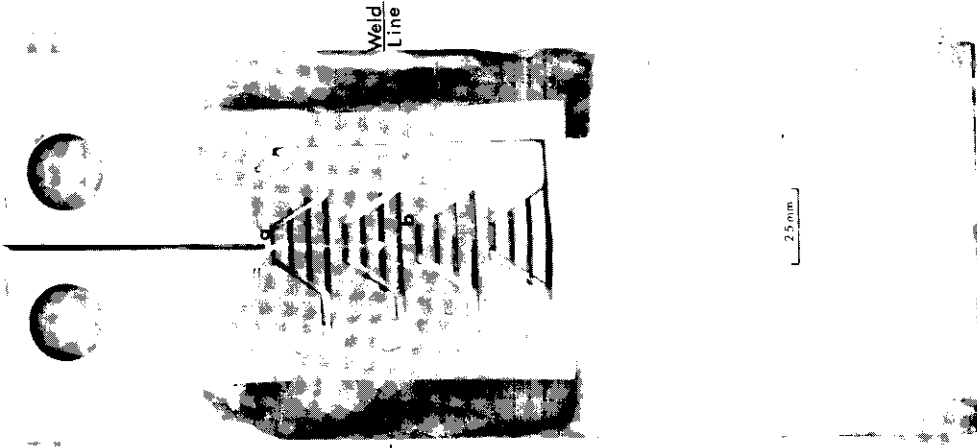


FIG. A-6. DUPLEX 4340/A517F DCB TEST PIECE 3VY1 (12.7 mm-THICK, TESTED AT 0°C). Fracture initiated at a and arrested in the A517F steel at b, shortly after penetrating the weld line

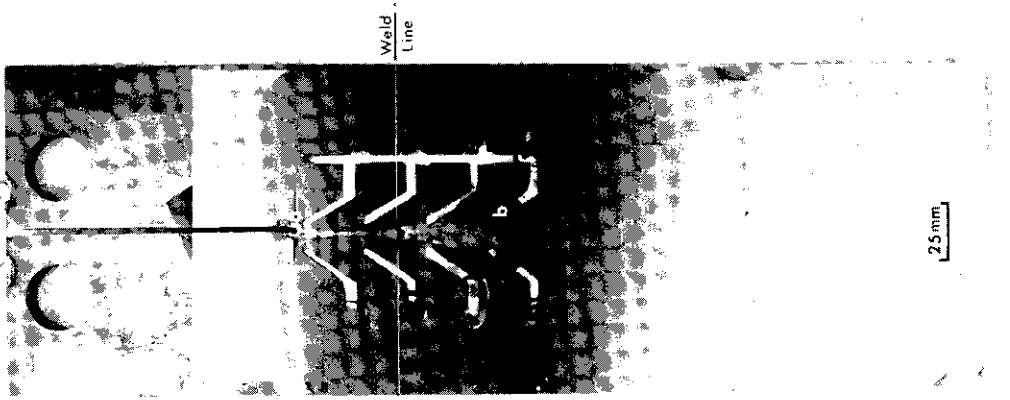


FIG. A-9. DUPLEX 4340/A517F DCB TEST PIECE 3VY10 (12.7 mm-THICK, TESTED AT -78°C). Fracture initiated at a and arrested at b.

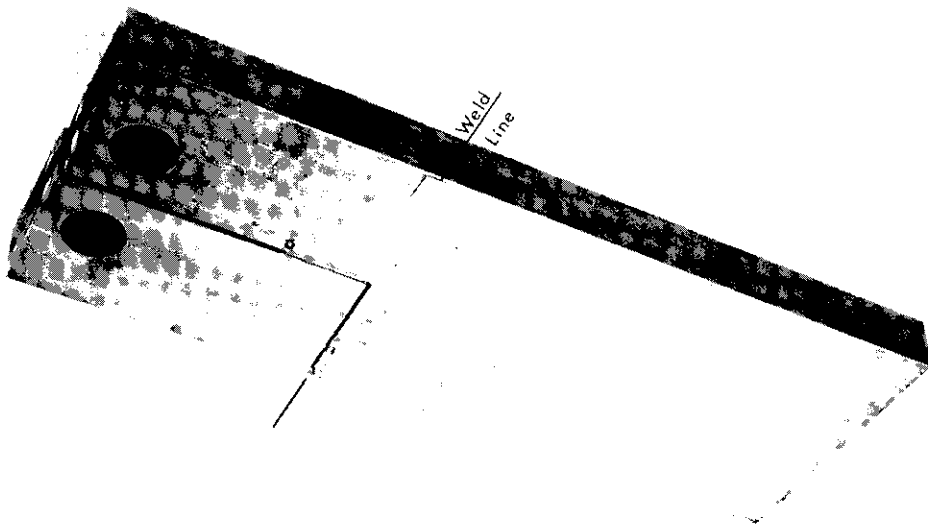


FIG. A-8. DUPLEX 4340/A517F DCB TEST PIECE 3VY-4 (25.4 mm-THICK, TESTED AT -78°C). Fracture initiated at a; propagated to the weld line, and then along the weld line because of incomplete penetration of the

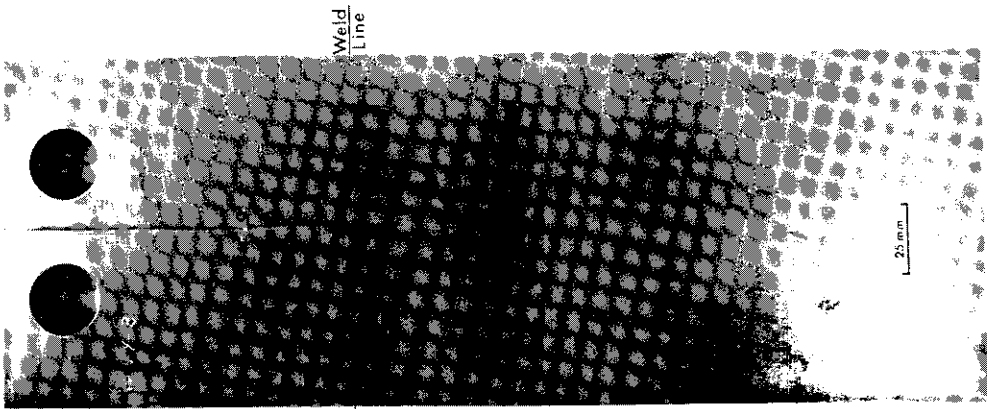


FIG. A-7. DUPLEX 4340/A517F DCB TEST PIECE 3VY3 (25.4 mm-THICK, TESTED AT -78°C). Fracture initiated at a and arrested at b. Subsequent studies indicated that weld penetration was probably incomplete in this specimen.

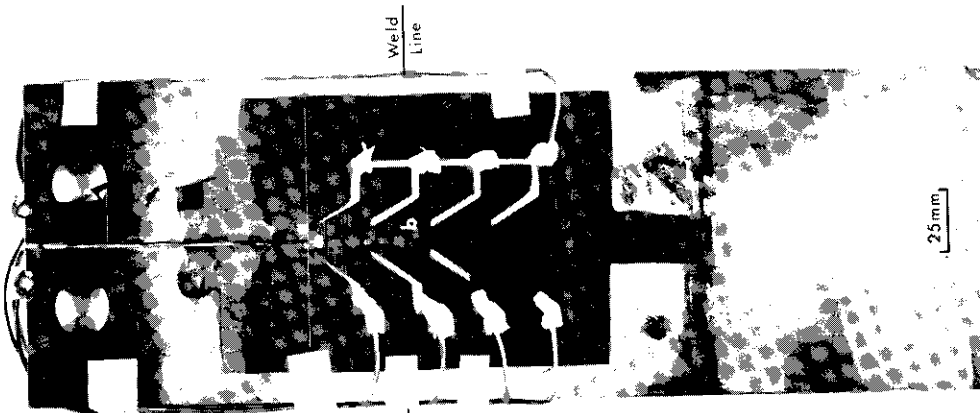


FIG. A-10. DUPLEX 4340/A517F
DCB TEST PIECE 3VY11
(12.7 mm-THICK, TESTED AT
0°C). Fracture initiated
at a and arrested in the
A517F steel at b, shortly
after penetrating the
weld line.

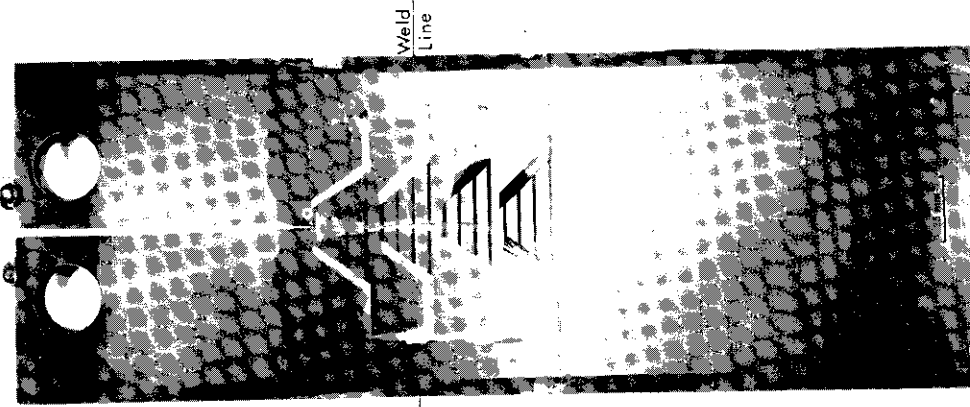


FIG. A-11. DUPLEX 4340/A517F
DCB TEST PIECE 3VY12
(12.7 mm-THICK, TESTED AT
-78°C). Fracture
initiated at a and
arrested at b.

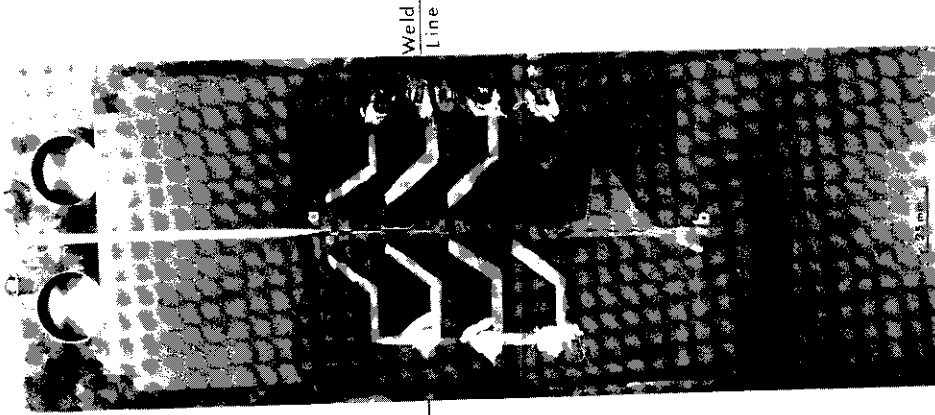


FIG. A-12. DUPLEX 4340/A517F
DCB TEST PIECE 3VY13 (12.7
mm-THICK, TESTED AT -78°C).
Fracture initiated at a
and arrested at b.

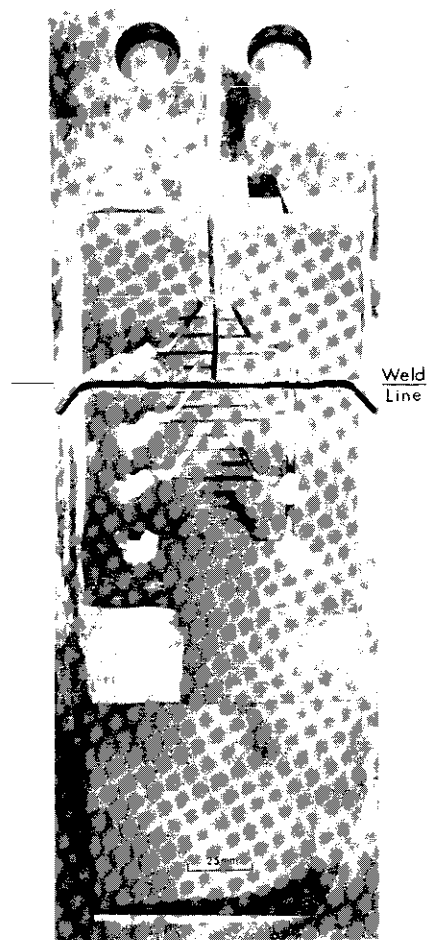


FIG. A-13. DUPLEX 4340/A517F DCB TEST PIECE 3VY22 (25.4 mm-THICK, TESTED AT -78°C). Fracture initiated at a and propagated close to the weld line. At this point, a second fracture, normal to the first was initiated from a long shallow surface crack in the weld near the center of the test piece and propagated through the weld before the main fracture could penetrate the test section. Note that the second fracture departed from the weld line at b, evidence that the weld was reasonably tough.

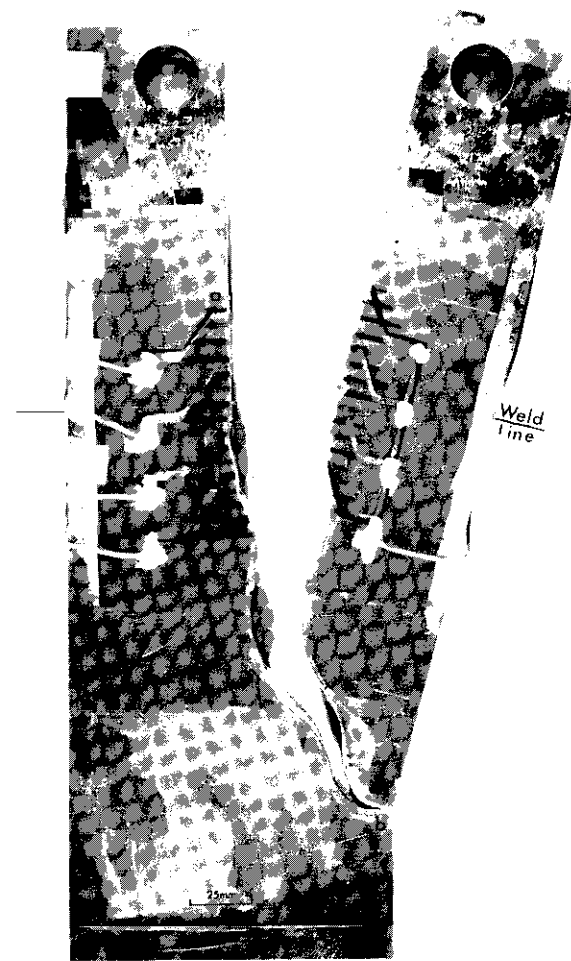


FIG. A-14. DUPLEX 4340/A517F DCB TEST PIECE 3VY23 (25.4 mm-THICK, TESTED AT -78°C). The fracture initiated at a and arrested at b.

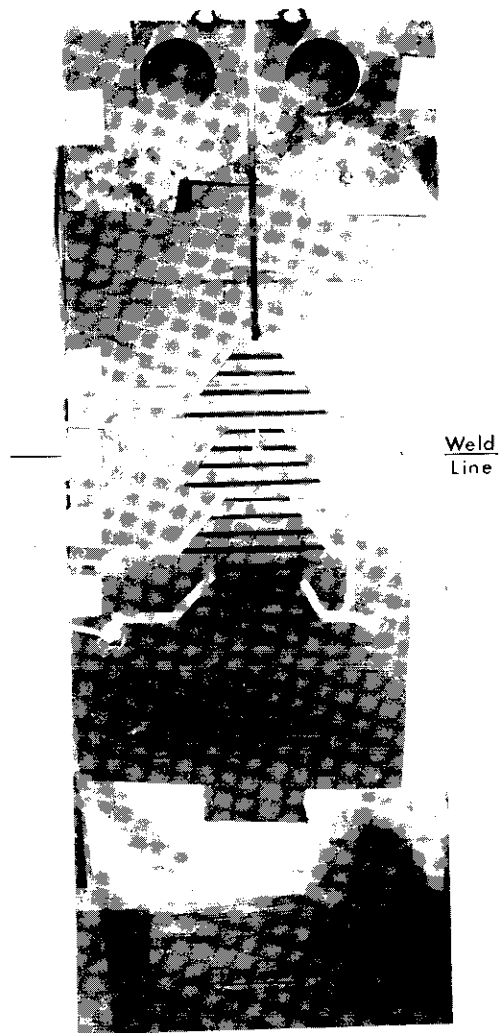
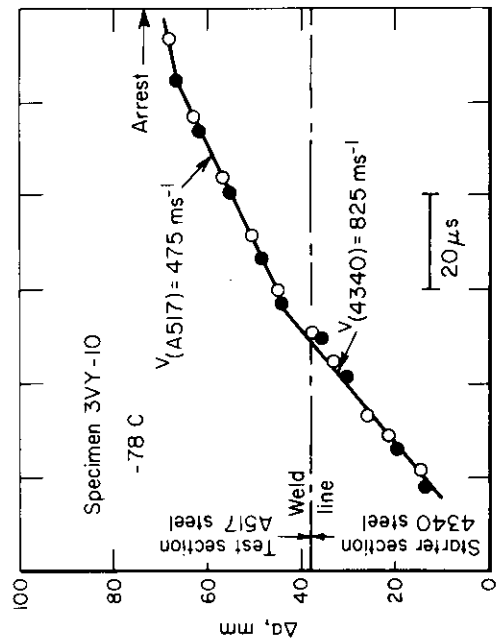


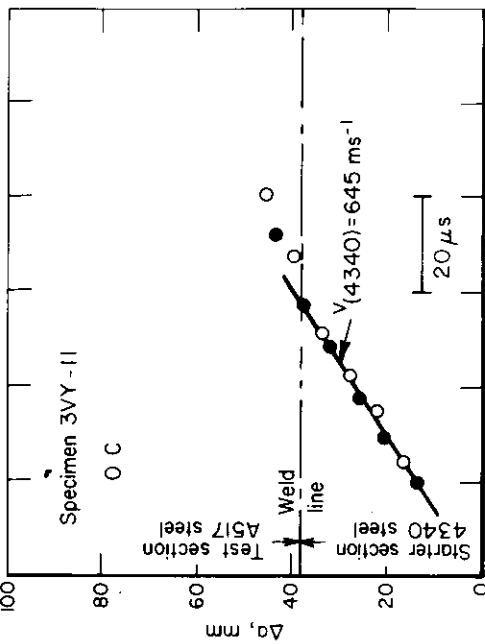
FIG. A-15. DUPLEX-4340/A517F DCB TEST PIECE 3VY24 (25.4 mm-THICK, TESTED AT 0°C). Fracture initiated at a and arrested on the A517F steel test section at b, shortly after penetrating the weld line.



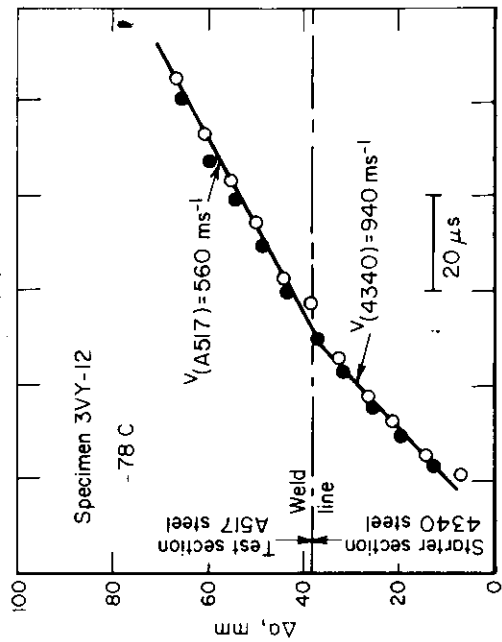
FIG. A-16. DUPLEX 4340/A517F DCB TEST PIECE 3VY28 (25.4 mm-THICK, TESTED AT -78°C). Fracture initiated at a and arrested at b.



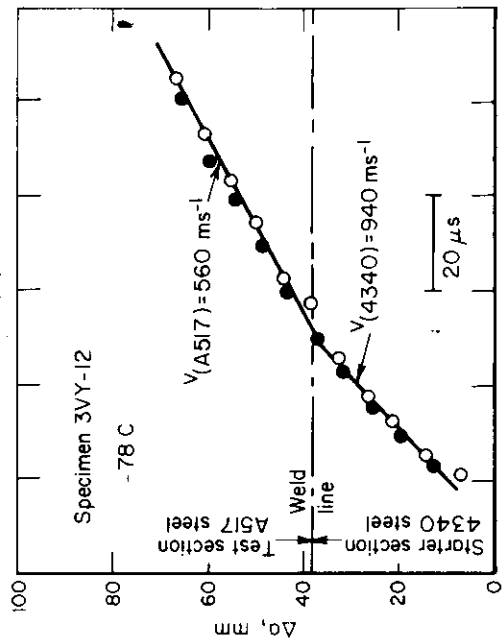
(a)



(b)



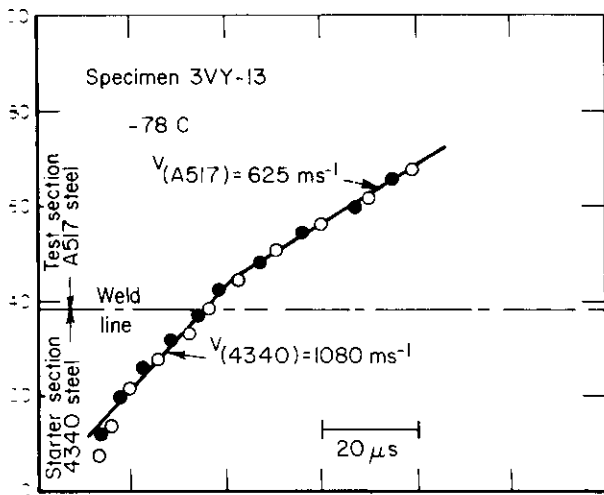
(c)



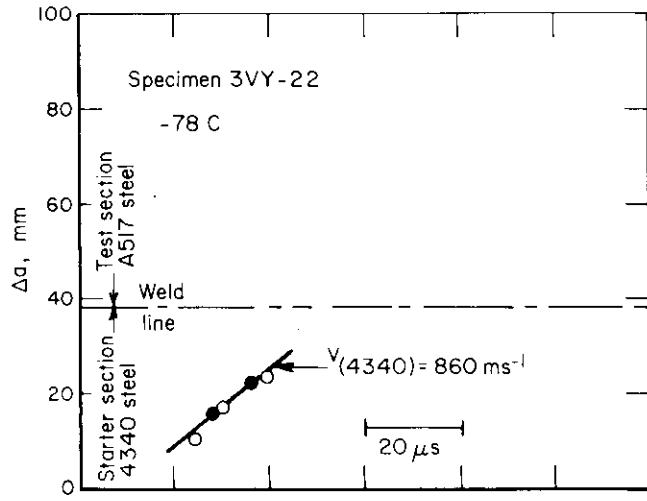
(d)

FIGURE A-17. CRACK VELOCITY MEASUREMENTS DERIVED FROM THE CONDUCTING STRIPS:

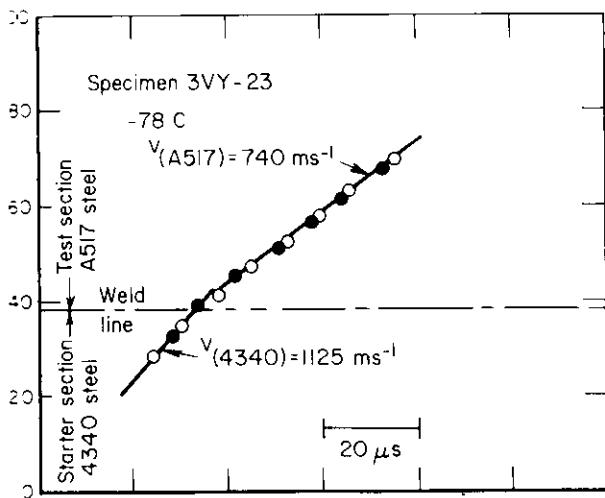
- (a) 3V44
- (b) 3VY10
- (c) 3VY11
- (d) 3VY12
- (e) 3VY13
- (f) 3VY22
- (g) 3VY23
- (h) 3VY24
- (i) 3VY28



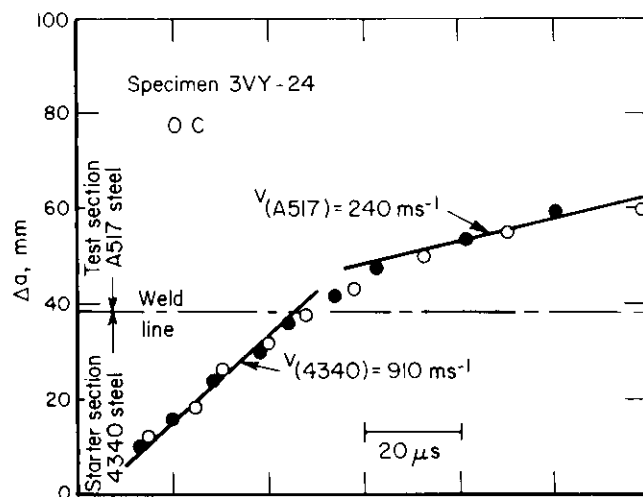
(e)



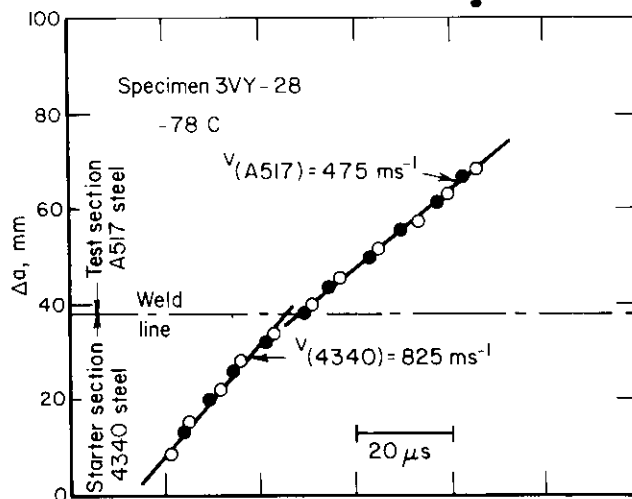
(f)



(g)



(h)



(i)

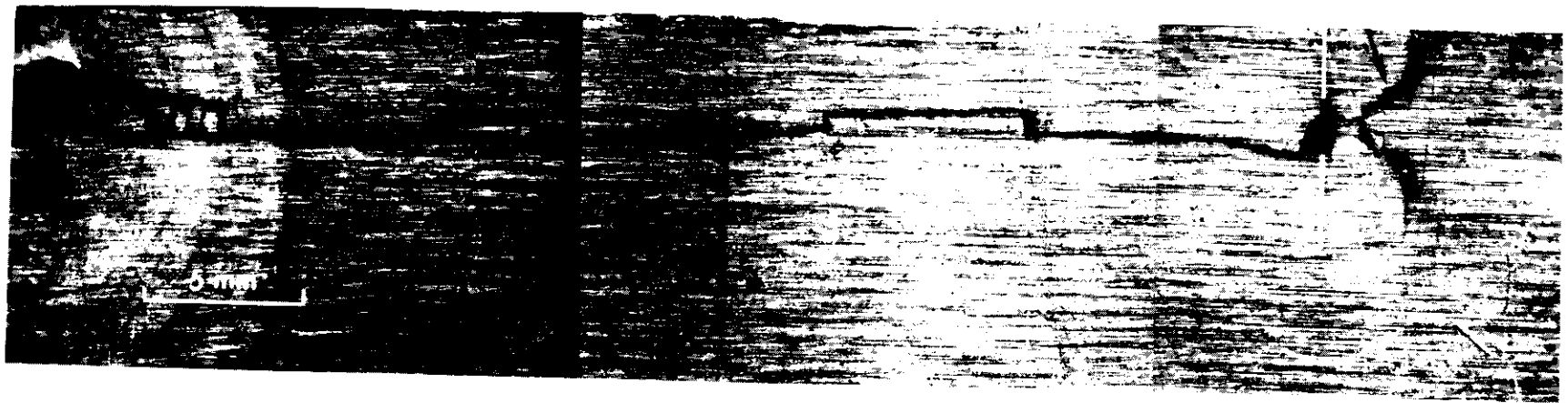
FIG. A-17 (Continued)



(a) Specimen Surface

(b) Specimen Midsection

FIGURE A-18. EXTENT OF FRACTURE PROPAGATION IN THE DUPLEX 4340/A517F DCB TEST PIECE 3VY10: (a) at the specimen surface and (b) on the specimen midsection. The arrow in (a) shows the extent of the crack on the surface. The dimple visible on the surface is associated with the tunneling of the crack in the inferior and extends much farther



(a) Specimen Surface



(b) Specimen Midsection

FIGURE A-19. EXTENT OF FRACTURE PROPAGATION IN THE DUPLEX 4340/A517F DCB TEST PIECE 3VY11: (a) at the specimen surface and (b) on the specimen midsection. The arrow in (a) shows the extent of the crack on the surface; (b) illustrates that the crack extended farther on the plate and midsection



(a)



(b)



(c)

FIGURE A-20. PROFILE OF THE ARRESTED CRACK IN THE A517F STEEL TEST SECTION OF SPECIMEN 3VY-10 (12.7 mm-THICK, TESTED AT -78°C). The profiles shown are on the plate midplane: (a) the arrested crack tip, (b) 0.3 to 0.6 mm behind the crack tip, and (c) 0.8 to 1.2 mm from the crack tip. An unbroken ligament a is visible in Figure A-20(c); ruptured ligaments, identified by b, are evident in all 3 photographs.

SECTION 3

DYNAMIC ANALYSIS OF CRACK PROPAGATION IN THE DCB TEST SPECIMEN

by

M. F. Kanninen

ABSTRACT

In this report an analysis of dynamic unstable crack propagation in the double-cantilever (DCB) test specimen is presented. The technique is based on the beam-on-elastic foundation model of the DCB specimen used previously but with the simple beam and foundation representations replaced by a Timoshenko beam and a generalized elastic foundation. Crack speeds and energy levels calculated with this model using a finite-difference method are presented and discussed. A complete derivation of the governing equations of the model and of the computational procedure is also given.

DYNAMIC ANALYSIS OF CRACK PROPAGATION IN THE DCB SPECIMEN

I. INTRODUCTION

The criteria which govern unstable crack propagation and crack arrest have not yet been definitely established. In fact, this problem presently constitutes a controversial topic in fracture mechanics. Two points of view are current: one based upon an "arrest-toughness" criterion, the other upon an "energy-balance" criterion.

Many investigators subscribe to the idea that crack arrest can be treated as simply the reverse (in time) of crack initiation. In other words, that each material has an intrinsic crack-arrest toughness which is a property of the material to the same extent that K_{Ic} is a property of that material. It follows that the unstable propagation of the crack which precedes its arrest is of no concern in an engineering design aimed at preventing catastrophic failure by insuring crack arrest. An alternative point of view is that a crack will continue to propagate until the system can no longer provide sufficient energy to support further crack growth. This means that crack arrest depends on the nature of the crack-extension process prior to arrest, not merely on the end point itself.

Experimental results and analyses which would decisively reveal the correct criterion for crack arrest are presently lacking. However, the energy-balance approach appears to be more viable for the following reasons. First, it permits analytical progress to be made towards an engineering solution to the problem. Second, because an energy balance must always be satisfied, such an analysis will undeniably have a fundamentally correct basis. Third, even though the two approaches are not necessarily incompatible (they will coincide when the kinetic energy of the system is negligible), the energy-balance approach always provides the more conservative prediction of crack arrest. In this report, an analysis based on the energy-balance point of view is developed for the double-cantilever-beam (DCB) test specimen.

II. SUMMARY OF PREVIOUS WORK

On the basis of work conducted in this laboratory⁽¹⁻⁴⁾, it now seems certain that the inertia forces must be explicitly taken into account in the analysis of rapid unstable crack propagation. For the DCB specimen this can be readily accomplished because a one-dimensional spatial degree-of-freedom (i.e., beam theory) representation suffices. Hence, the time variable can be accommodated without an inordinate increase in the mathematical complexity of the problem. It should perhaps be emphasized that there is no intent to use beam theory to predict local stresses or strains in the neighborhood of the "crack tip" in this work. Rather, the beam analysis is used only to calculate nonlocal quantities (e.g., strain energy, kinetic energy) that can be determined much more accurately. This is the basic reason that the simple theory is successful.

A beam model has been used by a large number of different investigators over the years. In most cases, a pair of built-in cantilever beams, having a length equal to the crack length, were taken to represent the cracked portion of the specimen. The deformation of the uncracked portion was thereby neglected although empirical corrections have been introduced to compensate for this neglect. We have developed an extended model in which the beams are of the same length as the specimen but are partly connected by a continuous array of linear springs which simulate the transverse elasticity of the uncracked region*. In the case of symmetrically located crack, of course, this is equivalent to a single beam partly supported by an elastic foundation and, because this offers a more convenient way of formulating the problem, it will be used in the following discussion. The beam-on-elastic foundation model of the DCB specimen is shown in Figure 1.

As a first attempt, the simplest possible representations for the two components of the beam-on-elastic foundation model were employed: a simple Euler-Bernoulli beam and a Winkler layer.⁽¹⁾ Omitting the details, a solution for the beam deflection satisfying appropriate boundary conditions is then readily obtained for a constant length crack. Having the beam deflection, the strain energy can be computed and an expression for the stress-intensity factor deduced. When the "uncracked length" is not too small, the result is

$$K = 2/3 \frac{P_2}{bh^{3/2}} \left[1 + \alpha \frac{h}{a} \right] \quad (1)$$

where K = stress-intensity factor
 P = load applied at the end of the specimen
 a = crack length
 2h = height of the specimen
 b = thickness of the specimen

and α is the number $(6)^{-1/4} = 0.64$. Because Equation (1) was found to be in excellent agreement both with two-dimensional analyses and with experimental results, it is believed that the beam-on-elastic-foundation model can be used in the dynamic situation where the realistic two-dimensional solutions are virtually unobtainable.

The initial use of the beam-on-elastic-foundation model in the analysis of unstable crack propagation was in a quasi-static approximation.** This work was reported in Reference 1. The results, when compared later with experiments, revealed a two-fold inadequacy of this approach. First, the predicted crack speeds were greatly in excess of the observed speeds. Second, the calculation did not predict essentially constant-speed propagation as was observed in the experiments. To remedy this, a dynamic version of the model was developed by incorporating the

* Prandtl⁽⁵⁾ has used a beam-spring fracture model but had in mind an atomic bond breaking picture like that developed later by Goodier and Kanninen. Hence, Prandtl's springs have a finite spacing associated with them (in contrast to the continuous foundation envisioned here) so that both the springs and the beam have a distinctly different physical interpretation from that of the model developed in this paper.

** Inertia forces were not included in the equation of motion. Strain energy and kinetic energy were computed from the resulting static configurations and the crack speed deduced from a postulated energy balance.⁽¹⁾

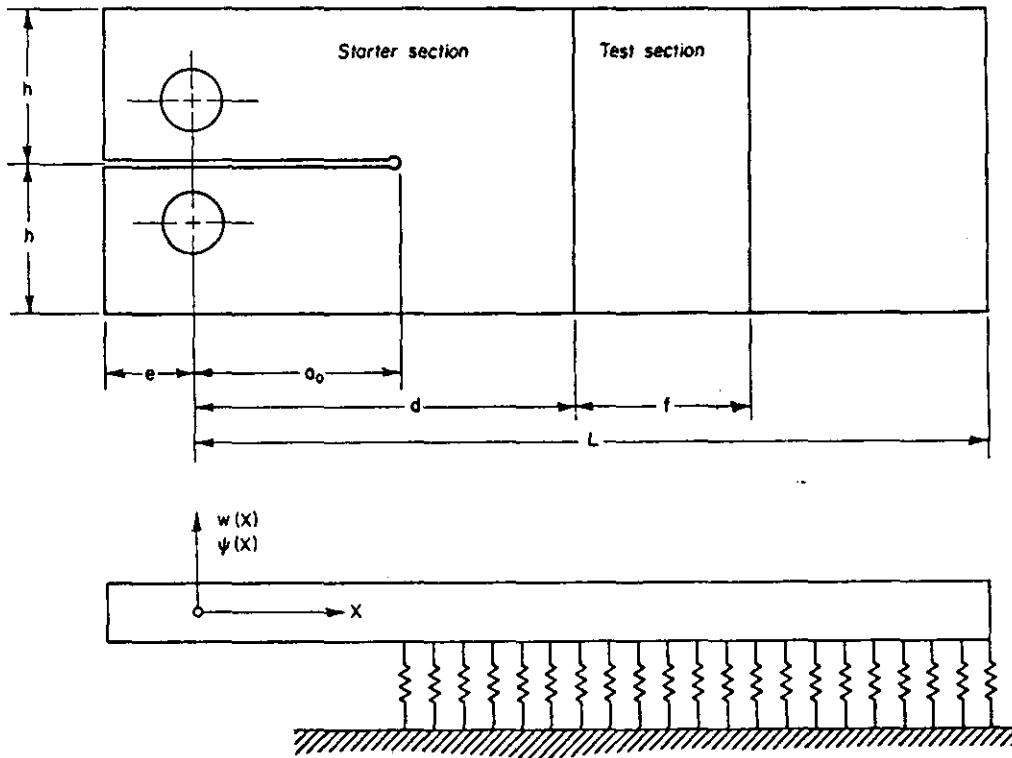


FIGURE 1. THE DOUBLE CANTILEVER BEAM (DCB) TEST SPECIMEN AND THE BEAM-ON-ELASTIC FOUNDATION MODEL.

lateral-inertia forces into the equation governing the beam deflection. The equation to be solved is then given by

$$EI \frac{\partial^4 w}{\partial x^4} + \rho A \frac{\partial^2 w}{\partial t^2} + kH (w_c - w)w = 0 \quad (2)$$

where w is the beam deflection, w_c is a critical deflection for the rupture of the foundation, H denotes the Heaviside step function, and other parameters are as given below.

The boundary conditions accompanying Equation (2) were those representing a fixed displacement δ with no applied torque at the load pins and zero stress at the right-hand end of the specimen. Hence, using the notation given in Figure 1,

$$w(0, t) = \delta$$

and (3)

$$w''(0, t) = w''(L, t) = w'''(L, t) = 0$$

The initial conditions were obtained by solving the static counterpart of Equation (2), subject to the above boundary conditions.

Notice that the parameters δ and w_c appearing in this formulation can be alternatively expressed in terms of more physically relevant parameters. Specifically, δ can be directly related to the applied stress-intensity factor K_q while w_c can be related to a fracture toughness (i.e., either K_c for the static problem or K_d for the dynamic problem). Without providing the details, this means that a dynamic-crack-propagation solution can be obtained by specifying only the ratio K_q/K_d in addition, of course, to the specimen geometry.

For an initially blunt crack, $K_q > K_c$. Hence, unless some additional refinement is introduced into the model represented by Equations (2) and (3), a portion of the beam that is supported by the foundation just beyond the crack tip will have a deflection exceeding w_c in the initial configuration. As described in Reference 2, crack propagation then commences with a substantial instantaneous increase in crack length. This awkward feature of the model was subsequently eliminated by introducing a "pinching force" Q at the crack tip in the initial configuration. (This is the essential difference between the work described in References 2 and 3.) The pinching force, which was intended to simulate the effect of the initial bluntness, was incorporated in the form of a jump discontinuity in w''' at $x = a_0$ equal to Q/EI . The parameter Q was then taken to be such that $w(a_0, 0) = w_c$. Then, crack propagation can occur smoothly (once the pinching force is removed) from the beginning of the computation.

The solution to the initial-value problem given by Equations (2) and (3) was obtained numerically using a finite-difference method.^(2,3) A constant dynamic fracture toughness was used, just as in the quasi-static calculations of Reference 1. A substantial improvement was realized in that the calculations predicted constant-speed propagation at much reduced speeds. Encouraged by this result, a more refined version of the beam-on-elastic foundation model was undertaken to eliminate the remaining discrepancy between the calculated speeds and the experimental values (roughly, a factor of two). The development of the model and the computational results obtained from it are the subject of this report.

Before discussing the details of the dynamic-crack-propagation model contained in this report, it may be useful to briefly mention other analytical treatments that have been offered. Most of these are quasi-static in nature and have been described in Reference 1 and elsewhere. The only dynamic treatment directly applicable to the DCB configuration is that of Bilek and Burns⁽⁶⁾. They have obtained a closed form solution by considering a built-in Euler-Bernoulli beam under various loading conditions: constant bending moment, constant displacement rate, or constant shearing force. The equation of motion for these conditions can thus be transformed into an ordinary differential equation by use of a similarity transform.* The solution determined in this way predicts that crack propagation occurs in such a way that the ratio a/\sqrt{t} is either a constant or changes slowly with the fracture energy's dependence on the crack speed. Here, a denotes the crack length and t the time.

While the work of Bilek and Burns is certainly useful, their approach suffers from a number of disadvantages in comparison to the model developed in this report. First, they are not able to specify initial conditions (the similarity transform restricts the analysis to the specific condition that $a = 0$ at $t = 0$). Among other drawbacks, the systematic variation of the parameter K_q by blunting the initial crack cannot therefore be treated. Second, the "built-in beam"

* The equation of motion for the Bilek-Burns model is the same as Equation (2) of this report when $k = 0$. The boundary conditions consequently contain the fracture criterion which is that of a critical bending moment at the crack tip.

condition at the crack tip, in addition to producing spurious wave effects, means that the size of the specimen increases in time. Hence, the energy apportionment calculated from the solution is somewhat suspect. Third, although a closed-form solution is obtained, it is sufficiently complicated (i.e., involving Fresnel, sine and cosine integrals), that the details of the results are not easily accessible without a computer. In this light the finite-difference procedure employed here is no more inconvenient.

III. A MODEL OF THE DCB SPECIMEN USING A TIMOSHENKO BEAM ON A GENERALIZED ELASTIC FOUNDATION

The very significant improvement in the analysis resulting from the incorporation of a single inertia term strongly suggests further development of the model in this direction. Two areas of improvement are immediately available: the beam characterization and the foundation characterization. In particular, the applicability of one-dimensional beam theory can be extended by taking account of transverse-shear deformations and, for moving beams, of rotary inertia. The formalism which includes these effects is usually referred to as Timoshenko's beam equations(7,8). Similarly, the Winkler foundation can be generalized to an elastic foundation which exhibits rotational stiffness in addition to an extensional stiffness**. The current model (Figure 1) employs these concepts.

1. The Equations of Motion

The governing equations for a model of the DCB specimen using a Timoshenko beam on a generalized elastic foundation are derived in Appendix A. The derivation starts from the equations of three-dimensional elasticity, adapting the method given by Cowper(10). The resulting relations are

$$EI \frac{\partial^2 \psi}{\partial x^2} + KGA \left(\frac{\partial w}{\partial x} - \psi \right) - F\psi - k_r H^*(\theta_c - \theta) \psi = \rho I \frac{\partial^2 \psi}{\partial t^2} \quad (4)$$

$$KGA \left(\frac{\partial^2 w}{\partial x^2} - \frac{\partial \psi}{\partial x} \right) - k_e H^*(\theta_c - \theta) w = \rho A \frac{\partial^2 w}{\partial t^2}$$

** As shown by Kerr(9), the generalized elastic foundation is equivalent to the Pasternak foundation model.

where,

- w = average deflection of the cross section
- Ψ = mean angle of rotation of the cross section about the neutral axis
- E = elastic modulus
- I = moment of inertia (= $bh^3/12$ for a rectangular cross section)
- G = shear modulus
- F = axial compressive force applied to the beam
- ρ = density
- A = cross-sectional area of beam (= bh for a rectangular cross section)
- k_e = extensional stiffness of the foundation
- k_r = rotational stiffness of the foundation
- K = shear-deflection coefficient of the beam
- θ = crack extension parameter
- θ_c = critical value of the crack-extension parameter

and $H^*(x)$ is the ordinary Heaviside step function modified such that a spring once broken always remains broken.

The boundary conditions to be imposed are those which correspond to stress-free conditions at the ends of the specimen. Using the equations derived in Appendix A, these are

$$\begin{aligned} w'(-e, t) - \Psi(-e, t) &= 0 \\ \Psi'(-e, t) &= 0 \\ w'(L, t) - \Psi(L, t) &= 0 \\ \Psi'(L, t) &= 0 \end{aligned} \tag{5}$$

where the prime notation indicates differentiation with respect to x and the coordinates are as shown in Figure 1. An additional constraint that must be imposed is that the deflection of the load point cannot be less than the deflection imposed initially. If δ denotes this initial displacement, then

$$w(0, t) \geq \delta$$

throughout the crack-extension process.

The initial conditions are obtained by finding the static solution that satisfies the above boundary conditions and has, in addition, a force Q and a couple M acting at $x = a_0$. The parameters Q and M , which are intended to simulate the effect of the initial bluntness, are chosen such that $\theta(a_0, 0) = \theta_c$ and the strain energy in the system initially is a minimum. The static solution can be obtained in closed form by, (i) separating the problem into the two intervals where the differential equations have constant coefficients (i.e., $-e \leq x \leq a_0$ and $a_0 \leq x \leq L$ where a_0 is the initial crack length), (ii) finding a solution valid for each interval, (iii) satisfying the boundary conditions of the problem together with the condition that $w = \delta$ at $x = 0$, and (iv) evaluating the remaining arbitrary constants such that w and Ψ are continuous at $x = a_0$ while w' and Ψ' experience jump discontinuities equal to Q/KGA and M/KGA , respectively. The details are given in Appendix C.

In the Timoshenko-beam equations, the effective transverse-shear strain is taken to be equal to the average shear stress on a cross section divided by the product of the shear modulus and a dimensionless "shear coefficient" K . This latter quantity is usually introduced to compensate for the fact that the shear stress and shear strain are not uniformly distributed over the cross section. A more fundamental derivation of K has been given by Cowper(10) by integration of the

equations of three-dimensional elasticity. His result for a rectangular cross section is

$$\kappa = \frac{10(1+\nu)}{12 + 11\nu}$$

where ν is Poisson's ratio. In the following it will be convenient to approximate this result by taking

$$\frac{\kappa G}{E} = \frac{1}{3} \quad (6)$$

which is exact for $\nu = 3/11$.

2. The Energy Components and the Crack-Extension Criterion

The crack-extension parameter θ appearing in Equations (4) can be evaluated by considering the energy of the system, as follows. Expressions for the energy components in a DCB specimen represented by a Timoshenko beam on a generalized foundation are developed in Appendix B. The results are

$$U = \int_0^L \left\{ EI \left(\frac{\partial \Psi}{\partial x} \right)^2 + \kappa GA \left(\frac{\partial w}{\partial x} - \Psi \right)^2 + F \Psi^2 + H^*(\theta_c - \theta) \left[k_c w^2 + k_r \Psi^2 \right] \right\} dx \quad (7)$$

and

$$T = \int_0^L \left\{ \rho A \left(\frac{\partial w}{\partial t} \right)^2 + \rho I \left(\frac{\partial \Psi}{\partial t} \right)^2 \right\} dx$$

where U and T are strain energy and the kinetic energy, respectively. Notice that the factor 1/2 ordinarily appearing in expressions of this kind is omitted because U and T each represent a total for the two halves of the specimen.

The total energy \mathcal{E} contained in the specimen at any point in time is the sum of $U+T$. Hence, from Equations (7)

$$\begin{aligned} \mathcal{E} = \int_0^L \left\{ EI \left(\frac{\partial \Psi}{\partial x} \right)^2 + \kappa GA \left(\frac{\partial w}{\partial x} - \Psi \right)^2 + \right. \\ \left. + \rho A \left(\frac{\partial w}{\partial t} \right)^2 + \rho I \left(\frac{\partial \Psi}{\partial t} \right)^2 + F \Psi^2 + \right. \\ \left. + H(x-a) \left[k_e w^2 + k_r \Psi^2 \right] \right\} dx \quad (8) \end{aligned}$$

where a is the crack length. It is assumed for simplicity that there are no "islands" of material remaining behind the crack tip whereupon the function $H(x-a)$ performs exactly the same service as does $H^*(\theta - \theta_c)$ and, therefore, can be used in its place.

The basic premise of fracture mechanics is that the energy absorbed by the extending crack must be just equal to that "released" by the body containing the crack. In the present case, where no work is done by external forces while the crack is propagating, this means that during an amount of crack advance da

$$Rbd\dot{a} = -d\dot{\mathcal{E}}$$

or

$$bR = -\frac{1}{V} \frac{d\mathcal{E}}{dt} \quad (9)$$

where R is the dynamic energy absorption per unit area of crack extension, and $V = da/dt$ is the crack speed. As shown in Appendix B, upon substituting Equation (8) into Equation (9), differentiating with respect to t , integrating by parts, using Equations (4) and (5), it is found that

$$bR = \left[k_e w^2 + k_r \psi^2 \right]_{x=a} \quad (10)$$

This reveals that the crack-extension parameter must be associated with a critical value of the bracketed quantity. Consequently, by definition

$$\theta = k_e w^2 + k_r \psi^2 \quad (11)$$

and

$$\theta_c = bR \quad (12)$$

are the parameters that must be used in the dynamic solution of Equations (4). Notice that this result could also have been obtained by simply equating the sum of the extensional and the rotational energy contained in the springs that must rupture to permit a unit of crack advance (which is therefore "lost" to the system) to the fracture toughness per unit of crack advance.

3. The Evaluation of the Foundation Parameters Using the Static Solution

In the development of the beam-on-elastic-foundation model of the DCB specimen using simple-beam theory, it was possible to intuitively determine the appropriate value of the foundation modulus. This choice was then verified by comparing the stress-intensity factor obtained from the model with established data for the DCB specimen. The same procedure is followed here, the essential difference being that there are now two foundation constants, k_e and k_r . Just as in the previous work, by solving Equations (4) and (5), an expression for the stress-intensity factor can be determined. By comparing this result to existing experimental and two-dimensional computational results(11-13), confidence that appropriate choices of the system parameters has been made is gained.

The foundation parameters k_e and k_r can be evaluated from a simple one-dimensional "tensile specimen" picture of the foundation elements. In particular, by equating the extension of the element to the beam deflection, equating the force acting on the element to $k_e w$, and taking the elastic properties of the element to be the same as those of the beam, it is found that

$$k_e = \frac{2Eb}{h} \quad (13)$$

Similarly, by associating the change in shape of the element when shearing forces given by $k_r \Psi$ are applied to its sides with the mean rotation of the beam cross section, the result

$$k_r = \frac{KGA}{2} \quad (14)$$

is obtained. Using the approximate form of Cowper's shear coefficient given by Equation (6) and taking $A = bh$ then gives

$$k_r = \frac{Ebh}{6} \quad (15)$$

which is appropriate for a rectangular cross section and a material for which $\nu \approx 0.272$. For other types of cross section, appropriate expressions for K can be obtained from Cowper⁽¹⁰⁾.

The derivation of general expressions for the specimen compliance and the stress-intensity factor appear in Appendix C. Using the results given there together with Equations (13) and (15), it is found that*

$$\frac{\delta}{P} = \frac{4a^3}{Ebh^3} \left\{ 1 + \frac{3\sqrt{5}}{4} \left(\frac{h}{a}\right) + \frac{2}{3} \left(\frac{h}{a}\right)^2 + \frac{3\sqrt{5}}{16} \left(\frac{h}{a}\right)^3 \right\} \quad (16)$$

and

$$K = \frac{2\sqrt{3} P a}{bh^{3/2}} \left\{ 1 + \frac{\sqrt{5}}{2} \left(\frac{h}{a}\right) + \frac{1}{2} \left(\frac{h}{a}\right)^2 \right\}^{1/2} \quad (17)$$

when the "uncracked length", $L-a$, is large in comparison to h .

To test the validity of these results, comparison with the stress-intensity factors calculated using two-dimensional elasticity theory (e.g., boundary-point collocation) can be made. Such a comparison is shown in Figure 2 using the data of Gross and Srawley⁽¹²⁾ and of Wiederhorn, Shorb and Moses⁽¹³⁾. To put these results into perspective, the values obtained at various stages of the development of the beam-on-elastic foundation model are also shown. In obtaining the curves appearing in the figure, the values of the foundation constants were either those of Equations (13) and (15) or were zero. Notice that the simple built-in cantilever-beam model is included here as the special case of a beam supported by an infinitely rigid foundation to which it is mathematically equivalent.

The results given in Figure 2 show that the rigid-foundation models are clearly inadequate. The two "self-consistent" beam-on-elastic foundation model models, on the other hand, provide an excellent representation of the established data for the DCB specimen. It is worth pointing out that it may be possible to obtain precise agreement with the established data by introducing further numerical factors into the relations for the foundation parameters. However, the simplicity afforded by Equations (13) and (14) is felt to be more valuable than the modest improvement that would accrue by complicating them.

* Equation (17) represents the stress-intensity factor for crack extension under constant load. To obtain the stress-intensity factor for crack extension under constant displacement, Equation (16) can be used to eliminate P from Equation (17) in favor of δ .

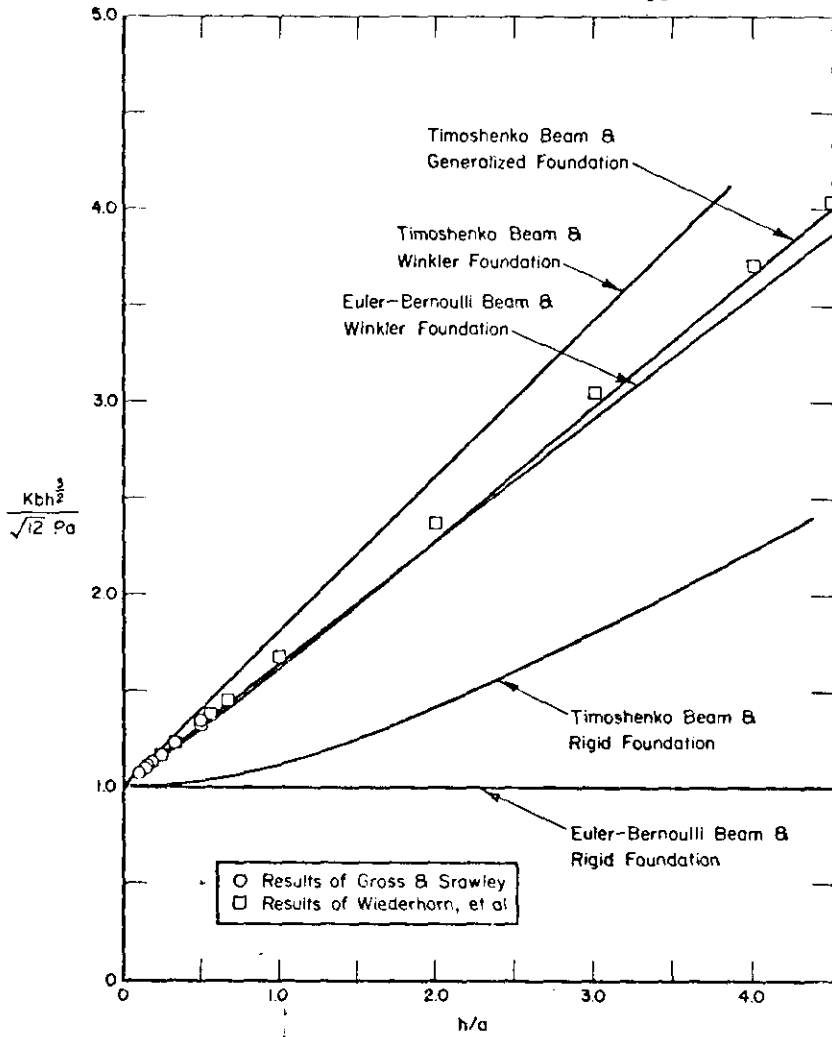


FIGURE 2. COMPARISON BETWEEN STRESS INTENSITY FACTORS FOR THE DCB SPECIMEN CALCULATED USING TWO DIMENSIONAL ELASTICITY THEORY WITH THOSE FROM VARIOUS DIFFERENT BEAM-ON-ELASTIC FOUNDATION MODELS.

4. Computational Procedure for Dynamic Crack Propagation

For computational purposes, it is convenient to introduce a unit of length of the order of the spring deflections. Let this parameter be denoted as w_c and defined such that

$$k_e w_c^2 = \theta_c \tag{18}$$

where $\theta_c = bR$ is a critical value of the parameter appearing in Equation (11). Introducing Equation (13), it can be seen that

$$w_c = \left(\frac{h R}{2 E} \right)^{1/2} \tag{19}$$

Or, in analogy with the static situation, by defining $K_d^2 = ER$

$$w_c = \left(\frac{h}{2} \right)^{1/2} \frac{K_d}{E} \tag{20}$$

where K_d is the dynamic fracture toughness. Notice that when the energy stored in rotational deformation of the foundation is zero (i.e., in a Winkler foundation), the crack-extension parameter is satisfied by having the beam deflection become just equal to a critical deflection w_c . This was the case in the model represented by Equation (2). However, in the more general case where $k_r \neq 0$, the deflection w_c will have no such specific role.

Dimensionless variables can be introduced as follows. First, let the new independent variables be

$$\xi = \frac{x}{h} \quad (21)$$

and

$$\tau = \left(\frac{E}{12\rho} \right)^{1/2} \frac{t}{h} \quad (22)$$

Then, let the new dependent variables be

$$W = \frac{w}{w_c} \quad (23)$$

and

$$Y = \frac{h}{w_c} \psi \quad (24)$$

A dimensionless crack-extension parameter can similarly be introduced by defining

$$\hat{\theta} = \frac{\theta}{\theta_c} \quad (25)$$

Equivalently, using Equations (11) and (18)

$$\hat{\theta} = \left(\frac{w}{w_c} \right)^2 + \frac{k_r}{k_e} \left(\frac{\psi}{w_c} \right)^2$$

Or, with Equations (13), (15), (23), and (24)

$$\hat{\theta} = W^2 + \frac{1}{12} Y^2 \quad (26)$$

As can be readily seen from Equation (25), the critical value of the θ parameter is unity.

Substituting Equations (21-25) into Equations (4) then gives, in the most general case

$$\frac{\partial^2 Y}{\partial \xi^2} + \frac{\kappa}{2(1+\nu)} \frac{Ah^2}{I} \left\{ \frac{\partial W}{\partial \xi} - Y \right\} - \frac{Fh^2}{EI} Y - \frac{k_r h^2}{EI} H^*(1-\theta) Y = \frac{1}{12} \frac{\partial^2 Y}{\partial \tau^2} \quad (27)$$

$$\frac{6\kappa}{1+\nu} \left\{ \frac{\partial^2 W}{\partial \xi^2} - \frac{\partial Y}{\partial \xi} \right\} - 12 \frac{k_e h^2}{EA} H^*(1-\theta) W = \frac{\partial^2 W}{\partial \tau^2}$$

Similarly, Equations (5) become

$$W'(-e/h, \tau) - Y(-e/h, \tau) = 0$$

$$Y'(-e/h, \tau) = 0$$

$$W'(L/h, \tau) - Y(L/h, \tau) = 0$$

$$Y'(L/h, \tau) = 0$$

(28)

The initial conditions are obtained, just as in the above, by solving the time-independent version of Equations (27). Again, the boundary conditions at the left-hand end are replaced by

$$W(0,0) = \delta/w_c$$

and

$$Y'(0,0) = 0$$

where δ is the initial deflection of the load pins. The ratio δ/w_c can be related to the ratio K_q/K_d which is more convenient for comparison with experiment. This is accomplished through Equations (16), (17) and (20) to obtain

$$\frac{\delta}{w_c} = \left(\frac{8}{3}\right)^{1/2} \left(\frac{a_0}{h}\right)^2 \frac{K_q}{K_d} \frac{\left[1 + \frac{3/5}{4} \left(\frac{h}{a}\right) + \frac{2}{3} \left(\frac{h}{a}\right)^2 + \frac{3/5}{16} \left(\frac{h}{a}\right)^3\right]}{\left[1 + \frac{\sqrt{5}}{2} \left(\frac{h}{a}\right) + \frac{1}{2} \left(\frac{h}{a}\right)^2\right]^{1/2}} \quad (29)$$

Also, if the wedge is considered to be stationary, the condition

$$W(0, \tau) \geq \delta/w_c$$

must be imposed during the crack-propagation process.

Because Equations (27) represent a hyperbolic system, the characteristics should be obtained in order to set the integration step properly. In the present circumstance, the characteristics correspond to the roots of the equation

$$\left(\alpha_1^2 - \frac{1}{12} \alpha_2^2\right) \left(\frac{6K}{1+\nu} \alpha_1^2 - \alpha_2^2\right) = 0$$

This can be solved by inspection and the result used in connection with standard procedures in the solution of differential equations by finite-difference technique; see for example Forsythe and Wasow⁽¹⁴⁾. In particular,

$$\frac{\Delta\tau}{\Delta\xi} < \min \left\{ \frac{1}{2\sqrt{3}}, \left(\frac{1+\nu}{6K}\right)^{1/2} \right\}$$

where $\Delta\xi$ and $\Delta\tau$ denote the step sizes of the two independent variables in the finite-difference computation.

Equations (27) are valid for arbitrary specimen cross-sectional geometries. For present purposes they can be simplified by specializing to a rectangular cross section. The result is

$$\frac{\partial^2 Y}{\partial \xi^2} + 4 \frac{\partial W}{\partial \xi} - 4Y - 2H*(1-\hat{\theta})Y = \frac{1}{12} \frac{\partial^2 Y}{\partial \tau^2}$$

and

$$\frac{\partial^2 W}{\partial \xi^2} - \frac{\partial Y}{\partial \xi} - 6H*(1-\hat{\theta})W = \frac{1}{4} \frac{\partial^2 W}{\partial \tau^2}$$

(30)

where it has been assumed that the axial force F can be neglected. The boundary conditions remain unchanged. The integration step sizes in the finite-difference computation are now subject to the requirement that

$$\Delta\xi > \sqrt{12} \Delta\tau \quad (31)$$

which could also have been obtained directly from Equations (30).

An important part of the computation is the evaluation of the energy components during unstable crack propagation. By substituting the various parameters introduced above into Equations (7), suitable expressions for a rectangular cross section are found to be

$$\frac{U}{RA} = \int_0^{L/h} \left\{ \frac{1}{24} \left(\frac{\partial Y}{\partial \xi}\right)^2 + \frac{1}{6} \left(\frac{\partial W}{\partial \xi} - Y\right)^2 + H*(1-\hat{\theta}) \left[W^2 + \frac{1}{12} Y^2 \right] \right\} d\xi$$

and

$$\frac{T}{RA} = \int_0^{L/h} \left\{ \frac{1}{24} \left(\frac{\partial W}{\partial \tau}\right)^2 + \frac{1}{288} \left(\frac{\partial Y}{\partial \tau}\right)^2 \right\} d\xi$$

(32)

To compute the rates of change of the energy components, it suffices to calculate the "kinetic energy release rate" $\frac{dT}{dz}$. Hence,

$$\frac{dT}{da} = \frac{RbC_o}{V} \int_0^{L/h} \left\{ \frac{\partial W}{\partial \tau} \cdot \frac{\partial^2 W}{\partial \tau^2} + \frac{\partial Y}{\partial \tau} \cdot \frac{\partial^2 Y}{\partial \tau^2} \right\} d\xi$$

with the "strain energy release rate" - $\frac{dU}{da}$ being determined by appealing to an energy balance.

Details of the finite-difference formulation of Equations (30) and (32) used in the computing program are given in Appendix D. Also given there are the results of computations in which the step sizes $\Delta\xi$ and $\Delta\tau$ are systematically varied. As can be seen from these results, the computation is remarkably insensitive to the particular choices (provided, of course, inequality (31) is satisfied) which affords a very economical computation. On the average, each computation reported here was obtained in about two minutes of CDC 6600 central processor time.

IV. RESULTS AND CONCLUSIONS ON DYNAMIC CRACK PROPAGATION

To perform a computation of unstable crack growth and arrest in a single-section DCB specimen using the analytical model described in the above, it is only necessary to specify the geometric dimensions of the specimen together with the ratio K_q/K_d . For a duplex specimen the ratio R_T/R_S --the ratio of the energy absorption ratio in the test section and the starter section, respectively--must also be given. In order to identify the results of particular computations in a concise manner, these numbers will be given together with a "specimen designation letter" representing the geometry. The specimen designations together with the actual dimensions corresponding to that designation are given in Table 1. Two material constants, $C_o = 5190$ M/s and $\nu = 0.272$, are also used in this work. These values are appropriate for steel.

The most important feature to be expected from the computational results is that they exhibit constant speed propagation over a sizable portion of the event. This is found to be the case provided K_q/K_d is not too large. For the K_q/K_d values corresponding to the experimental data obtained so far, essentially constant speed propagation is obtained.

A typical result is shown in Figure 3 where the crack lengths computed as a function of time are shown as open circles for the standard cases: specimen type A with $K_q/K_d = 2$. The best least-squares linear representation of the computational results is shown by the solid line in Figure 3. The slope of this line then provides a measure of the "steady state" speed V . The least-squares calculation has been performed routinely to determine V using the computed data over the first 80% of crack growth. Hence, for each computation the key results to be reported are the steady state speed V and the crack length at arrest, a_T .

Accompanying the crack length-time computational results are the values of the strain energy, kinetic energy and the absorbed energy. These are routinely computed at the time that the critical condition for crack extension is met at one of the finite-difference mesh points. A plot of the three energy components as a function of crack length for the standard case (whose crack length-time record is shown in Figure 3) is shown in Figure 4. In the figure the strain energy is designated by U , the kinetic energy by T , and the absorbed energy by R . Notice that, in accord with Equations (32), the actual values of these quantities are not computed--only the ratios of the energy components to the constant quantity Rbh^* .

* In a duplex specimen the value of R is that of the starter section.

TABLE I - DIMENSIONS OF DCB SPECIMENS USED IN THE COMPUTATIONS*

| Parameter** | SPECIMEN DESIGNATION | | | | | | | | | | |
|-------------|----------------------|-------|-------|-------|-------|-------|-------|-------|-------|-------|-------|
| | A | B | C | D | E | F | G | H | J | K | L |
| a_0 | 92.4 | 92.4 | 92.4 | 184.8 | 184.8 | 90.0 | 90.0 | 90.0 | 180.0 | 90.0 | 90.0 |
| h | 63.5 | 63.5 | 63.5 | 127.0 | 63.5 | 70.0 | 70.0 | 70.0 | 70.0 | 90.0 | 90.0 |
| L | 360.7 | 360.7 | 360.7 | 721.4 | 721.4 | 360.0 | 360.0 | 360.0 | 720.0 | 360.0 | 360.0 |
| d | -- | 132.1 | 132.1 | -- | -- | -- | 115.0 | 115.0 | -- | -- | 115.0 |
| e | 20.3 | 20.3 | 20.3 | 40.6 | 20.3 | 25.0 | 25.0 | 25.0 | 25.0 | 25.0 | 25.0 |
| f | -- | -- | 25.0 | -- | -- | -- | -- | 25.0 | -- | -- | -- |
| b | 12.7 | 12.7 | 12.7 | 25.4 | 12.7 | 12.5 | 12.5 | 12.5 | 12.5 | 12.5 | 12.5 |
| D | 25.4 | 25.4 | 25.4 | 50.8 | 25.4 | 25.4 | 25.4 | 25.4 | 25.4 | 25.4 | 25.4 |
| l | 88.0 | 88.0 | 88.0 | 176.0 | 88.0 | 90.0 | 90.0 | 90.0 | 90.0 | 90.0 | 90.0 |

* All dimensions are in mm.

** Parameters are as shown in Figure 1 (page 4). Additional parameters are D = pin diameter, l = pin length.

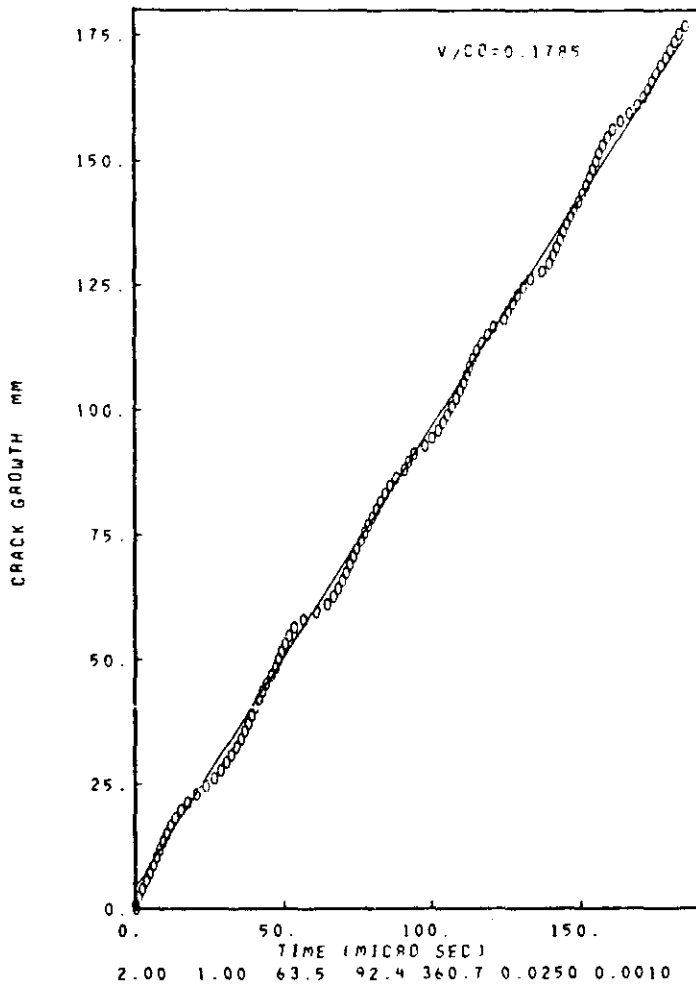


FIGURE 3. SPECIMEN A,
 $K_q/K_d = 2$

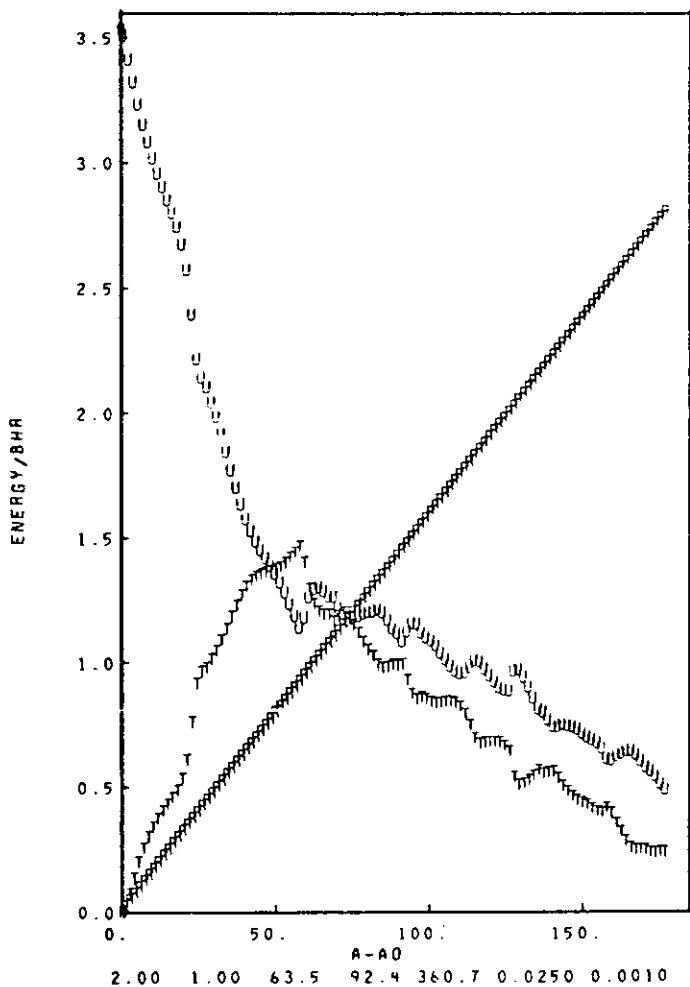


FIGURE 4. SPECIMEN A,
 $K_q/K_d = 2$

In Tables 2 and 3 the steady-state crack speeds (defined as above) and the distance propagated at arrest are shown for single-section and duplex specimens, respectively. Plots of the crack length-time data and the linear least-squares representation of these data are given in Appendix E. From the plots it can readily be seen that no steady-state speed exists when K_q/K_d exceeds ~ 2.5 . Below this figure, however, the linear representation is apparently quite accurate. At least for the computations shown in Table 2, it can be stated that the linear representation is roughly valid for cracks that arrest within the specimen but not otherwise.

Perhaps the most striking result of the computations is the support that is given to the following idea: that the steady-state speed achieved by the crack at some point in time depends only upon the conditions existing at the time, and not upon the prior history of crack propagation. This is most easily seen by the results obtained for duplex specimens. In particular, the relation

$$\left(\frac{K_q}{K_d}\right)_T = \frac{\left(\frac{K_q}{K_d}\right)_S}{\left(\frac{R_T}{R_S}\right)^{1/2}} \quad (33)$$

TABLE II - COMPUTATIONAL RESULTS FOR SINGLE-SECTION DCB SPECIMENS

| K_q/K_d | a_o/h | $a_r - a_o$ (mm) | a_r/h | v/c_o |
|---------------------------------|---------|---------------------|---------|---------|
| <u>Specimen Configuration A</u> | | | | |
| 1.2 | 1.45 | 26 | 1.875 | .056 |
| 1.5 | 1.45 | 75 | 2.650 | .116 |
| 2.0 | 1.45 | 176 | 4.250 | .180 |
| 2.5 | 1.45 | * | * | .217 |
| 3.0 | 1.45 | * | * | .234 |
| 3.5 | 1.45 | * | * | .237 |
| 4.0 | 1.45 | * | * | .422 |
| <u>Specimen Configuration D</u> | | | | |
| 2.0 | 1.45 | 352 | 4.250 | .180 |
| <u>Specimen Configuration E</u> | | | | |
| 1.5 | 2.90 | 113 | 4.70 | .075 |
| 2.0 | 2.90 | 246 | 6.80 | .127 |
| 3.0 | 2.90 | * | * | .173 |
| <u>Specimen Configuration F</u> | | | | |
| 1.2 | 1.30 | 26 | 1.70 | .061 |
| 1.5 | 1.30 | 75 | 2.40 | .124 |
| 2.0 | 1.30 | 187 | 4.00 | .188 |
| 2.5 | 1.30 | * | * | .226 |
| 3.0 | 1.30 | * | * | .253 |
| <u>Specimen Configuration J</u> | | | | |
| 2.0 | 2.55 | 247 | 6.10 | .136 |
| <u>Specimen Configuration K</u> | | | | |
| 1.2 | 1.00 | 29 | 1.35 | .071 |
| 1.5 | 1.00 | 83 | 1.95 | .150 |
| 2.0 | 1.00 | 218 | 3.45 | .217 |
| 2.5 | 1.00 | * | * | .275 |
| 3.0 | 1.00 | * | * | .283 |

* Crack did not arrest within the specimen.

TABLE III - COMPUTATIONAL RESULTS FOR DUPLEX DCB SPECIMENS

| $(K_q/K_d)_S$ | R_T/R_S | $(K_q/K_d)_T$ | $a_r - a_o$ (mm) | $(v/c_o)_S$ | $(v/c_o)_T$ |
|---------------------------------|-----------|---------------|---------------------|-------------|-------------|
| <u>Specimen Configuration B</u> | | | | | |
| 2.0 | 1.2 | 1.83 | 148 | .171 | .16 |
| 2.0 | 1.5 | 1.63 | 122 | .171 | .14 |
| 2.0 | 2.0 | 1.41 | 91 | .171 | .10 |
| 2.0 | 4.0 | 1.00 | 40 | .171 | -- |
| 2.5 | 2.0 | 1.77 | 163 | .192 | .16 |
| 3.0 | 2.0 | 2.12 | 252 | .533 | .20 |
| 3.0 | 2.25 | 2.00 | 220 | .533 | .19 |
| <u>Specimen Configuration C</u> | | | | | |
| 2.0 | 2.0 | 1.41 | 148 | .170 | .09 |
| <u>Specimen Configuration G</u> | | | | | |
| 2.0 | 1.2 | 1.83 | 152 | .259 | .17 |
| 2.0 | 1.5 | 1.63 | 117 | .259 | .15 |
| 2.0 | 2.0 | 1.41 | 82 | .259 | .12 |
| <u>Specimen Configuration H</u> | | | | | |
| 2.5 | 2.0 | 1.77 | 268 | .398 | .22 |
| <u>Specimen Configuration L</u> | | | | | |
| 2.0 | 1.2 | 1.83 | 178 | .289 | .20 |
| 2.0 | 1.5 | 1.63 | 137 | .289 | .19 |
| 2.0 | 2.0 | 1.41 | 92 | .289 | .17 |

can be used to put the speeds obtained in the two different sections on a common basis. Here, the subscript T denotes properties of the test section, S the starting section. The statement made above is then equivalent to stating that, by plotting the speeds obtained in each section as a function of K_q/K_d for that section, the results will fall on a single curve. Notice, however, that the distance propagated at arrest is very definitely dependent on the entire process, as evidenced by the data shown in Table 3.

Figures 5 and 6 show the computational results for a duplex specimen in which $K_q/K_d = 2$ in the test section. The value of K_q/K_d in the starter section is 3 which allows a very high crack speed to be achieved prior to its entry into the test section. Despite this, the steady-state speed that is achieved in the test section is $0.191 C_0$ which compares well with the value $0.180 C_0$ calculated in Figure 3. Crack arrest, on the other hand, occurs at $a_r/h = 4.925$. This is in contrast to the value $a_r/h = 4.250$ obtained for a single-section specimen with $K_q/K_d = 2$ and no arrest within the specimen when $K_q/K_d = 3$.

One of the attractive features of having an analytical model in conjunction with an experimental program is that it makes possible a systematic investigation of some aspect of the problem that would be quite awkward to accomplish experimentally. As an example, the effect of load pin mass can be approximately determined. Within the confines of beam theory, the contribution of the mass of the load pins can most conveniently be taken into account by varying the beam density while leaving its dimensions unchanged. This introduces a correction into the equations of motion for the load point which is related to the quantity

$$\Delta M = \frac{\pi D}{4 h} \left(\frac{\ell}{b} - 1 \right)$$

where D is the pin diameter, ℓ is the pin length and, as above, b and h are the specimen thickness and half height, respectively. It has been assumed that the density of the pin material and the specimen material are the same although differing densities could be accounted for in an obvious way.

In Table 4 are shown the relative effect of the additional mass contributed by the load pins on the distance propagated at arrest and on the average crack speed in a typical case. It can be seen that while these results are not especially sensitive to the pin mass, there may well be instances where the effect should be considered. In addition, the movement of the pins while the propagation event is in progress can be important in interpreting the experimental results. Such results can be obtained from the analysis and are also shown in Table 4 at two different stages of the crack propagation event. It should be pointed out that in the current calculation the wedge is considered to be fixed. In actuality some movement occurs. Finally, it is interesting to notice that the oscillations of the computed crack length-time calculation generally diminish as the load pins become relatively more massive.

In conclusion, the analytical model for unstable crack propagation developed in this report has now been demonstrated to predict results that are in very good accord with the experimental observations. This is taken as conclusive support for the energy-balance approach to crack propagation and arrest. In fact, the most important result of the work described here is to certify the correctness of this approach for use in less specialized applications. Possibly the most direct proof of the validity of the energy balance point of view are plots, typified by Figure 3, which show that the kinetic energy at the time of crack arrest is practically zero.

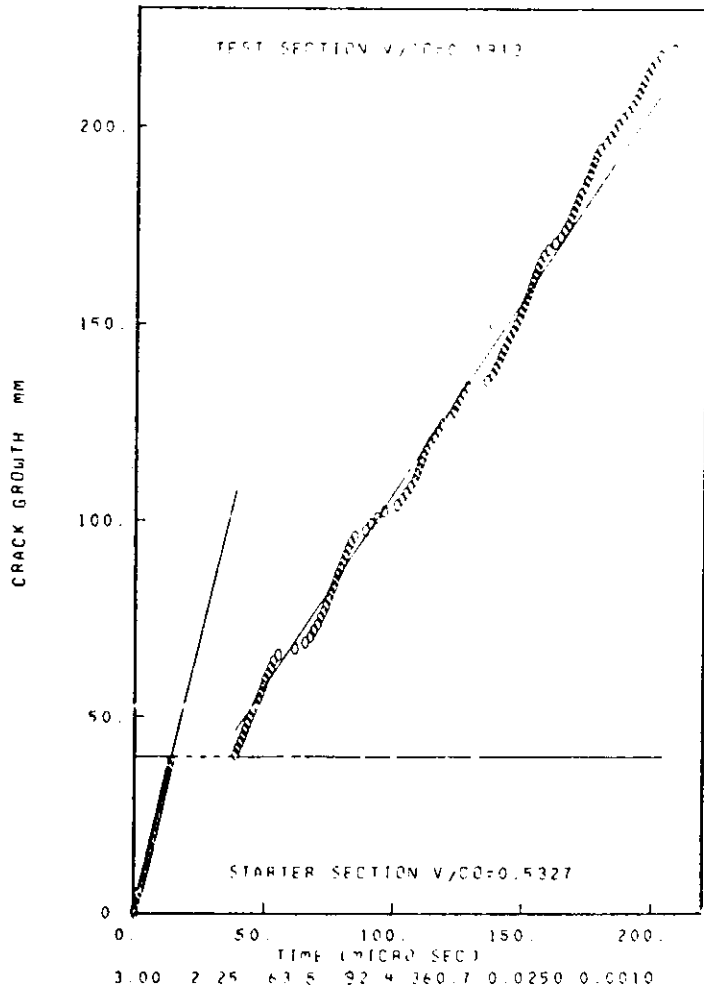


FIGURE 5. SPECIMEN B, $(K_q/K_d)_S = 3.0$,
 $(K_q/K_d)_T = 2.0$

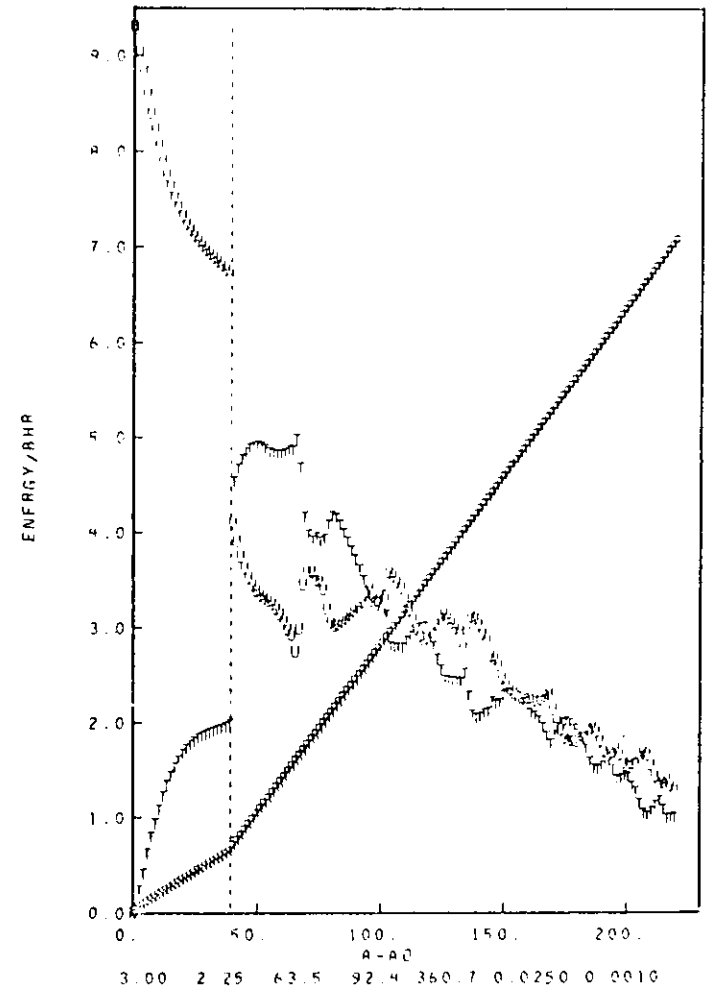


FIGURE 6. SPECIMEN B, $(K_q/K_d)_S = 3.0$,
 $(K_q/K_d)_T = 2.0$

TABLE IV - COMPUTATIONAL RESULTS SHOWING THE RELATIVE EFFECTS OF VARYING THE MASS OF THE LOAD PINS*

| $K_q/K_d = 2$ Specimen A | | | | |
|--|--------------------------------|--|---|--|
| <u>Comparative increase in mass at load point due to the load pins</u> | <u>Comparative crack speed</u> | <u>Comparative crack growth at point of arrest</u> | <u>Ratio of pin displacement from initial configuration</u> | |
| | | | <u>at time of arrest</u> | <u>120 μ sec after arrest</u> |
| 0.0 | 1.105 | 0.928 | 1.193 | 1.325 |
| 0.5 | 1.079 | 0.928 | 1.110 | 1.176 |
| 1.0 | 1.000 | 1.000 | 1.072 | 1.120 |
| 1.5 | 0.887 | 1.000 | 1.033 | 1.046 |
| 2.0 | 0.780 | 0.982 | 1.005 | 1.002 |

* The entries in this table are the ratios of the given result to the result determined in the standard case. In the standard case the load pins had a diameter of 25.4 mm., a length of 88.0 mm., the specimen thickness was 25.4 mm. with the density of the pin and the specimen being equal. For the results of the standard case, see Table 3.

There are, to be sure, aspects of the analytical model that could still be improved upon. In particular, the simulation of the crack-blunting effect by imposing a point force and couple at the crack tip in the initial configuration is a gross oversimplification. This was acceptable in the previous models (i.e., with a Euler-Bernoulli beam) because it introduced a discontinuity only in the third derivative of w . In a parabolic system, this effect is inconsequential. In the present formulation, however, discontinuities exist in the first derivatives of the two dependent variables and, the equation is hyperbolic. Consequently, the spurious effects introduced by the point force and couple remain highly visible throughout the computation. This is believed to be the reason for the high amplitude of the periodic oscillation about the mean as seen, for example, in Figure 2.

In addition to a more precise treatment of the initial bluntness, consideration might also be given in improving the model to account for the interaction between the wedge and the load pins. Currently being neglected is the possibility that a torque is applied to the specimen due to friction at the contacting surfaces. Movement of the wedge and the related contact forces (acting on both ends of the specimen) while the crack is propagating are similarly neglected. Of even more importance is the current restriction to a single value of K_d throughout the entire crack propagation process. However, these improvements are almost certainly second-order effects and, while desirable, they are not likely to change the gross features of the results given in this report.

V. REFERENCES

1. M. F. Kanninen, "An Augmented Double Cantilever Beam Model for Studying Crack Propagation and Arrest", Int. J. Fracture Mech., Vol. 9, p. 83, 1973.
2. G. T. Hahn, R. G. Hoagland, M. F. Kanninen, and A. R. Rosenfield, "A Preliminary Study of Fast Fracture and Arrest in the DCB-Test Specimen", Dynamic Crack Propagation Conference, Lehigh University, 1972.
3. M. F. Kanninen, A. R. Rosenfield, and R. G. Hoagland, "Fast Fracture in PMMA", Deformation and Fracture of High Polymers, H. Kausch, et al., eds. (in press).
4. G. T. Hahn, R. G. Hoagland, M. F. Kanninen, and A. R. Rosenfield, "The Characterization of Fast Fracture and Arrest in Structural Materials", Third International Conference on Fracture, Munich, Germany, April, 1973.
5. L. Prandtl, "Ein Gedankenmodell für den Zerreißvorgang spröder Körper", ZAMM, Vol. 13, p. 129, 1933.
6. Z. J. Bilek and S. J. Burns, "The Dynamics of Crack Propagation in Double Cantilever Beam Specimens", Dynamic Crack Propagation, Lehigh University, 1972.
7. S. P. Timoshenko, "On the Correction for Shear of the Differential Equation for Transverse Vibrations of Prismatic Bars", Phil. Mag., Vol. 41, p. 744, 1921.
8. S. P. Timoshenko, "On the Transverse Vibrations of Bars of Uniform Cross-Section", Phil. Mag., Vol. 43, p. 125, 1922.
9. A. D. Kerr, "Elastic and Viscoelastic Foundation Models", J. Appl. Mech., Vol. 31, p. 491, 1964.
10. G. R. Cowper, "The Shear Coefficient in Timoshenko's Beam Theory", J. Appl. Mech., Vol. 33, p. 335, 1966.
11. S. Mostovoy, P. B. Crosley, and E. J. Ripling, "Use of the Crack-Line-Loaded Specimens for Measuring Plane Strain Fracture Toughness", J. Mat., Vol. 2, p. 661, 1967.
12. B. Gross and J. E. Srawley, "Stress Intensity Factors by Boundary Collocation for Single-Edge-Notch Specimens Subject to Splitting Forces", NASA Tech. Note D-3295, 1966.
13. S. M. Wiederhorn, A. M. Shorb, and R. L. Moses, "Critical Analysis of the Theory of the Double Cantilever Method of Measuring Fracture Surface Energies", J. Applied Physics, Vol. 39, p. 1569, 1968.
14. G. E. Forsythe and W. R. Wasow, "Hyperbolic Equations In Two Independent Variables", Chapter 1, Finite Difference Methods for Partial Differential Equations, Wiley, New York, pp. 15-87, 1960.

APPENDIX 3-A

DERIVATION OF THE GOVERNING EQUATIONS FOR THE
TIMOSHENKO BEAM-GENERALIZED ELASTIC
FOUNDATION MODEL OF THE DCB SPECIMEN

The incorporation of the Timoshenko beam and generalized elastic foundation ideas into the model of the DCB specimen can best be accomplished by using three-dimensional elasticity theory, thereby generalizing the derivation given by Cowper(10). Let x be the coordinate along the length of the beam and consider that beam cross sections lie in the y - z plane with the beam deflection taking place in the z -direction. Then, following Cowper, the quantities ordinarily arising in elementary beam theory are given precise definitions in terms of the variables of three-dimensional theory of elasticity. In particular, the beam deflection w is defined as the net displacement of the cross section via the relation

$$w = \frac{1}{A} \iint u_z dydz \quad (A-1)$$

where A is the area of the cross section and u_z is the displacement component in the z -direction. Similarly, the transverse-shearing force S acting on the cross section is defined as

$$S = \iint \tau_{xz} dydz \quad (A-2)$$

where τ_{xz} is a component of the shearing stress. In both of these equations, of course, the integration extends over the cross section.

The equation of motion of a beam element with respect to forces in the z -direction is

$$\frac{\partial \tau_{xz}}{\partial x} + \frac{\partial \tau_{yz}}{\partial y} + \frac{\partial \sigma_z}{\partial z} + F_z = \rho \frac{\partial^2 u_z}{\partial t^2} \quad (A-3)$$

where F_z is the body force, ρ is the mass density and t denotes time. Integration of Equation (A-3) over the cross section gives

$$\begin{aligned} \frac{\partial}{\partial x} \iint \tau_{xz} dydz + \iint \left\{ \frac{\partial \tau_{yz}}{\partial y} + \frac{\partial \sigma_z}{\partial z} + F_z \right\} dy dz = \\ = \rho \frac{\partial^2}{\partial t^2} \iint u_z dy dz \end{aligned} \quad (A-4)$$

By application of the divergence theorem, Cowper shows that the second term in the above is simply p , the total transverse load applied to the beam. In the present situation this is just the force exerted by the springs. Hence, for linear springs

$$p = -k_e w \quad (A-5)$$

Using this relation together with Equations (A-1) and (A-2), Equation (A-4) becomes

$$\frac{\partial S}{\partial x} - k_e w = \rho A \frac{\partial^2 w}{\partial t^2} \quad (A-6)$$

which is the first of four basic equations of the model.

Cowper next introduces a parameter Ψ which represents the mean angle of rotation of a beam cross section about the neutral axis.* Hence

$$\Psi = -\frac{1}{I} \iiint z u_x \, dy \, dz \quad (A-7)$$

where $I (= bh^3/12$ for a rectangular cross section of height h and width b) is the moment of inertia of the cross section with respect to the neutral axis. Notice that if (as in the elementary beam theory) cross sections remain plane, then u_x would be proportional to $-z$ whereupon Ψ would be exactly equal to the slope of the beam. In general, however, there is warping in addition to rotation and the equality does not hold.

The equation of motion of a beam element with respect to forces in the x -direction is

$$\frac{\partial \sigma_x}{\partial x} + \frac{\partial \tau_{xy}}{\partial y} + \frac{\partial \tau_{xz}}{\partial z} + F_x = \rho \frac{\partial^2 u_x}{\partial t^2} \quad (A-8)$$

Multiplying each term by z and integrating over the cross section gives

$$\begin{aligned} \frac{\partial}{\partial x} \iint z \sigma_x \, dy \, dz + \iint z \left\{ \frac{\partial \tau_{xy}}{\partial y} + \frac{\partial \tau_{xz}}{\partial z} + F_x \right\} \, dy \, dz = \\ = \rho \frac{\partial^2}{\partial t^2} \iint z u_x \, dy \, dz \end{aligned} \quad (A-9)$$

The first integral can be interpreted as the net bending moment acting at any cross section. Hence, let

* Cowper's parameter is just the same as that given by Equation (A-7) but with the minus sign omitted. The negative is used here to conform with the more commonly accepted form.

$$M = \iiint z \sigma_x \, dy \, dz \quad (A-10)$$

The second term can be interpreted by rewriting it in order to apply the divergence theorem. That is,

$$\begin{aligned} \iiint z \left\{ \frac{\partial \tau_{xy}}{\partial y} + \frac{\partial \tau_{xz}}{\partial z} + F_x \right\} dy \, dz &= \\ &= \iiint \left\{ \frac{\partial}{\partial y} (z \tau_{xy}) + \frac{\partial}{\partial z} (z \tau_{xz}) - \tau_{xz} + z F_x \right\} dy \, dz \\ &= \oint z \left\{ n_y \tau_{xy} + n_z \tau_{xz} \right\} ds + \iiint \left\{ z F_x - \tau_{xz} \right\} dy \, dz \end{aligned}$$

Here, n_y and n_z are the components of the unit normal to the cross section and ds is an element of arc of the cross section boundary. The first term represents q , the moment of the applied forces, while the second term is just S when, as assumed here, F_x is either constant or zero. There are two contributions to the applied bending moment: that due to the torsional stiffness of the foundation and that due to the axial force F . Both are proportional to the mean angle of rotation of the cross section. Specifically,

$$q = k_r \Psi + F \Psi \quad (A-11)$$

where k_r is the foundation modulus for rotational deformation and F is the axial compressive force. Finally, substituting Equations (A-2), (A-7) and (A-10) into Equation (A-9) gives

$$\frac{\partial M}{\partial x} + (k_r + F) \Psi - S = -\rho I \frac{\partial^2 \Psi}{\partial t^2} \quad (A-12)$$

which is the second equation of the model.

A relation between the bending moment and the rotation is obtained next from the Hooke's law equation for deformation in the x -direction,

$$E \epsilon_x = E \frac{\partial u_x}{\partial x} = \sigma_x - \nu (\sigma_y + \sigma_z) \quad (A-13)$$

Following Cowper, the stresses σ_y and σ_z are considered to be negligible in comparison to σ_x and are dropped. Then, multiplying (A-13) through by z and integrating over the cross section, it is found that

$$E \frac{\partial}{\partial x} \iiint z u_x \, dy \, dz = \iiint z \sigma_x \, dy \, dz$$

Substituting Equations (A-7) and (A-10) then gives

$$-EI \frac{\partial \Psi}{\partial x} = M \quad (A-14)$$

which is the third equation of the model. Notice that in deriving this relation, for the first time an assumption other than that normally arising in linear elasticity was used.

The Hooke's law equation for shear deformation in the plane of the cross section is

$$G \gamma_{xz} = G \left\{ \frac{\partial u_x}{\partial z} + \frac{\partial u_z}{\partial x} \right\} = \tau_{xz} \quad (A-15)$$

Integrating over the cross section gives

$$\iint \frac{\partial u_x}{\partial z} dy dz + \frac{\partial}{\partial x} \iint u_z dy dz = \frac{1}{G} \iint \tau_{xz} dy dz$$

Now, defining a "residual" displacement u'_x such that

$$u_x = \frac{1}{A} \iint u_x dy dz - z\psi + u'_x \quad (A-16)$$

Then

$$\frac{\partial u_x}{\partial z} = -\psi + \frac{\partial u'_x}{\partial z}$$

Using this result together with Equation (A-1), then, gives

$$\iint \left\{ -\psi + \frac{\partial u'_x}{\partial z} \right\} dy dz + \frac{\partial}{\partial x} \{Aw\} = \frac{1}{G} \iint \tau_{xz} dy dz$$

or

$$-\psi + \frac{\partial w}{\partial x} = \frac{1}{GA} \iint \left\{ \tau_{xz} - G \frac{\partial u'_x}{\partial z} \right\} dy dz \quad (A-17)$$

The raison d'etre of Cowper's work is the evaluation of the integral in Equation (A-17) and its interpretation of the "shear coefficient" κ which, in effect, is defined such that

$$\frac{1}{GA} \iint \left\{ \tau_{xz} - G \frac{\partial u'_x}{\partial z} \right\} dy dz = \frac{S}{\kappa GA} \quad (A-18)$$

The evaluation of this integral involves the further assumption that the shearing stresses do not vary too rapidly along the length of the beam. Given this, κ can be evaluated for a number of cross-section shapes. Of interest here is the result for a rectangular cross section which is $\kappa = 10(1+\nu)/(12+11\nu)$. Consequently, the fourth and final basic equation of the model is given by combining Equations (A-17) and (A-18) to get

$$\frac{\partial w}{\partial x} - \psi = \frac{S}{\kappa GA} \quad (A-19)$$

which relates the shearing force to the deflection and rotation of the beam.

A more convenient form is obtained by eliminating M and S from Equations (A-6), (A-12), (A-14) and (A-19) in order to have two equations in two unknowns. This is accomplished by first substituting (A-19) into (A-6) to get

$$\kappa GA \frac{\partial}{\partial x} \left\{ \frac{\partial w}{\partial x} - \Psi \right\} - k_e w = \rho A \frac{\partial^2 w}{\partial t^2}$$

Then, substituting (A-14) and (A-19) into (A-12) gives

$$-EI \frac{\partial^2 \Psi}{\partial x^2} + (k_r + F)\Psi - \kappa GA \left\{ \frac{\partial w}{\partial x} - \Psi \right\} = -\rho I \frac{\partial^2 \Psi}{\partial t^2}$$

Finally, the two governing equations can be written in terms of a foundation partially supporting the beam by introducing an arbitrary (at this point at least) crack extension parameter θ . Then

$$\begin{aligned} EI \frac{\partial^2 \Psi}{\partial x^2} + \kappa GA \left\{ \frac{\partial w}{\partial x} - \Psi \right\} - F\Psi - k_r H^* (\theta_c - \theta)\Psi &= \\ &= \rho I \frac{\partial^2 \Psi}{\partial t^2} \end{aligned} \quad (A-20)$$

and

$$\kappa GA \left\{ \frac{\partial^2 w}{\partial x^2} - \frac{\partial \Psi}{\partial x} \right\} - k_e H^* (\theta_c - \theta)w = \rho A \frac{\partial^2 w}{\partial t^2} \quad (A-21)$$

where θ_c denotes a critical value of the crack extension parameter and H^* is the ordinary Heaviside step function.

$$H(x) = \begin{cases} 1, & x > 1 \\ 0, & x < 1 \end{cases} \quad (A-22)$$

which is modified to allow a switch from unity to zero but not vice versa. Equations (A-20) and (A-21) are the governing equations for the Timoshenko beam-generalized elastic foundation model of the DCB specimens that are used in this work.

APPENDIX 3-B

DERIVATION OF THE COMPONENTS OF ENERGY AND
THE CRACK-EXTENSION CRITERION FOR THE TIMOSHENKO
BEAM-GENERALIZED ELASTIC FOUNDATION DCB MODEL

A completely general statement of the strain energy per unit volume in three-dimensional isotropic elasticity theory is

$$dU = \frac{1}{2} \left\{ \sigma_x \epsilon_x + \sigma_y \epsilon_y + \sigma_z \epsilon_z + \tau_{xy} \gamma_{xy} + \tau_{yz} \gamma_{yz} + \tau_{xz} \gamma_{xz} \right\} \quad (B-1)$$

Consistent with the derivation given in Appendix A, all of the stress components in the Timoshenko beam can be neglected with the exception of σ_x and τ_{xz} . Hence, for the beam, exclusive of the foundation

$$dU_b = \frac{1}{2} \left\{ \sigma_x \epsilon_x + \tau_{xz} \gamma_{xz} \right\}$$

or

$$dU_b = \frac{1}{2} \left\{ \sigma_x \frac{\partial u_x}{\partial x} + \tau_{xz} \left[\frac{\partial u_z}{\partial x} + \frac{\partial u_x}{\partial z} \right] \right\} \quad (B-2)$$

In order to use the results of Appendix A it is necessary to integrate over the beam cross section separately, deferring the integration over the length (i.e., in the x-direction) until later. Hence, let

$$U_b = \int U_{b,x} dx \quad (B-3)$$

so that

$$U_{b,x} = \frac{1}{2} \iint \left\{ \sigma_x \frac{\partial u_x}{\partial x} + \tau_{xz} \left[\frac{\partial u_z}{\partial x} + \frac{\partial u_x}{\partial z} \right] \right\} dy dz \quad (B-4)$$

where the integration is taken over the beam cross section.

To evaluate the integral in Equation (B-4), it is convenient to introduce two "residual" displacement components such that

$$u_z = w + u'_z \quad (B-5)$$

and

$$u_x = \bar{u}_x - z\psi + u'_x \quad (B-6)$$

where, by definition

$$\bar{u}_x = \frac{1}{A} \iint u_x dy dz$$

and other quantities are as in Appendix A. It should be recognized that u'_z and u'_x would be exactly zero if the beam cross sections remain plane in bending and, therefore, are likely to be small with respect to the total displacements.

Substituting Equations (B-5) and (B-6) into Equation (B-4), noting that w , Ψ and \bar{u}_x are functions of x only, gives a result that can be written

$$2U_{b,x} = -\frac{\partial \Psi}{\partial x} \int \int z \sigma_x dydz + \left\{ \frac{\partial w}{\partial x} - \Psi \right\} \int \int \tau_{xz} dydz + \int \int \left\{ \sigma_x \left[\frac{\partial \bar{u}_x}{\partial x} + \frac{\partial u'_x}{\partial x} \right] + \tau_{xz} \left[\frac{\partial u'_z}{\partial x} + \frac{\partial u'_x}{\partial z} \right] \right\} dydz \quad (B-7)$$

Now, on the basis of the statement made above and consistent with the assumptions introduced by Cowper, the third integral in Equation (B-7) can be assumed to be negligible. Then, the remaining two integrals can be evaluated using results derived in Appendix A. In particular, by combining Equation (A-10) with (A-14) and Equation (A-2) with (A-19), it is found that

$$\int \int z \sigma_x dydz = -EI \frac{\partial \Psi}{\partial x} \quad (B-8)$$

and

$$\int \int \tau_{xz} dydz = KGA \left\{ \frac{\partial w}{\partial x} - \Psi \right\} \quad (B-9)$$

Substituting these into Equation (B-7) and the result into Equation (B-3) then gives

$$U_b = \frac{1}{2} \int \left\{ EI \left(\frac{\partial \Psi}{\partial x} \right)^2 + KGA \left[\frac{\partial w}{\partial x} - \Psi \right]^2 \right\} dx \quad (B-10)$$

for the strain energy of the beam.

The strain energy of the foundation and the kinetic energy of the beam can be written down by inspection. These are, respectively,

$$U_s = \frac{1}{2} \int \left\{ k_e w^2 + k_r \Psi^2 \right\} dx \quad (B-11)$$

and

$$T = \frac{1}{2} \int \left\{ \rho A \left(\frac{\partial w}{\partial t} \right)^2 + \rho I \left(\frac{\partial \Psi}{\partial t} \right)^2 \right\} dx \quad (B-12)$$

To the energies given by Equations (B-10), (B-11) and (B-12) must be added the energy $F\Psi^2$ which then completely accounts for the energy contained in a Timoshenko beam on a generalized elastic foundation. For the DCB model, however, the energy

released by crack extension must be accounted for as well. To evaluate this, Equations (B-10) and (B-11) are first combined to obtain the strain energy of a DCB specimen of length L using a beam partly supported by an elastic foundation. This is

$$U = \int_0^L \left\{ EI \left(\frac{\partial \Psi}{\partial x} \right)^2 + KGA \left(\frac{\partial w}{\partial x} - \Psi \right)^2 + F\Psi^2 + H^*(\theta_c - \theta) \left[k_e w^2 + k_r \Psi^2 \right] \right\} dx \quad (B-13)$$

where H^* is the function defined by Equation (A-22). Notice that the factor $\frac{1}{2}$ has been omitted because U now represents the total strain energy of the DCB specimen which is considered to be composed of two identical beams. Similarly, the kinetic energy of the DCB specimen is

$$T = \int_0^L \left\{ \rho A \left(\frac{\partial w}{\partial t} \right)^2 + \rho I \left(\frac{\partial \Psi}{\partial t} \right)^2 \right\} dx \quad (B-14)$$

To both verify the correctness of Equations (B-13) and (B-14) and as a preliminary step in deducing the appropriate fracture criterion, the time derivative of the total energy of the system will now be calculated.

Beginning with (B-14), upon differentiation with respect to t , it can readily be seen that

$$\frac{dT}{dt} = 2 \int_0^L \left\{ \rho A \frac{\partial w}{\partial t} \cdot \frac{\partial^2 w}{\partial t^2} + \rho I \frac{\partial \Psi}{\partial t} \cdot \frac{\partial^2 \Psi}{\partial t^2} \right\} dx \quad (B-15)$$

Next, differentiating Equation (B-13) with respect to t and simplifying by appropriate use of integration by parts gives

$$\begin{aligned} \frac{dU}{dt} = 2 \int_0^L \left\{ -EI \frac{\partial \Psi}{\partial t} \cdot \frac{\partial^2 \Psi}{\partial x^2} + KGA \left[-\frac{\partial w}{\partial t} \cdot \frac{\partial^2 w}{\partial x^2} + \right. \right. \\ \left. \left. - \frac{\partial \Psi}{\partial t} \cdot \frac{\partial w}{\partial x} + \frac{\partial w}{\partial t} \cdot \frac{\partial \Psi}{\partial x} + \Psi \cdot \frac{\partial \Psi}{\partial t} \right] + F\Psi + \right. \\ \left. + H^*(\theta_c - \theta) \left[k_e w \cdot \frac{\partial w}{\partial t} + k_r \Psi \cdot \frac{\partial \Psi}{\partial t} \right] + \right. \\ \left. + \frac{1}{2} \left[k_e w^2 + k_r \Psi^2 \right] \frac{\partial H^*(\theta_c - \theta)}{\partial t} \right\} dx + \\ \left. + \left[EI \frac{\partial \Psi}{\partial x} \cdot \frac{\partial \Psi}{\partial t} + KGA \frac{\partial w}{\partial t} \left(\frac{\partial w}{\partial x} - \Psi \right) \right]_0^{-L} \end{aligned} \quad (B-16)$$

The final term in the above is the rate at which work is being done by shearing forces and moments acting at the ends of the specimen. Under the conditions being considered here, these contributions are zero. This term can be dropped, therefore.

Now, it is unlikely that the crack-extension criterion will be simultaneously met at more than one position, but the possibility can nevertheless be admitted as follows. Let $x = \alpha_0, x = \alpha_1, \dots, x = \alpha_N$ be the positions which at time t , $\theta(x) = \theta_c$ and $\frac{d\theta}{dx} < 0$. Let $x = \beta_1, x = \beta_2, \dots, x = \beta_N$ be similar positions except that $\frac{d\theta}{dx} > 0$. Notice that unless there are "islands" of uncracked material, $N = 0$. Hence,

$$H^*(\theta - \theta_c) = H(x - \alpha_0) + \sum_{i=1}^N \{H(x - \alpha_i) - H(x - \beta_i)\} \quad (B-17)$$

Recalling that the step function H^* permits a transition from 1 to 0 but not vice versa,

$$\frac{\partial H^*(\theta_c - \theta)}{\partial t} = - \sum_{i=0}^N \frac{\partial \alpha_i}{\partial t} \cdot \Delta(x - \alpha_i)$$

where Δ denotes the Dirac delta function. Substituting this into Equation (B-16) then gives

$$\begin{aligned} \frac{dU}{dt} = & -2 \int_0^L \frac{\partial \Psi}{\partial t} \left\{ EI \frac{\partial^2 \Psi}{\partial x^2} + KGA \left[\frac{\partial w}{\partial x} - \Psi \right] - F\Psi - k_r H^*(\theta_c - \theta) \Psi \right\} dx + \\ & - 2 \int_0^L \frac{\partial w}{\partial t} \left\{ KGA \left[\frac{\partial^2 w}{\partial x^2} - \frac{\partial \Psi}{\partial x} \right] - k_e H^*(\theta_c - \theta) w \right\} dx + \\ & - \sum_{i=0}^N \frac{\partial \alpha_i}{\partial t} \left[k_c w^2 + k_r \Psi^2 \right]_{x=\alpha_i} \end{aligned} \quad (B-18)$$

Adding Equations (B-15) and (B-18) then gives

$$\begin{aligned} \frac{dU}{dt} + \frac{dT}{dt} = & 2 \int_0^L \frac{\partial \Psi}{\partial t} \left\{ \rho I \frac{\partial^2 \Psi}{\partial t^2} - EI \frac{\partial^2 \Psi}{\partial x^2} - KGA \left[\frac{\partial w}{\partial x} - \Psi \right] + \right. \\ & \left. + F\Psi + k_r H^*(\theta_c - \theta) \Psi \right\} dx + 2 \int_0^L \frac{\partial w}{\partial t} \left\{ \rho A \frac{\partial^2 w}{\partial t^2} + \right. \\ & \left. - KGA \left[\frac{\partial^2 w}{\partial x^2} - \frac{\partial \Psi}{\partial x} \right] + k_e H^*(\theta_c - \theta) w \right\} dx + \\ & - \sum_{i=0}^N \frac{\partial \alpha_i}{\partial t} \left[k_e w^2 + k_r \Psi^2 \right]_{x=\alpha_i} \end{aligned}$$

Comparison with Equations (A-20) and (A-21) shows that the two integrals are identically zero. Thus,

$$\frac{dU}{dt} + \frac{dT}{dt} = - \sum_{i=0}^N \left(\frac{d\alpha_i}{dt} \right) \cdot \left[k_e w^2 + k_r \psi^2 \right]_{x=\alpha_i} \quad (B-19)$$

which proves that energy is conserved for a nonrupturing foundation and, therefore, shows that the basic formulation of the energy terms is consistent with the governing equations of motion.

Under the condition that no external work is done on the specimen during crack extension, the total energy of the system is U+T minus the energy absorbed at the crack tip. Let \mathcal{R}_i denote the energy absorbed in the foundation of new crack surfaces per unit area of crack advance at the point $x = \alpha_i$. Application of the fundamental energy balance principle of fracture mechanics then requires that

$$\frac{dU}{dt} + \frac{dT}{dt} + \sum_{i=0}^N b_i \mathcal{R}_i \frac{d\alpha_i}{dt} = 0 \quad (B-20)$$

where b_i denotes the thickness of the specimen at $x = \alpha_i$. Combining Equations (B-19) and (B-20) then gives

$$\sum_{i=0}^N \left(\frac{d\alpha_i}{dt} \right) \left\{ b_i \mathcal{R}_i - \left[k_e w^2 + k_r \psi^2 \right]_{x=\alpha_i} \right\} = 0 \quad (B-21)$$

which is for the general situation wherein "islands" of uncracked material exist, each being ruptured at a different rate.

In the simpler situation of a unique crack tip at the point $x = a$ in a constant-thickness constant-toughness specimen, Equation (B-21) reduces to

$$b\mathcal{R} = \left[k_e w^2 + k_r \psi^2 \right]_{x=a} \quad (B-22)$$

which reveals that the crack-extension parameter must be associated with a critical value of the bracketed quantity. Notice that for a Winkler foundation (where $k_e = 2Eb/h$ and $k_r = 0$), Equation (B-22) defines a critical beam deflection w_c . This is

$$w_c = \left(\frac{h}{2} \frac{\mathcal{R}}{E} \right)^{\frac{1}{2}} \quad (B-23)$$

which remains useful as a reference length even in the more general situation now being considered.

APPENDIX 3-C

SOLUTION FOR INITIAL CRACK EXTENSION IN
THE TIMOSHENKO BEAM-GENERALIZED ELASTIC FOUNDATION DCB MODEL

The governing equations for a DCB specimen modeled by a Timoshenko beam and a generalized elastic foundation for initial crack extension can be obtained by simply omitting the inertia terms in Equations (A-20) and (A-21). This gives

$$EI \frac{d^2 \Psi}{dx^2} + KGA \left\{ \frac{dw}{dx} - \Psi \right\} - k_r H(x) \Psi = 0 \quad (C-1)$$

and

$$KGA \left\{ \frac{d^2 w}{dx^2} - \frac{d\Psi}{dx} \right\} - k_e H(x) w = 0 \quad (C-2)$$

Note that it is convenient here to take the origin at the crack tip and the Heaviside step function has been adjusted accordingly. The boundary conditions are those corresponding to an applied shearing force P and zero bending moment at the cracked end with stress-free conditions at the other. Using Equations (A-14) and (A-19), these can be expressed as

$$KGA [w'(-a) - \Psi(-a)] = P$$

and

$$\Psi'(-a) = \Psi'(c) = w'(c) - \Psi(c) = 0 \quad (C-3)$$

where $c = L-a$ is the "uncracked" length of the specimen. Notice that in the case of the semi-infinite beam considered below, the dimension c is considered to greatly exceed all other beam dimensions.

The procedure to be followed here is, (1) to separate the problem into the two regions where the differential equations (C-1) and (C-2) have constant coefficients, (2) to determine the solutions for the two regions independently, using the Laplace transform technique for the $x > 0$ region, (3) satisfy the boundary conditions on the extremities of the region, and (4) match the solutions at the interface between regions. From the result so obtained, expressions can be deduced for the strain-energy-release rate and, in turn, the stress-intensity factor. The latter quantity will then be compared with known experimental and two-dimensional computational results to establish the validity of the model for the dynamic situation. As a second benefit, the solution will provide the initial conditions for the dynamic solution in closed form. Thirdly, the exact value of the total energy so obtained can be used to help judge the accuracy of the finite difference calculation.

Preliminary Analysis

In the region $x < 0$, the beam is free and Equations (C-1) and (C-2) reduce to

$$EI \frac{d^2 \Psi}{dx^2} + KGA \left\{ \frac{dw}{dx} - \Psi \right\} = 0$$

and

$$KGA \left\{ \frac{d^2 w}{dx^2} - \frac{d\Psi}{dx} \right\} = 0$$

These can be integrated easily. To facilitate the matching requirement, the results are most conveniently written as

$$w(x) = \frac{P}{6EI} \left\{ x^3 + 3ax^2 - \frac{6EI}{KGA} x \right\} + \Psi(0^-)x + w(0^-) \quad (C-4)$$

and

$$\Psi(x) = \frac{P}{2EI} \left\{ x^2 + 2ax \right\} + \Psi(0^-) \quad (C-5)$$

where $w(0^-)$ and $\Psi(0^-)$ denote the values at the interface between the regions. Notice that Equations (C-4) and (C-5) already satisfy the boundary conditions at $x = -a$; i.e., Equations (C-3).

In the region $x > 0$, the beam is supported by the foundation whereupon Equations (C-1) and (C-2) become

$$EI \frac{d^2 \Psi}{dx^2} + KGA \left\{ \frac{dw}{dx} - \Psi \right\} - k_r \Psi = 0 \quad (C-6)$$

$$KGA \left\{ \frac{d^2 w}{dx^2} - \frac{d\Psi}{dx} \right\} - k_e w = 0 \quad (C-7)$$

The integration of these two equations can be accomplished by use of the Laplace Transform. That is, let

$$\bar{w}(s) = \int_0^{\infty} e^{-sx} w(x) dx$$

$$\bar{\Psi}(s) = \int_0^{\infty} e^{-sx} \Psi(x) dx$$

Applying these to Equations (C-6) and (C-7) then gives

$$\kappa G A s \bar{w} + [E I s^2 - (k_r + \kappa G A)] \bar{\psi} = E I [\psi'(0^+) + s \psi(0^+)] + \kappa G A w(0^+)$$

$$[\kappa G A s^2 - k_e] \bar{w} - \kappa G A s \bar{\psi} = \kappa G A [w'(0^+) + s w(0^+) - \psi(0^+)]$$

By defining the parameters

$$\begin{aligned} \beta_e^2 &= \frac{k_e}{\kappa G A} \\ \beta_r^2 &= \frac{k_r}{E I} \\ \epsilon^2 &= \frac{\kappa G A}{E I} \end{aligned} \quad (C-8)$$

and solving the pair of simultaneous algebraic equations, it is found that

$$\begin{aligned} \bar{w}(s) &= \{w(0^+)s^3 + w'(0^+)s^2 + [\psi'(0^+) - \beta_r^2 w(0^+)] + \\ &\quad - [\beta_r^2 + \epsilon^2] [w'(0^+) - \psi(0^+)]\} \cdot \{s^4 - [\beta_r^2 + \beta_e^2]s^2 + \beta_e^2 [\beta_r^2 + \epsilon^2]\}^{-1} \end{aligned} \quad (C-9)$$

and

$$\begin{aligned} \bar{\psi}(s) &= \{\psi(0^+)s^3 + \psi'(0^+)s^2 - [\beta_e^2 \psi(0^+) + \epsilon^2 (w'(0^+) - \psi(0^+))]\} s + \\ &\quad - \beta_e^2 [\psi'(0^+) + \epsilon^2 w(0^+)]\} \cdot \{s^4 - [\beta_r^2 + \beta_e^2]s^2 + \beta_e^2 [\beta_r^2 + \epsilon^2]\}^{-1} \end{aligned} \quad (C-10)$$

The inverse transform can be obtained from Equations (C-9) and (C-10) by standard techniques. As is often the case, the form of the solution will depend on the relative sizes of the parameters appearing in the problem. In particular, it is assumed that

$$4\beta_e^2(\beta_r^2 + \epsilon^2) > (\beta_r^2 + \beta_e^2)^2$$

or, using Equation (C-8), that

$$4 \frac{k_e}{E I} > \left\{ \frac{k_e}{\kappa G A} - \frac{k_r}{E I} \right\}^2 \quad (C-11)$$

Provided Inequality (C-11) is satisfied, the solutions to Equations (C-6) and (C-7) are

$$\begin{aligned}
 w(x) = \frac{1}{2\xi\eta} & \left[\left[w(0^+) (\xi^2 - \eta^2 - \beta_r^2) + \psi'(0^+) \right] \sinh \xi x \sin \eta x + \right. \\
 & + \left[w'(0^+) \left(1 - \frac{\beta_r^2 + \epsilon^2}{\xi^2 + \eta^2} \right) \xi + \psi(0^+) \frac{\beta_r^2 + \epsilon^2}{\xi^2 + \eta^2} \xi \right] \cosh \xi x \sin \eta x + \\
 & + \left[w'(0^+) \left(1 + \frac{\beta_r^2 + \epsilon^2}{\xi^2 + \eta^2} \right) \eta - \psi(0^+) \frac{\beta_r^2 + \epsilon^2}{\xi^2 + \eta^2} \eta \right] \sinh \xi x \cos \eta x + \\
 & \left. + 2\xi\eta w(0^+) \cosh \xi x \cos \eta x \right]
 \end{aligned} \tag{C-12}$$

and

$$\begin{aligned}
 \psi(x) = \frac{1}{2\xi\eta} & \left[\left[\psi(0^+) (\xi^2 - \eta^2 + \epsilon^2 - \beta_e^2) - \epsilon^2 w'(0^+) \right] \sinh \xi x \sin \eta x + \right. \\
 & + \left[\psi'(0^+) \left(1 - \frac{\beta_e^2}{\xi^2 + \eta^2} \right) \xi - w(0^+) \frac{\beta_e^2 \epsilon^2}{\xi^2 + \eta^2} \xi \right] \cosh \xi x \sin \eta x + \\
 & + \left[\psi'(0^+) \left(1 + \frac{\beta_e^2}{\xi^2 + \eta^2} \right) \eta + w(0^+) \frac{\beta_e^2 \epsilon^2}{\xi^2 + \eta^2} \eta \right] \sinh \xi x \cos \eta x + \\
 & \left. + 2\xi\eta \psi(0^+) \cosh \xi x \cos \eta x \right]
 \end{aligned} \tag{C-13}$$

where

$$\begin{aligned}
 \xi^2 &= \frac{1}{2} \beta_e (\beta_r^2 + \epsilon^2)^{\frac{1}{2}} + \frac{1}{4} (\beta_r^2 + \beta_e^2) \\
 \eta^2 &= \frac{1}{2} \beta_e (\beta_r^2 + \epsilon^2)^{\frac{1}{2}} - \frac{1}{4} (\beta_r^2 + \beta_e^2)
 \end{aligned} \tag{C-14}$$

Notice that Equations (C-13) and (C-14) are general solutions and do not satisfy any particular boundary conditions or continuity conditions.

Determination of the Foundation Constants From the Stress-Intensity Factor for a Semi-Infinite Specimen

In the special case where the "uncracked" length of the DCB specimen greatly exceeds its other dimensions, the appropriate boundary conditions to be applied to Equations (C-12) and (C-13) are for the vanishing of $w(x)$ and $\Psi(x)$ as x becomes large. It can be shown that this condition is satisfied by taking

$$w'(0^+) = \frac{(\xi^2 + \eta^2)\Psi(0^+) - 2\xi\beta_e^2 w(0^+)}{\xi^2 + \eta^2 + \beta_e^2} \quad (C-15)$$

and

$$\Psi'(0^+) = - \frac{\beta_e^2 \epsilon^2 w(0^+) + 2\xi(\xi^2 + \eta^2)\Psi(0^+)}{\xi^2 + \eta^2 + \beta_e^2}$$

From Equations (C-4) and (C-5), the solutions for the cracked portion of the specimen, it is found that

$$w'(0^-) = \Psi(0^-) - \frac{P}{KGA} \quad (C-16)$$

and

$$\Psi'(0^-) = \frac{PQ}{EI}$$

Now, referring to the relations given in Appendix A, continuity of deflection, slope, shearing force and bending moment require that w , Ψ , w' and Ψ' all be continuous. (Note that when Q and M are acting at the interface, this is not the case.) Hence, equating the right-hand sides of Equations (C-15) and (C-16) allows a determination of $w(0)$ and $\Psi(0)$ to be made. This is

$$w(0) = \frac{\xi^2 + \eta^2 + \beta_e^2}{4\xi^2(\xi^2 + \eta^2) - \beta_e^2 \epsilon^2} \left\{ \epsilon^2 a + 2\xi \frac{\xi^2 + \eta^2}{\beta_e^2} \right\} \frac{P}{KGA} \quad (C-17)$$

$$\Psi(0) = - \frac{\xi^2 + \eta^2 + \beta_e^2}{4\xi^2(\xi^2 + \eta^2) - \beta_e^2 \epsilon^2} \left\{ 2\epsilon^2 \xi a + \epsilon^2 \right\} \frac{P}{KGA}$$

where the distinction between 0^- and 0^+ is now superfluous and has therefore been dropped.

The compliance of the DCB specimen--the deflection of the free end per unit of applied force--can be obtained from Equation (C-4) by setting $\delta = w(-a)$. This gives, in general

$$\delta = \frac{P\alpha^3}{3EI} \left\{ 1 + \left(\frac{3EI}{KGA} \right) \frac{1}{\alpha} \right\} - \Psi(0)\alpha + w(0) \quad (C-18)$$

or, substituting Equations (C-17) for the semi-infinite specimen

$$\delta = \frac{P\alpha^3}{3EI} \left\{ 1 + C_1 \left(\frac{h}{\alpha} \right) + C_2 \left(\frac{h}{\alpha} \right)^2 + C_3 \left(\frac{h}{\alpha} \right)^3 \right\} \quad (C-19)$$

where

$$C_1 = \frac{6\xi}{h} \left(\frac{\xi^2 + \eta^2 + \beta_e^2}{4\xi^2 (\xi^2 + \eta^2) - \beta_e^2 \epsilon^2} \right)$$

$$C_2 = \frac{3}{h^2 \epsilon^2} \left\{ 1 + 2\epsilon^2 \left(\frac{\xi^2 + \eta^2 + \beta_e^2}{4\xi^2 (\xi^2 + \eta^2) - \beta_e^2 \epsilon^2} \right) \right\} \quad (C-20)$$

$$C_3 = \frac{6\xi(\xi^2 + \eta^2)}{h^3 \epsilon^2 \beta_c^2} \left(\frac{\xi^2 + \eta^2 + \beta_e^2}{4\xi^2 (\xi^2 + \eta^2) - \beta_e^2 \epsilon^2} \right)$$

The stress-intensity factor can now be obtained since

$$K^2 = E\mathcal{L} = \frac{E}{b} \frac{d}{d\alpha} \quad (P6) \quad (C-21)$$

Using Equation (C-19) to eliminate δ in favor of P and using $I = bh^3/12$, then, for crack extension under constant load

$$K = 2\sqrt{3} \frac{P\alpha}{bh^{3/2}} \left\{ 1 + \frac{2}{3} C_1 \left(\frac{h}{\alpha} \right) + \frac{1}{3} C_2 \left(\frac{h}{\alpha} \right)^2 \right\}^{1/2} \quad (C-22)$$

Notice that if $C_1^2 = 3C_2$, Equation (C-22) reduces to

$$K = 2\sqrt{3} \frac{P\alpha}{bh^{3/2}} \left(1 + \frac{C_1}{3} \frac{h}{\alpha} \right) \quad (C-23)$$

which is identical to Equation (1) provided $C_1 = 3\alpha$.

Values of the beam and foundation constants that will put the model of the DCB specimen in good accord with experimental and with the more precise two-dimensional computations, can be obtained by using the expressions for the foundation parameters given as Equations (13) and (15). It is then found that

$$C_1 = 3\sqrt{5}/4$$

$$C_2 = 3/2$$

$$C_3 = 3\sqrt{5}/16$$

Upon substituting these into Equations (C-19) and (C-22), the results given as Equations (16) and (17) are obtained.

Finally, a comparison between the values of the coefficients obtained with the various analytical models can be made with the empirical values of Mostovoy, et al. This is shown in Table C-1. Unfortunately, there is little basis upon which to choose one set of these over another. However, it is instructive to notice that if the values given by Mostovoy, et al., were substituted into Equation (C-22), the result

$$K = \frac{2\sqrt{3} Pa}{bh^{3/2}} \left\{ 1 + 1.2\left(\frac{h}{a}\right) + 0.69\left(\frac{h}{a}\right)^2 \right\}^{1/2}$$

would be in relatively poor agreement with the values shown in Figure 2.

TABLE I - COEFFICIENTS IN THE RELATION FOR THE COMPLIANCE OF THE DCB SPECIMEN AS GIVEN BY VARIOUS DIFFERENT ANALYTICAL MODELS

$$\frac{\delta}{P} = \frac{a^3}{3EI} \left\{ 1 + C_1\left(\frac{h}{a}\right) + C_2\left(\frac{h}{a}\right)^2 + C_3\left(\frac{h}{a}\right)^3 \right\}$$

| <u>Analytical Model</u> | <u>C₁</u> | <u>C₂</u> | <u>C₃</u> |
|---|----------------------|----------------------|----------------------|
| Euler-Bernoulli beam on a rigid foundation | 0 | 0 | 0 |
| Timoshenko beam on a rigid foundation | 0 | 0.75 | 0 |
| Euler-Bernoulli beam on a Winkler foundation | 1.92 | 1.22 | 0.39 |
| Timoshenko beam on a Winkler foundation | 2.43 | 1.98 | 0.50 |
| Timoshenko beam on a generalized foundation | 1.68 | 1.50 | 0.42 |
| Semi-empirical extension of simple built-in beam model given by Mostovoy, et al. (12) | 1.80 | 2.08 | 0.22 |

APPENDIX 3-D

FINITE-DIFFERENCE APPROXIMATION TO EQUATIONS FOR
DYNAMIC-CRACK PROPAGATION IN THE TIMOSHENKO BEAM-GENERALIZED
ELASTIC FOUNDATION DCB MODEL

The governing equations for dynamic-crack propagation in a DCB specimen modeled by a Timoshenko beam on a generalized elastic foundation in dimensionless form are given by

$$Y'' + 4W' - 4Y - 2H*(1-\theta)Y = \frac{1}{12} \ddot{Y} \quad (D-1)$$

and

$$W'' - Y' - 6H*(1-\theta)W = \frac{1}{4} \ddot{W} \quad (D-2)$$

Here the prime notation indicates differentiation with respect to ξ , the dot with respect to τ . Hence, replacing the derivatives by finite-difference approximations gives

$$\begin{aligned} & \frac{1}{(\Delta\xi)^2} \{Y(\xi+\Delta\xi, \tau) - 2Y(\xi, \tau) + Y(\xi-\Delta\xi, \tau)\} + \\ & + \frac{2}{\Delta\xi} \{W(\xi+\Delta\xi, \tau) - W(\xi-\Delta\xi, \tau)\} - [4 + 2h*(1-\theta)] Y(\xi, \tau) = \end{aligned} \quad (D-3)$$

$$= \frac{1}{12(\Delta\tau)^2} \{Y(\xi, \tau+\Delta\tau) - 2Y(\xi, \tau) + Y(\xi, \tau-\Delta\tau)\}$$

and

$$\begin{aligned} & \frac{1}{(\Delta\xi)^2} \{W(\xi+\Delta\xi, \tau) - 2W(\xi, \tau) + W(\xi-\Delta\xi, \tau)\} + \\ & - \frac{1}{2\Delta\xi} \{Y(\xi+\Delta\xi, \tau) - Y(\xi-\Delta\xi, \tau)\} - 6H*(1-\theta)W(\xi, \tau) = \end{aligned} \quad (D-4)$$

$$= \frac{1}{4(\Delta\tau)^2} \{W(\xi, \tau+\Delta\tau) - 2W(\xi, \tau) + W(\xi, \tau-\Delta\tau)\}$$

Upon solving these for $Y(\xi, \tau + \Delta\tau)$ and $W(\xi, \tau + \Delta\tau)$, respectively, the following formulas are obtained.

$$\begin{aligned}
 Y(\xi, \tau + \Delta\tau) = & 12 \left(\frac{\Delta\tau}{\Delta\xi} \right)^2 \left\{ Y(\xi + \Delta\xi, \tau) + Y(\xi - \Delta\xi, \tau) \right\} + \\
 & + 24 \frac{(\Delta\tau)^2}{\Delta\xi} \left\{ W(\xi + \Delta\xi, \tau) - W(\xi - \Delta\xi, \tau) \right\} + \quad (D-5) \\
 & - \left\{ 24 \left(\frac{\Delta\tau}{\Delta\xi} \right)^2 - 2 + 24(\Delta\tau)^2 [2 + H^*(1-\theta)] \right\} Y(\xi, \tau) - Y(\xi, \tau - \Delta\tau)
 \end{aligned}$$

and

$$\begin{aligned}
 W(\xi, \tau + \Delta\tau) = & 4 \left(\frac{\Delta\tau}{\Delta\xi} \right)^2 \left\{ W(\xi + \Delta\xi, \tau) + W(\xi - \Delta\xi, \tau) \right\} + \\
 & - 2 \frac{(\Delta\tau)^2}{\Delta\xi} \left\{ Y(\xi + \Delta\xi, \tau) - Y(\xi - \Delta\xi, \tau) \right\} + \quad (D-6) \\
 & - \left\{ 8 \left(\frac{\Delta\tau}{\Delta\xi} \right)^2 - 2 + 24(\Delta\tau)^2 H^*(1-\theta) \right\} W(\xi, \tau) - W(\xi, \tau - \Delta\tau)
 \end{aligned}$$

These are the recursion relations used in the computations.

The components of energy can be computed from the finite-difference approximation as follows. It has been shown that

$$\frac{U}{RA} = \int_0^{L/h} \left\{ \frac{1}{24} (Y')^2 + \frac{1}{6} (W' - Y)^2 + H^*(1-\theta) \left[W^2 + \frac{1}{12} Y^2 \right] \right\} d\xi \quad (D-7)$$

and

$$\frac{T}{RA} = \int_0^{L/h} \left\{ \frac{1}{24} (\dot{W})^2 + \frac{1}{288} (\dot{Y})^2 \right\} d\xi \quad (D-8)$$

Hence, using central differences for the spatial derivatives

$$\begin{aligned}
 \frac{U}{RA} = & \sum \left\{ \frac{1}{24} \left[\frac{Y(\xi + \Delta\xi, \tau) - Y(\xi - \Delta\xi, \tau)}{2\Delta\xi} \right]^2 + \right. \\
 & + \frac{1}{6} \left[\frac{W(\xi + \Delta\xi, \tau) - W(\xi - \Delta\xi, \tau)}{2\Delta\xi} - Y(\xi, \tau) \right]^2 + \quad (D-9) \\
 & \left. + H^*(1-\theta) \left[W^2(\xi, \tau) + \frac{1}{12} Y^2(\xi, \tau) \right] \right\} \Delta\xi
 \end{aligned}$$

and, using forward differences for time derivatives

$$\frac{T}{RA} = \frac{1}{24} \sum \left\{ \left[\frac{3W(\xi, \tau) - 4W(\xi, \tau - \Delta\tau) + W(\xi, \tau - 2\Delta\tau)}{2\Delta\tau} \right]^2 + \right. \\ \left. + \frac{1}{12} \left[\frac{3Y(\xi, \tau) - 4Y(\xi, \tau - \Delta\tau) + Y(\xi, \tau - 2\Delta\tau)}{2\Delta\tau} \right]^2 \right\} \Delta\xi \quad (D-10)$$

where \sum implies summation over the beam length. These relations are also used in the computing program.

The final step preparatory to carrying out a large number of computations is to decide on suitable step sizes for the finite-difference procedure. Tables D-1 and D-2 show the results of a number of computations in which only the step sizes were varied. It can be seen that the solutions obtained are remarkably insensitive to these values and that, for the purposes of this report, the values $\Delta\xi = .05$ and $\Delta\tau = .01$ are entirely adequate. Most of these computations used these values. Nevertheless, a number of further check runs were carried out using more precise values. No substantial changes in the results were ever noted, however.

TABLE D-I - COMPARISON OF CRACK LENGTH VS TIME RESULTS COMPUTED USING DIFFERENT FINITE-DIFFERENCE STEP SIZES

Specimen Configuration A, $K_q/K_d = 2.0$

$$\tau = \frac{C_o t}{\sqrt{12} h}$$

| $\frac{a-a_o}{h}$ | $\Delta\xi = .200$ | | | $\Delta\xi = .100$ | | | $\Delta\xi = .050$ | | | $\Delta\xi = .025$ |
|-------------------|---------------------|---------------------|---------------------|---------------------|---------------------|---------------------|---------------------|---------------------|---------------------|---------------------|
| | $\Delta\tau = .010$ | $\Delta\tau = .005$ | $\Delta\tau = .001$ | $\Delta\tau = .010$ | $\Delta\tau = .005$ | $\Delta\tau = .001$ | $\Delta\tau = .010$ | $\Delta\tau = .005$ | $\Delta\tau = .001$ | $\Delta\tau = .001$ |
| 0.2 | 0 | 0 | 0 | 0.110 | 0.110 | 0.115 | 0.160 | 0.165 | 0.167 | 0.195 |
| 0.4 | .210 | .215 | .216 | 0.360 | 0.365 | 0.367 | 0.480 | 0.485 | 0.489 | 0.563 |
| 0.6 | .640 | .645 | .649 | 0.810 | 0.810 | 0.814 | 0.860 | 0.865 | 0.869 | 0.897 |
| 0.8 | .900 | .905 | .907 | 1.040 | 1.050 | 1.053 | 1.100 | 1.105 | 1.108 | 1.135 |
| 1.0 | 1.130 | 1.130 | 1.134 | 1.430 | 1.440 | 1.443 | 1.520 | 1.520 | 1.524 | 1.573 |
| 1.2 | 1.580 | 1.590 | 1.592 | 1.770 | 1.770 | 1.775 | 1.780 | 1.785 | 1.789 | 1.819 |
| 1.4 | 1.820 | 1.825 | 1.827 | 2.010 | 2.010 | 2.014 | 2.050 | 2.060 | 2.065 | 2.130 |
| 1.6 | 2.040 | 2.050 | 2.053 | 2.410 | 2.415 | 2.417 | 2.460 | 2.470 | 2.472 | 2.512 |
| 1.8 | 2.470 | 2.480 | 2.481 | 2.660 | 2.660 | 2.664 | 2.690 | 2.695 | 2.698 | 2.751 |
| 2.0 | 2.710 | 2.715 | 2.718 | 2.990 | 2.985 | 2.989 | 3.060 | 3.070 | 3.072 | 3.137 |
| 2.2 | 3.090 | 3.105 | 3.102 | 3.360 | 3.365 | 3.370 | 3.390 | 3.390 | 3.393 | 3.445 |
| 2.4 | 3.390 | 3.400 | 3.399 | 3.600 | 3.600 | 3.604 | 3.620 | 3.630 | 3.634 | 3.668 |
| 2.6 | 3.640 | 3.655 | 3.652 | 3.980 | 3.980 | 3.984 | 4.020 | 4.020 | 4.023 | 4.051 |
| 2.8 | 4.000 | 4.015 | 4.014 | 4.240 | 4.245 | 4.249 | 4.300 | 4.305 | 4.312 | 4.339 |

TABLE D-II - COMPARISON OF COMPUTATIONAL RESULTS USING DIFFERENT FINITE-DIFFERENCE STEP SIZES

Specimen Configuration A, $K_q/K_d = 2.0$

(a) Steady-State Crack Speeds

| $\Delta\xi$ | v/C_o | | |
|-------------|---------------------|---------------------|---------------------|
| | $\Delta\tau = .010$ | $\Delta\tau = .005$ | $\Delta\tau = .001$ |
| .200 | .1868 | .1862 | .1863 |
| .100 | .1783 | .1784 | .1783 |
| .050 | .1797 | .1796 | .1796 |
| .025 | | | .1785 |

(b) Crack Arrest Point

| $\Delta\xi$ | a_r/a_o | | |
|-------------|---------------------|---------------------|---------------------|
| | $\Delta\tau = .010$ | $\Delta\tau = .005$ | $\Delta\tau = .001$ |
| .200 | 3.33 | 3.33 | 3.33 |
| .100 | 2.87 | 2.87 | 2.87 |
| .050 | 2.93 | 2.93 | 2.93 |
| .025 | | | 2.93 |

APPENDIX 3-E

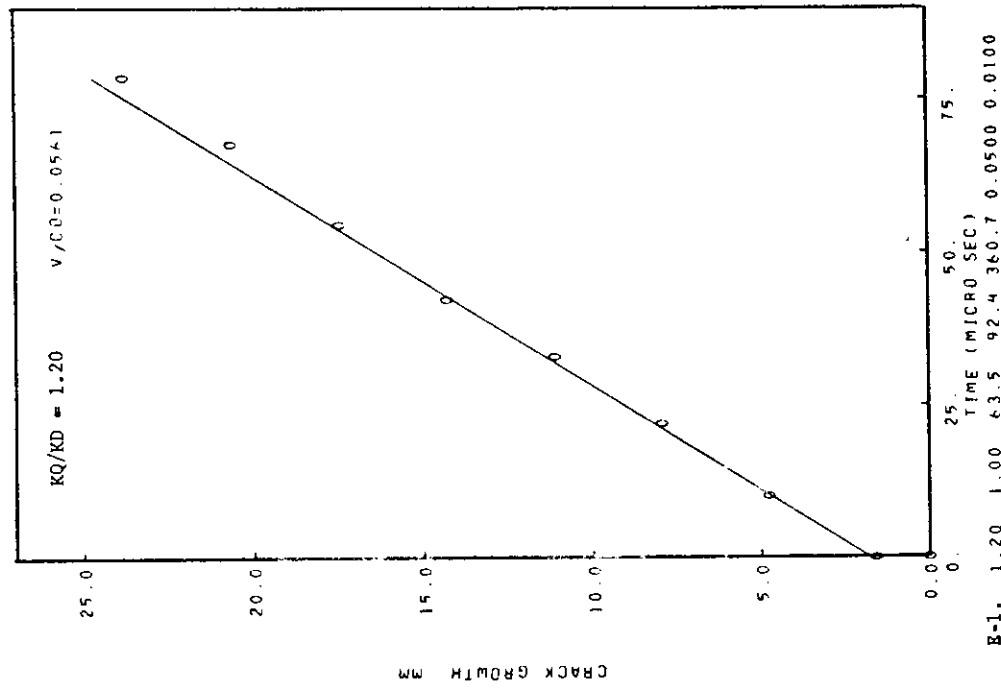
COMPUTER PLOTS OF RESULTS FOR DYNAMIC-CRACK
PROPAGATION IN STEEL DCB TEST SPECIMENS

In this appendix the computer plots obtained for a large number of different specimen geometries and loading conditions are presented. Two plots accompany each run: a crack length-time plot (using material constants appropriate for steel) and a plot of the energy apportionment as a function of crack length. Individual runs for single-section specimens are identified by a string of numbers under the abscissa. In order, these numbers correspond to K_q/K_d , R_T/R_S , $h(\text{mm})$, $a_0(\text{mm})$, $L(\text{mm})$, $\Delta\xi$, and $\Delta\tau$. These values suffice to identify a particular specimen so that dimensions not specifically given can be obtained from Table I.

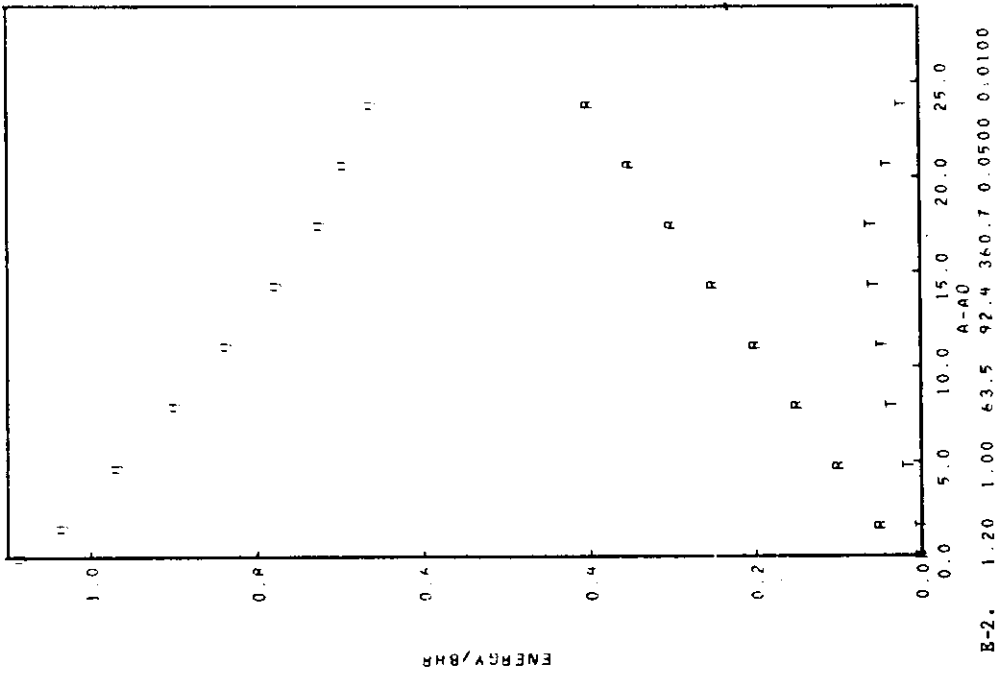
ACKNOWLEDGMENTS

The authors are grateful to J. K. Magor and George Mayer of the Army Research Office-Durham for their advice and encouragement. Valuable discussions have been held with members of the Advisory Group III of the Ship Research Committee.

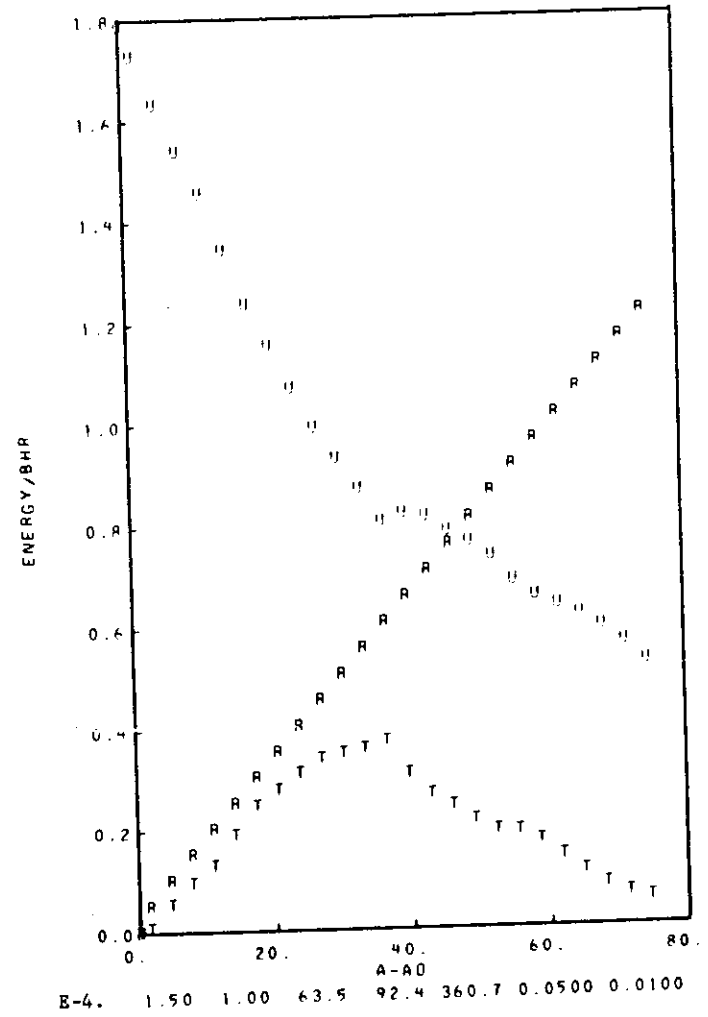
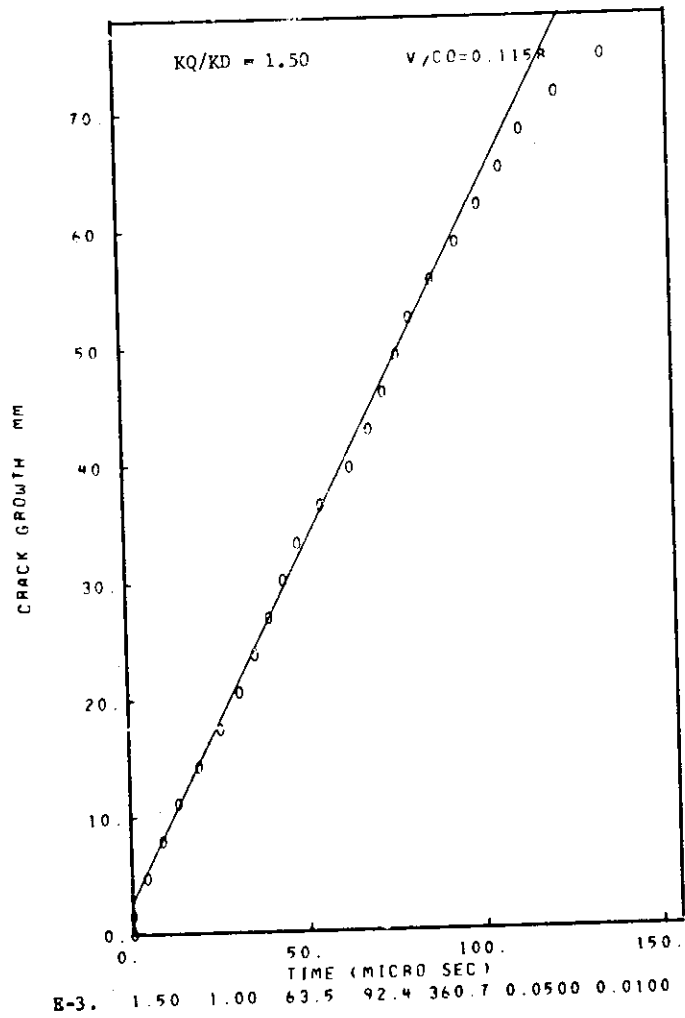
At Battelle-Columbus, the contributions of P. N. Mincer, C. R. Barnes, C. Pepper, J. Jarvis, and R. Speraw were particularly helpful.

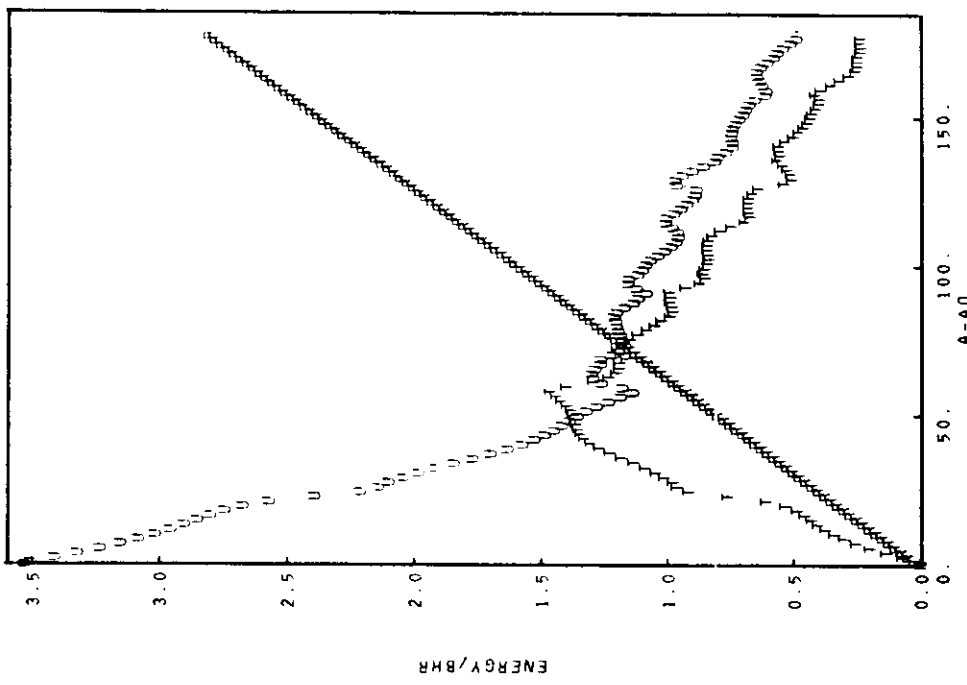


B-1. 1.20 1.00 63.5 92.4 360.7 0.0500 0.0100

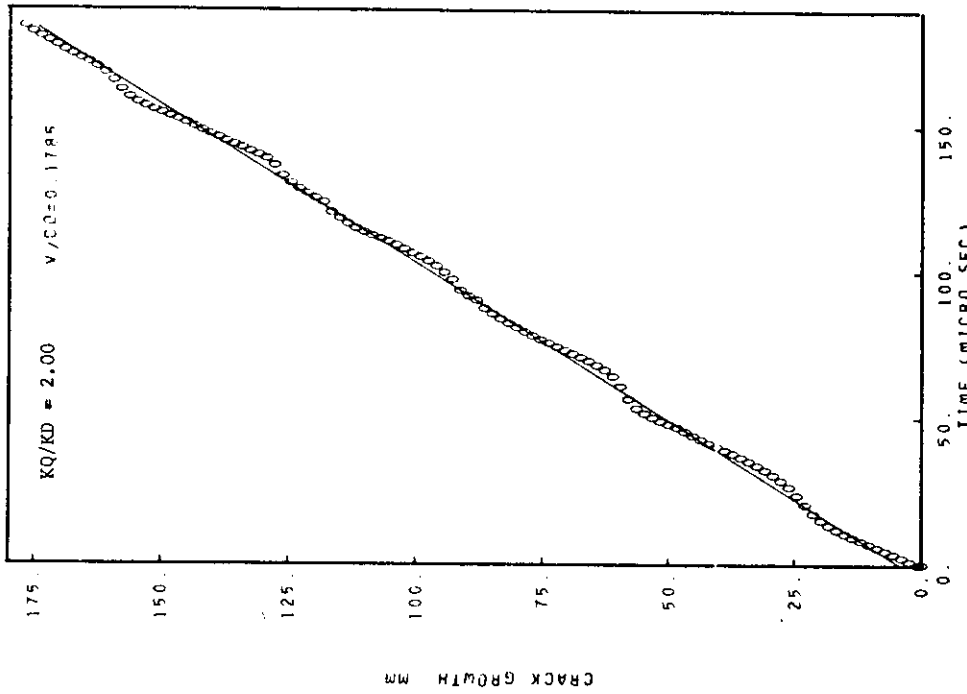


B-2. 1.20 1.00 63.5 92.4 360.7 0.0500 0.0100

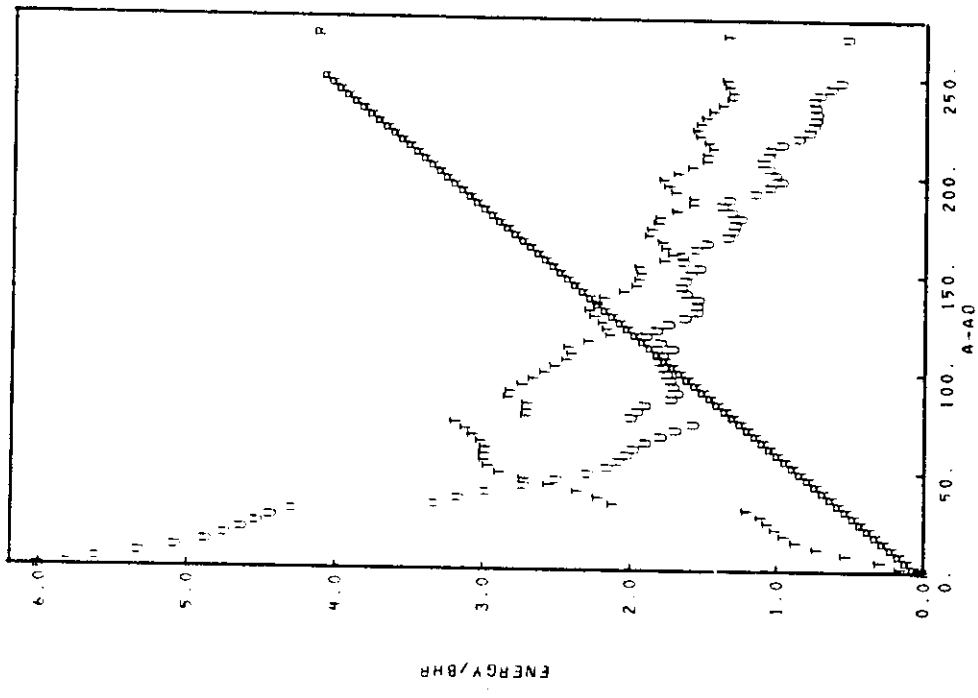




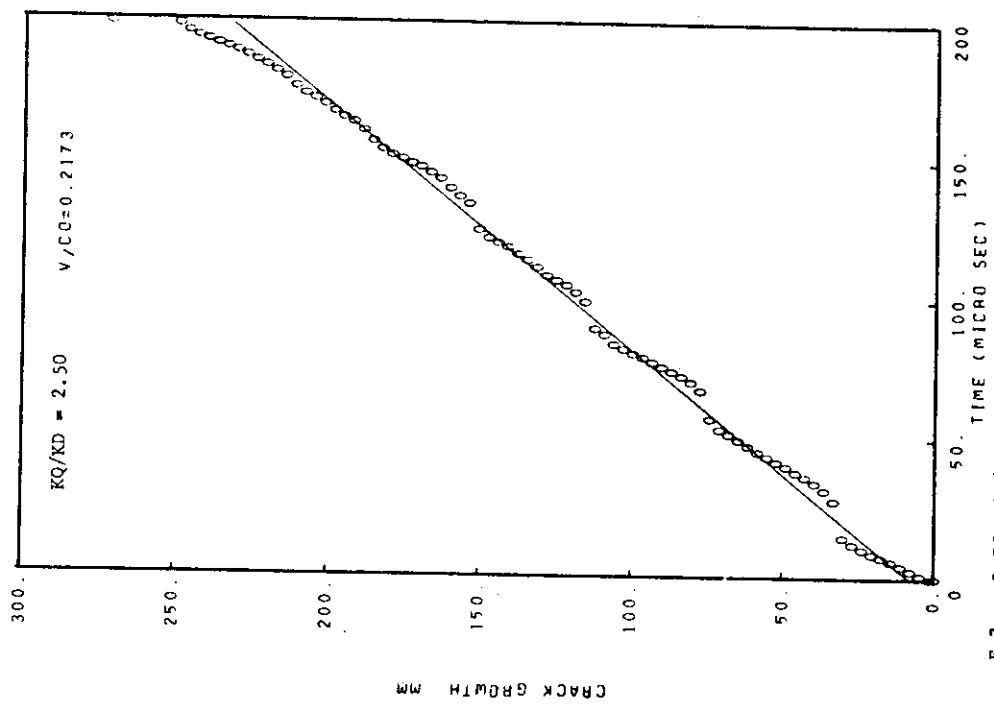
E-6. 2.00 1.00 63.5 92.4 360.7 0.0250 0.0010



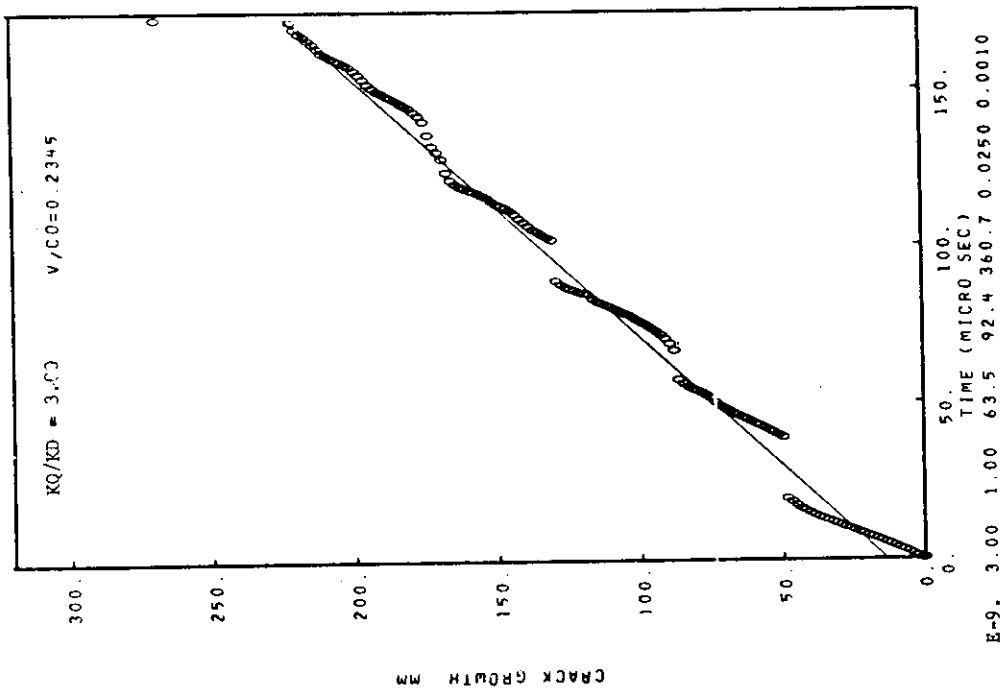
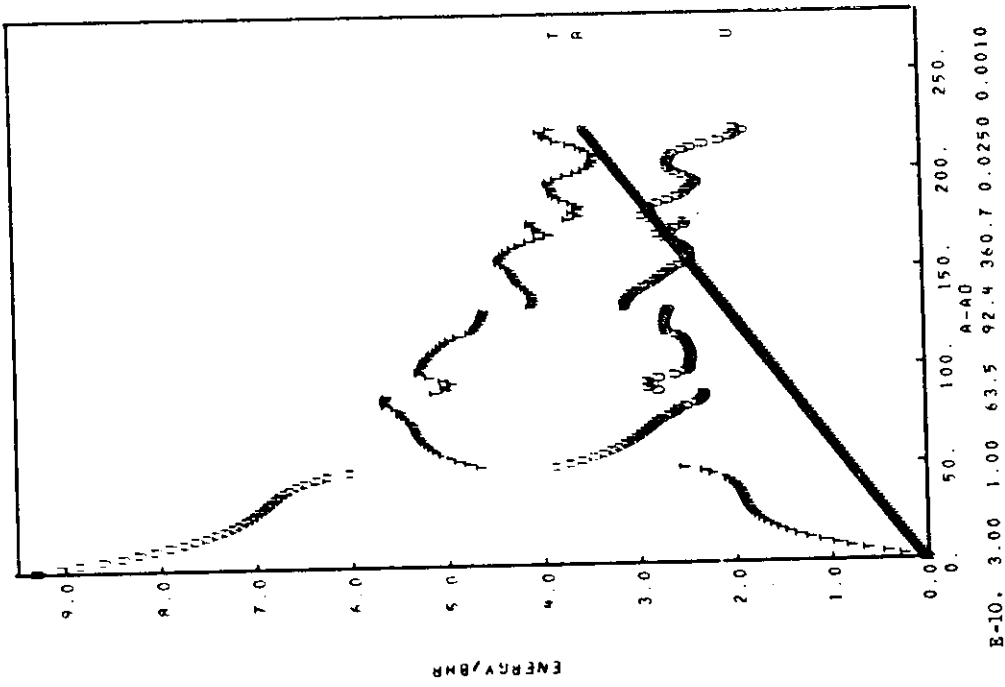
E-5. 2.00 1.00 63.5 92.4 360.7 0.0250 0.0010

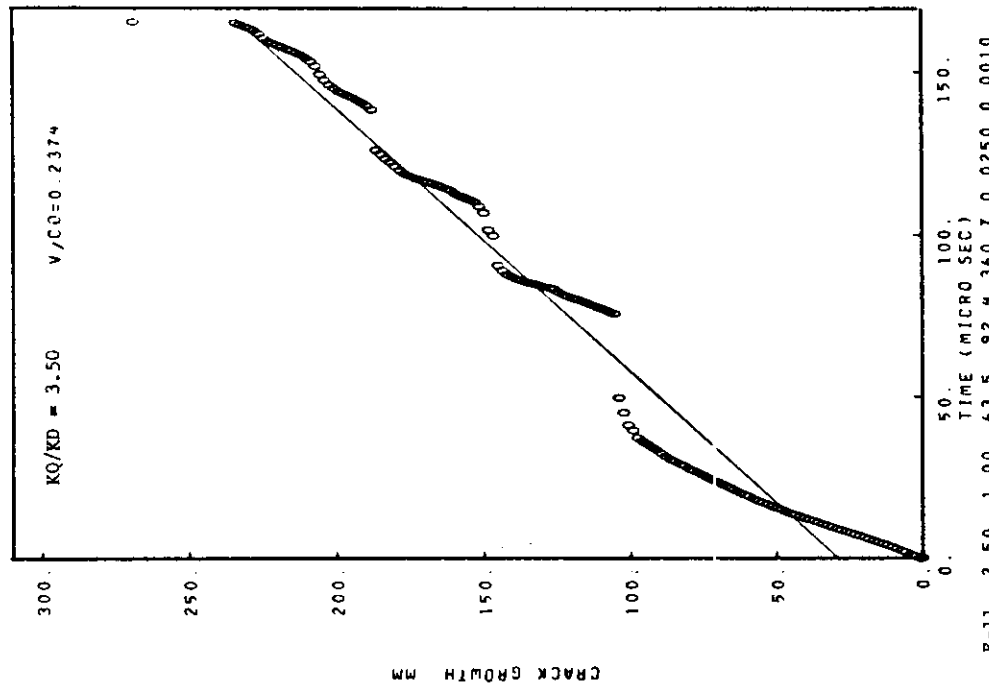


E-8. 2.50 1.00 63.5 92.4 360.7 0.0500 0.0100 A-A0

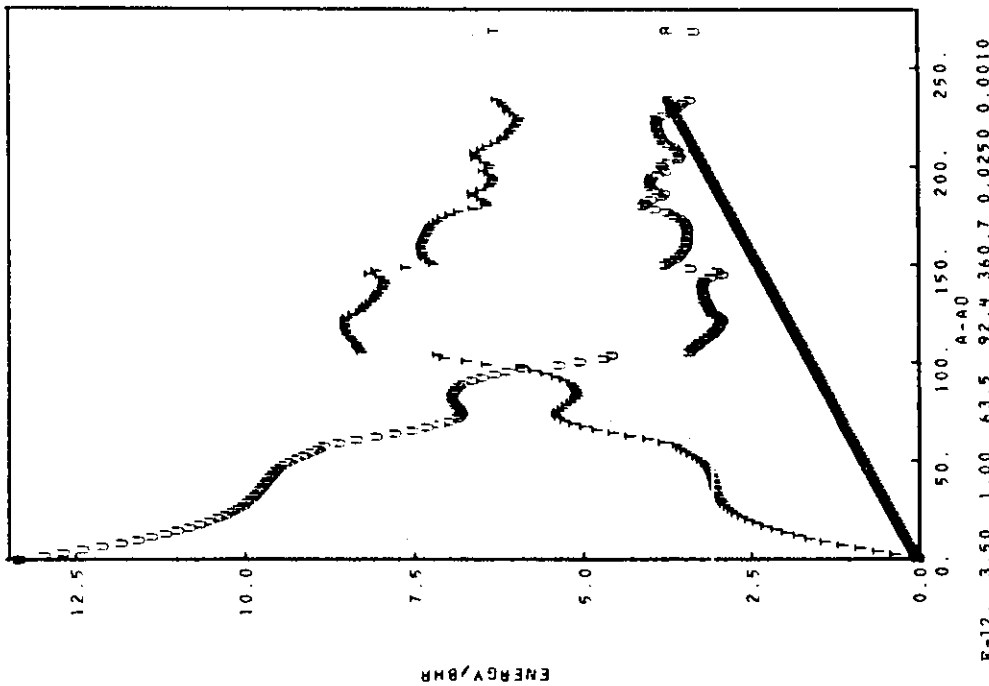


E-7. 2.50 1.00 63.5 92.4 360.7 0.0500 0.0100

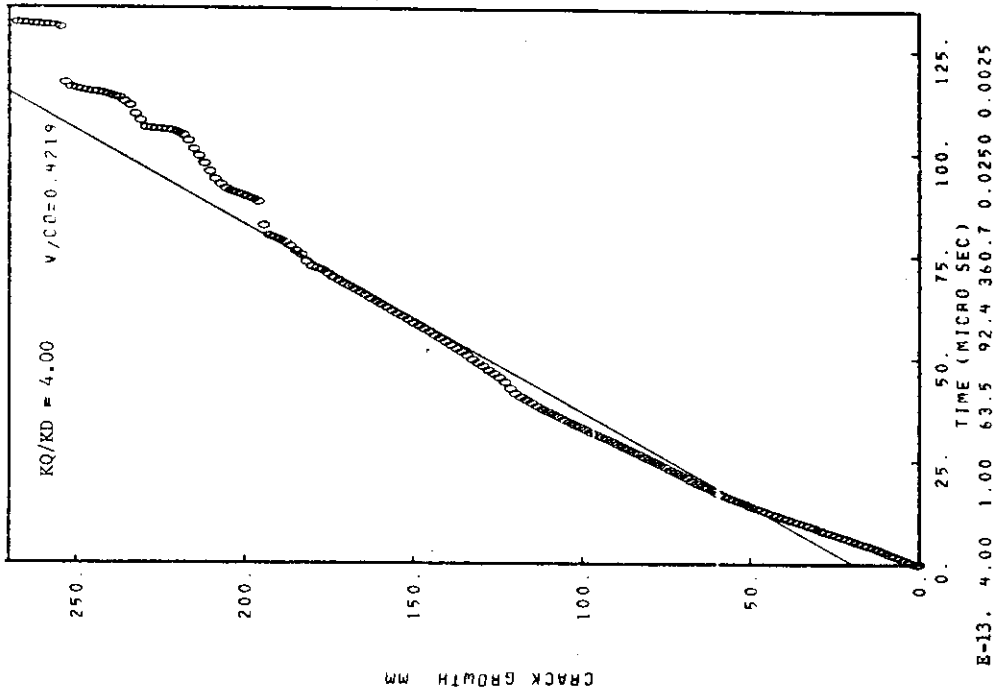
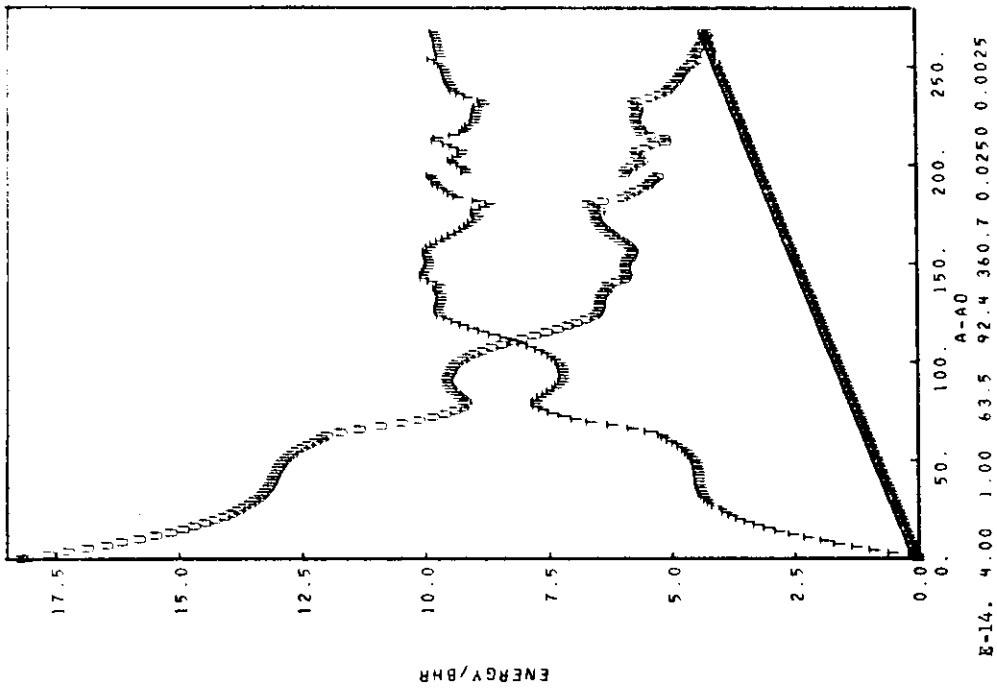


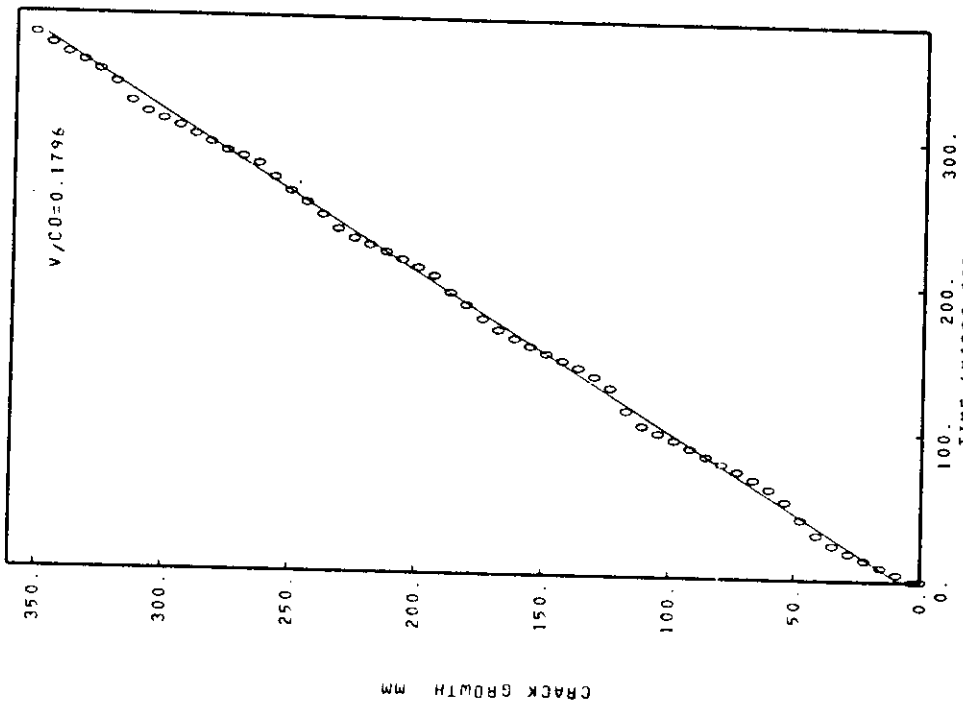


E-11. 3.50 1.00 63.5 92.4 360.7 0.0250 0.0010

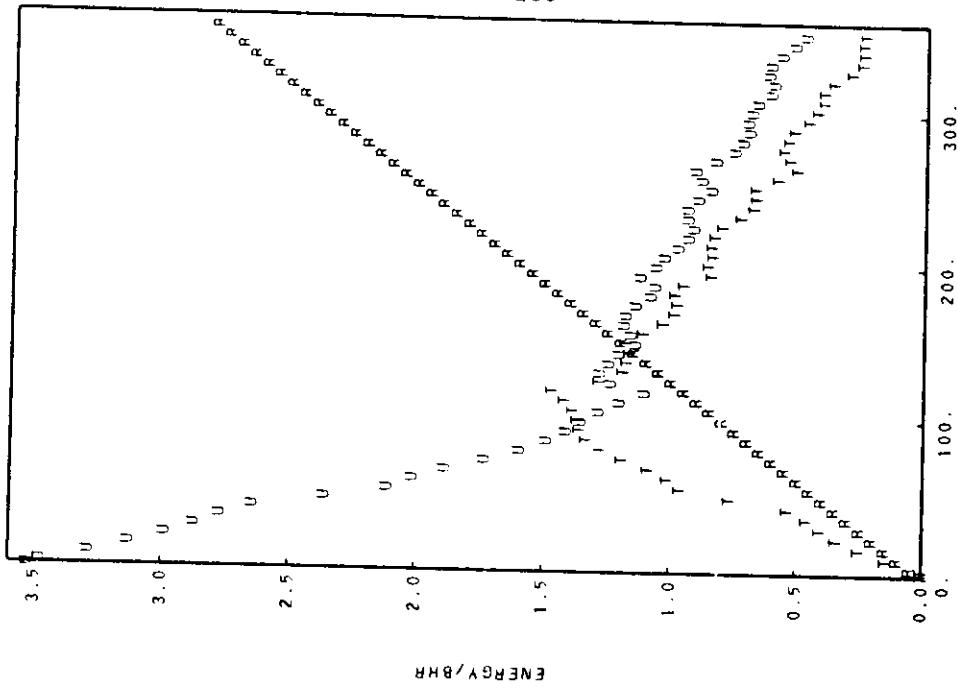


E-12. 3.50 1.00 63.5 92.4 360.7 0.0250 0.0010

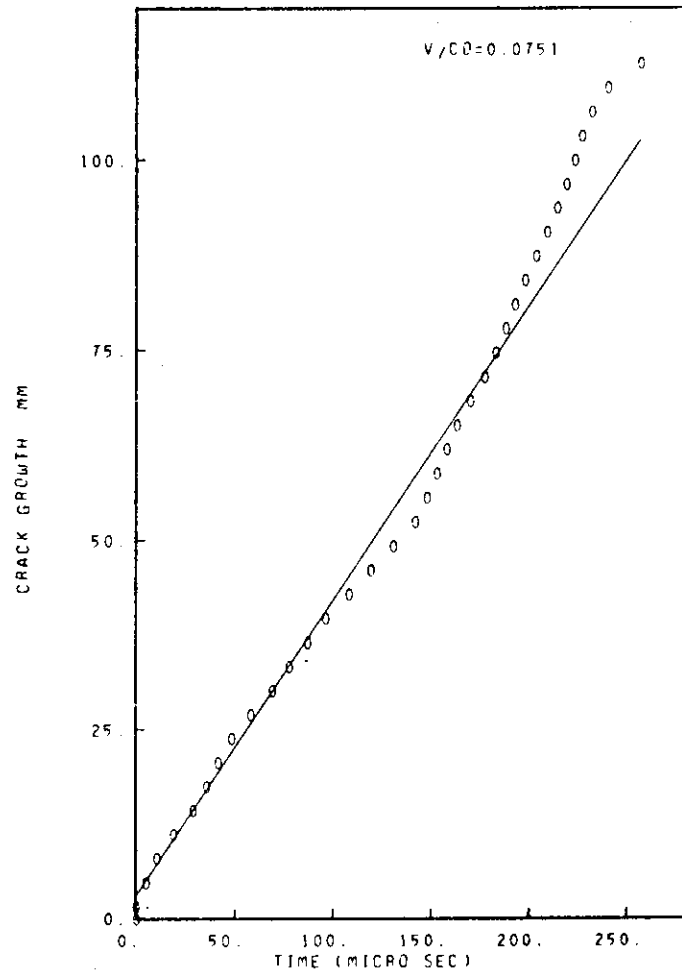




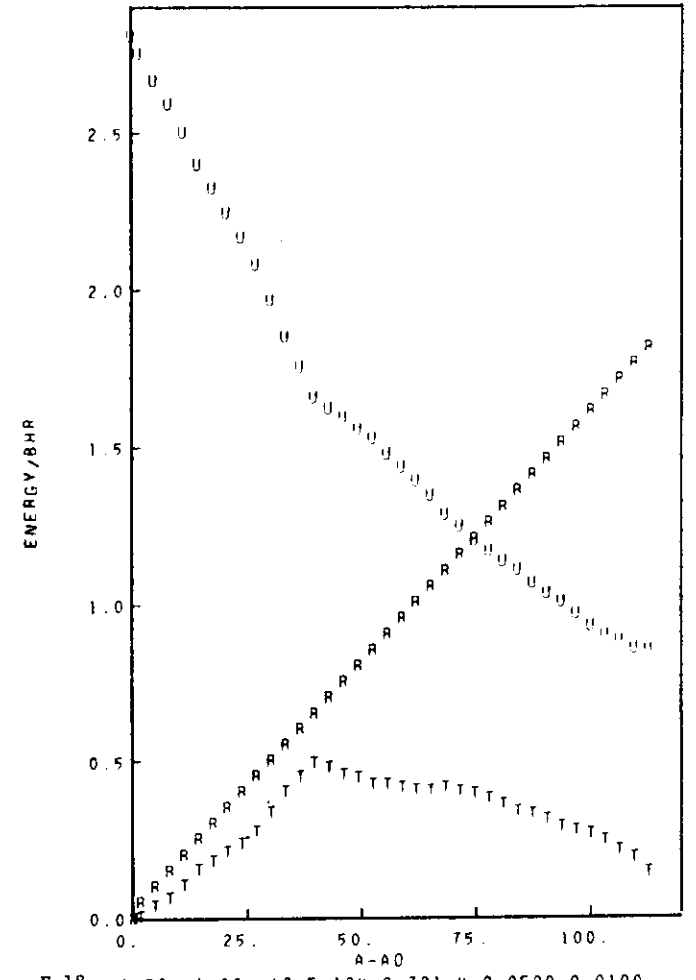
E-15. 2.00 1.00 127.0 184.8 721.4 0.0500 0.0010



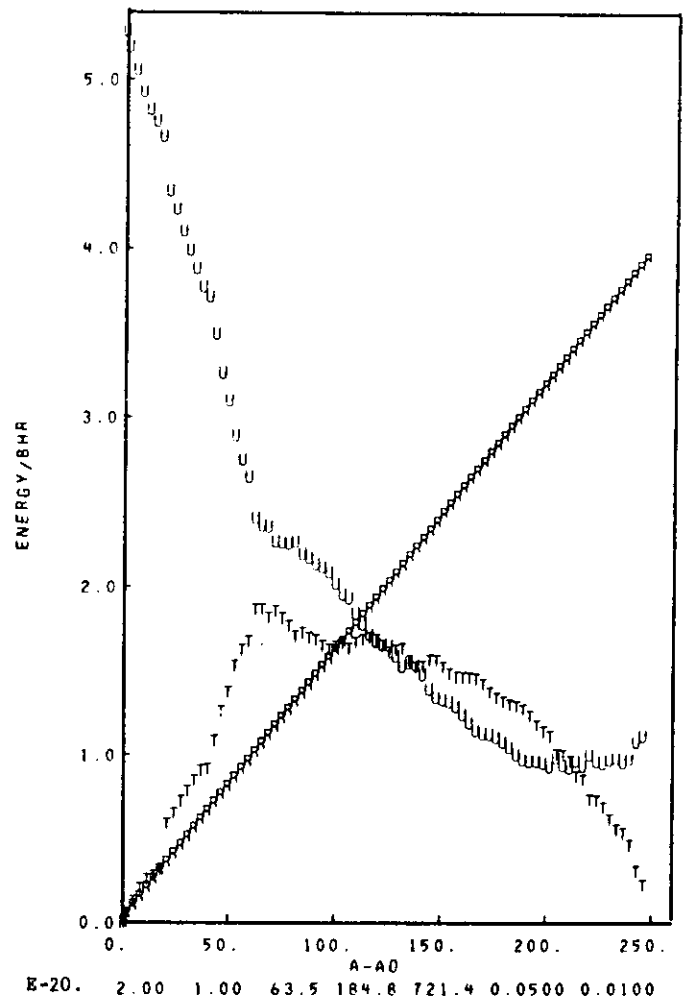
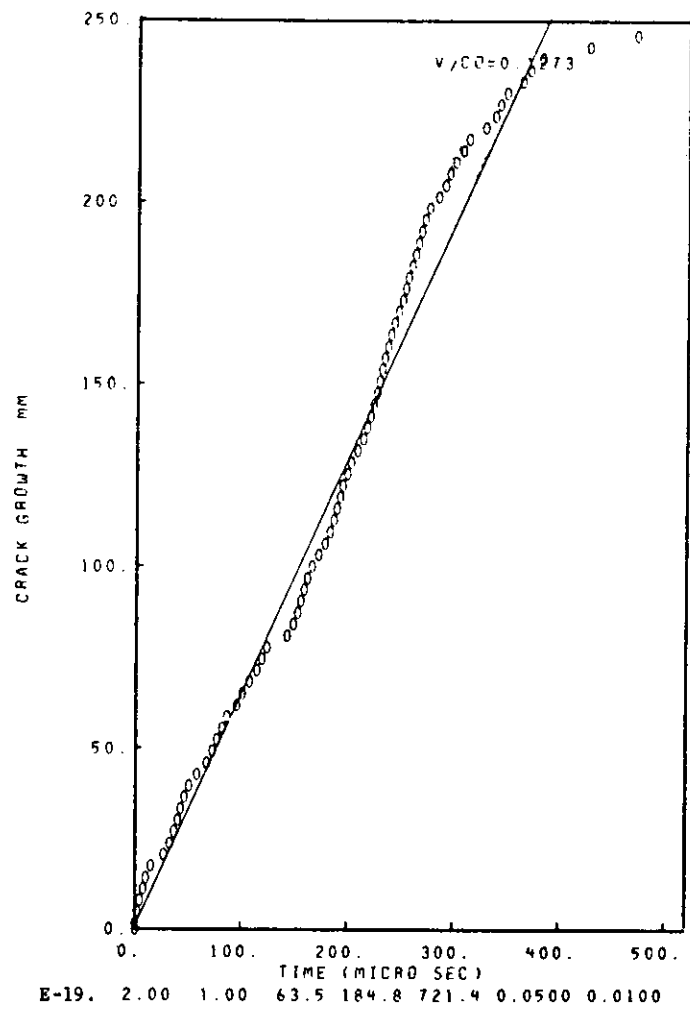
E-16. 2.00 1.00 127.0 184.8 721.4 0.0500 0.0010

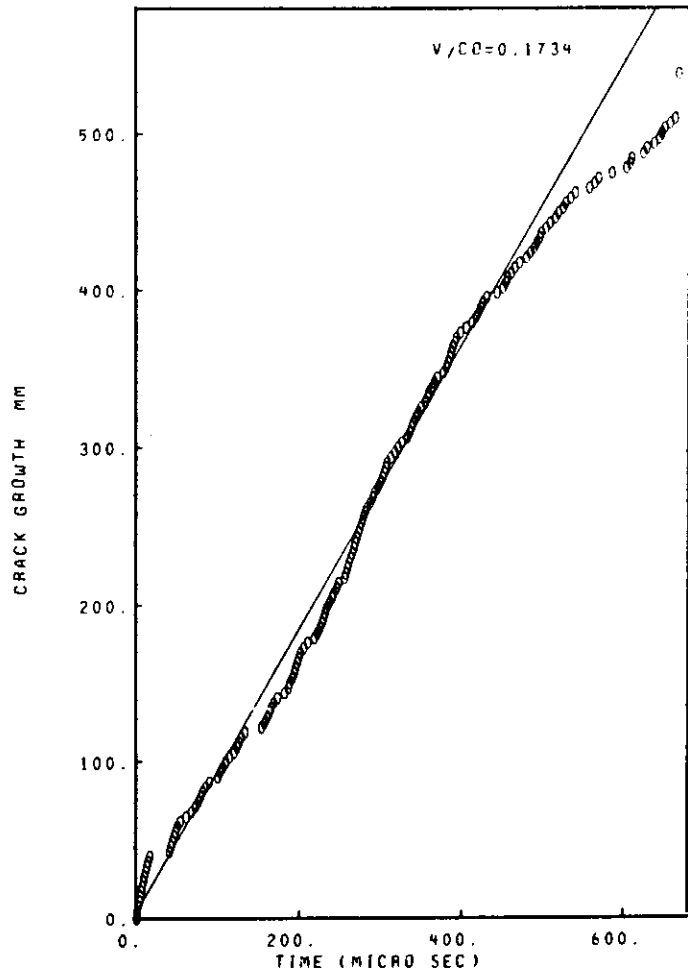


E-17. 1.50 1.00 63.5 184.8 721.4 0.0500 0.0100

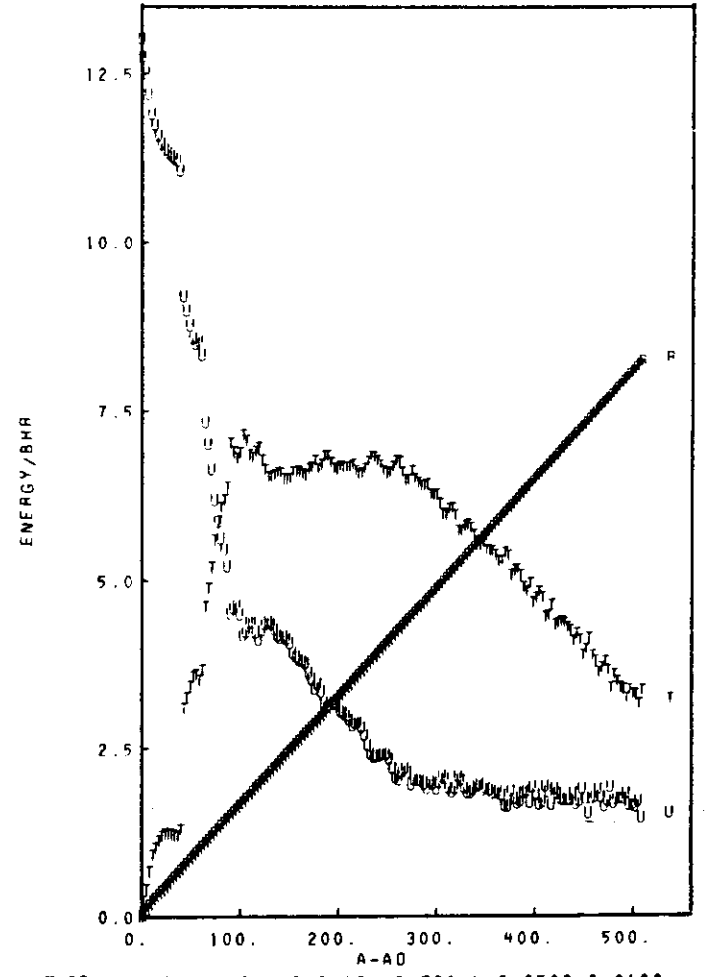


E-18. 1.50 1.00 63.5 184.8 721.4 0.0500 0.0100

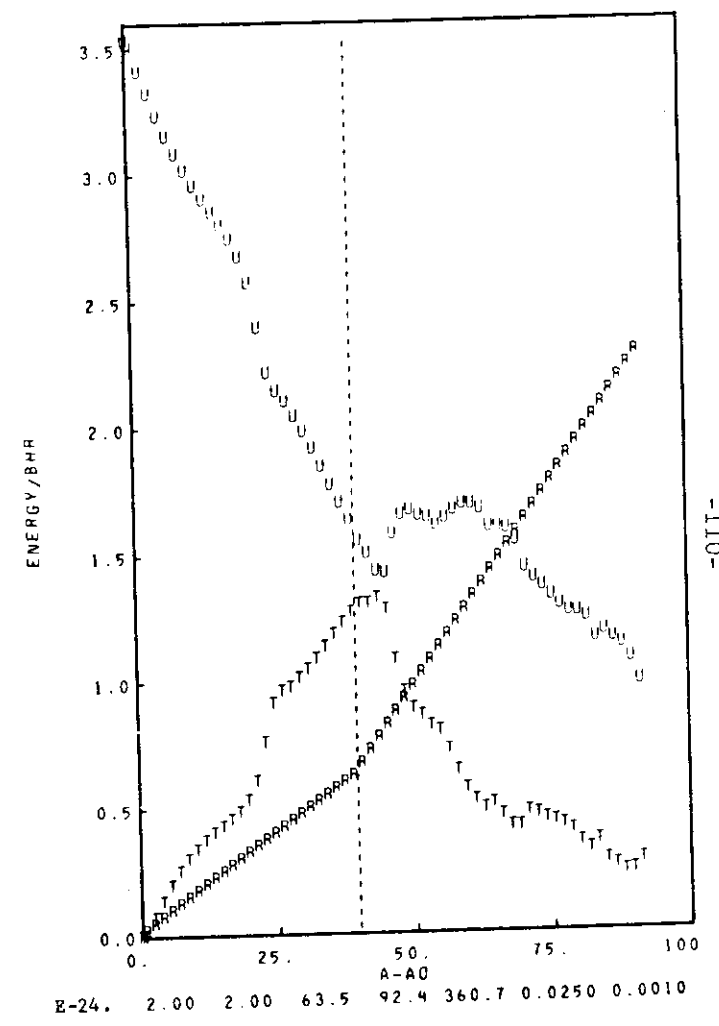
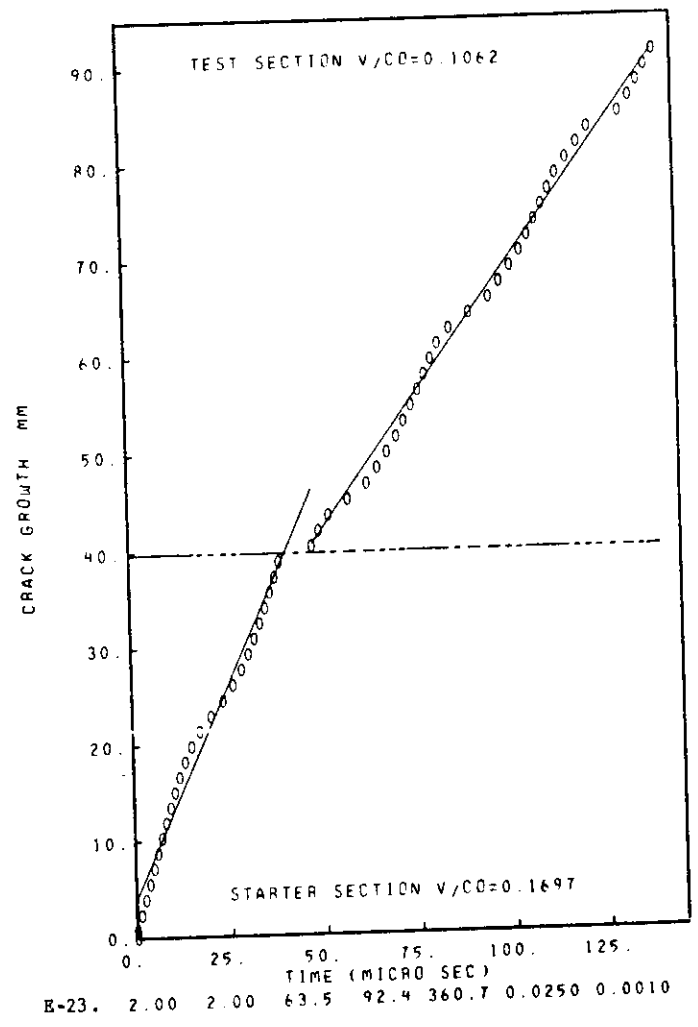


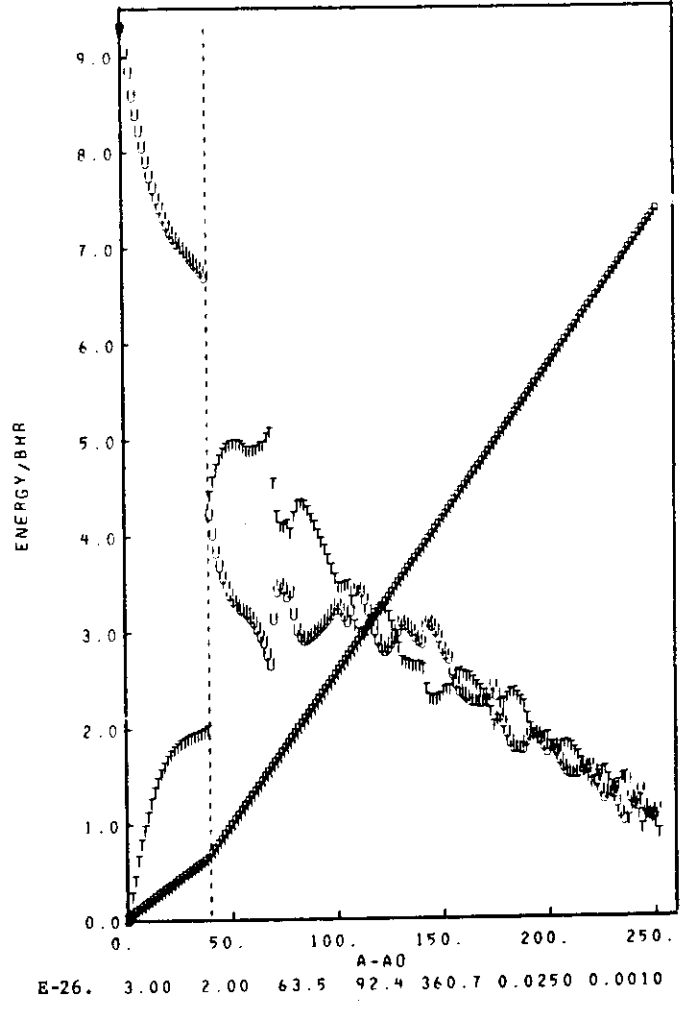
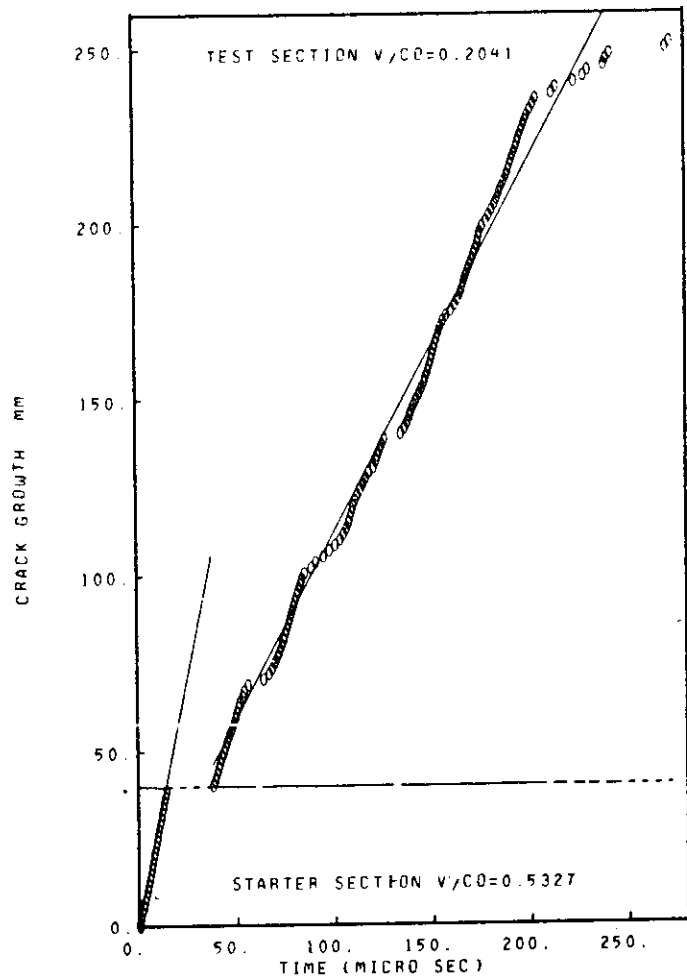


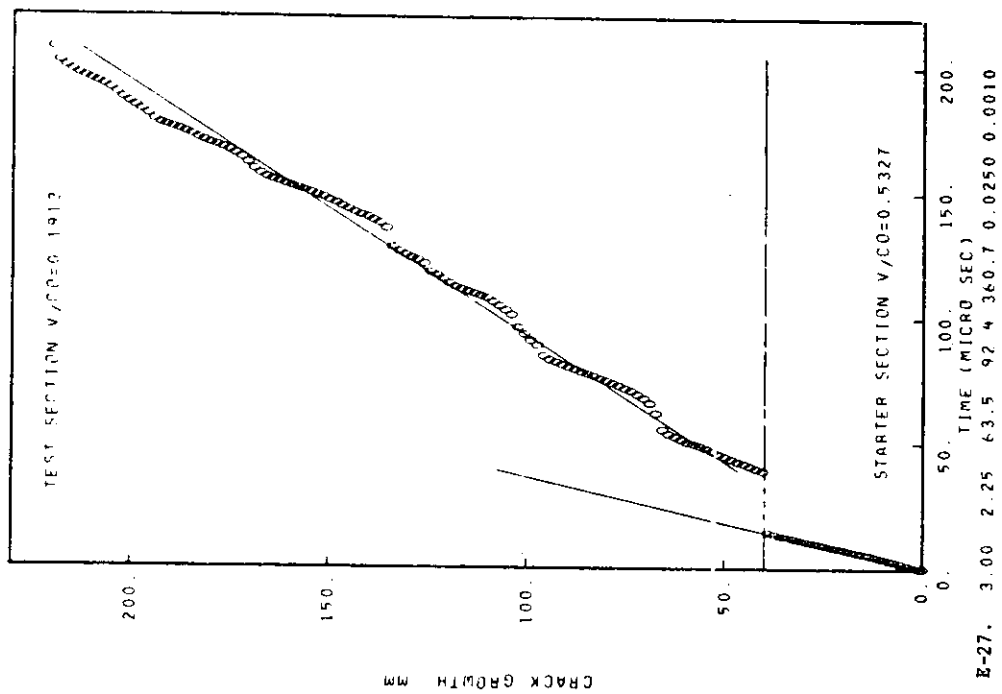
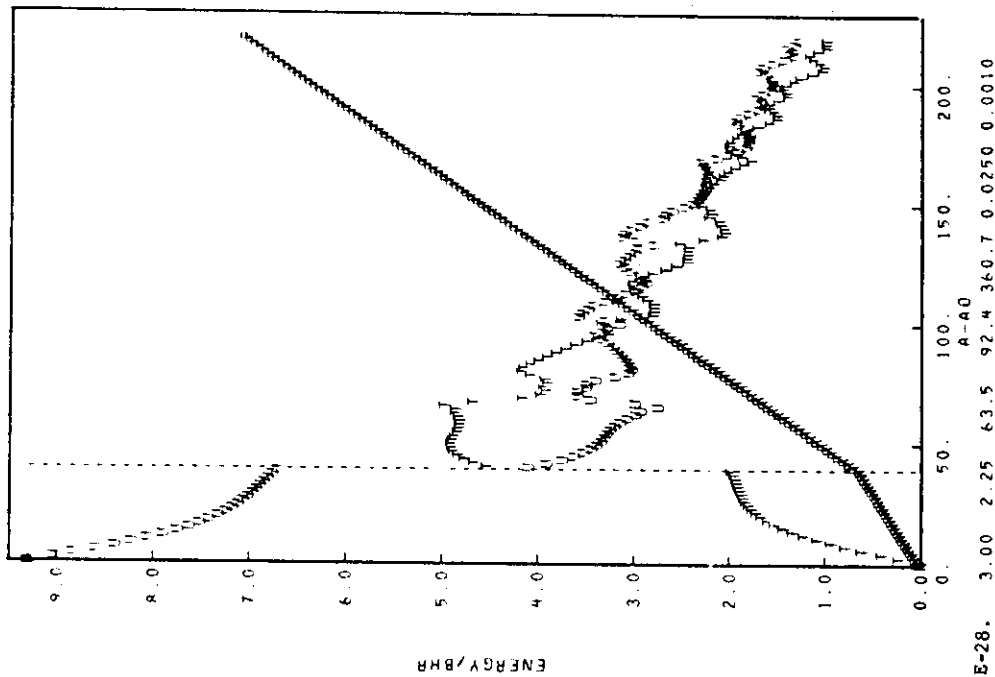
E-21. 3.00 1.00 63.5 184.8 721.4 0.0500 0.0100

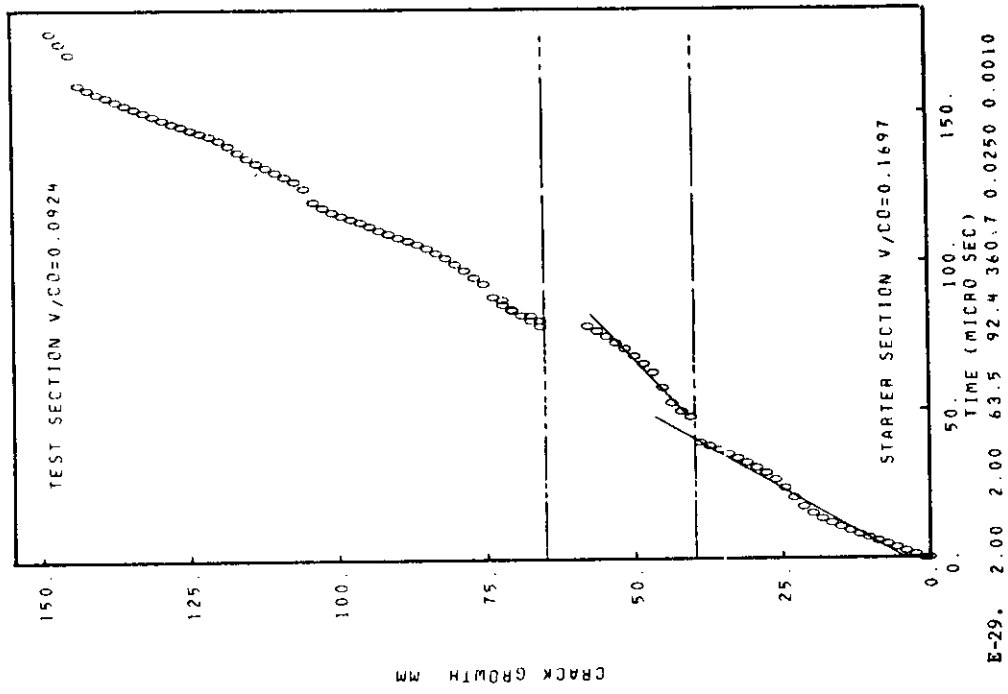
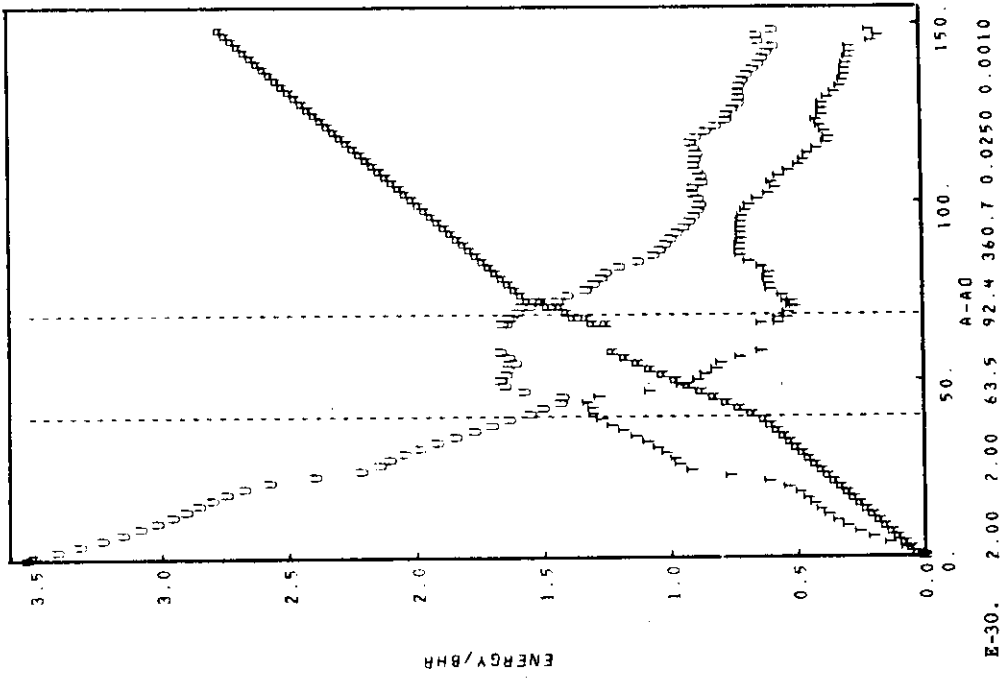


E-22. 3.00 1.00 63.5 184.8 721.4 0.0500 0.0100









DOCUMENT CONTROL DATA - R & D

(Security classification of title, body of abstract and indexing annotation must be entered when the overall report is classified)

| | | | |
|---|---|--|--|
| 1. ORIGINATING ACTIVITY (Corporate author) Battelle, Columbus Laboratories | | 2a. REPORT SECURITY CLASSIFICATION Unclassified | |
| | | 2b. GROUP | |
| 3. REPORT TITLE FAST FRACTURE RESISTANCE AND CRACK ARREST IN STRUCTURAL STEELS | | | |
| 4. DESCRIPTIVE NOTES (Type of report and inclusive dates) PROGRESS | | | |
| 5. AUTHOR(S) (First name, middle initial, last name) G. T. Hahn, R. G. Hoagland, M. F. Kanninen, A. R. Rosenfield, and R. Sejnoha | | | |
| 6. REPORT DATE June 1973 | 7a. TOTAL NO. OF PAGES 113 | 7b. NO. OF REFS 72 | |
| 8a. CONTRACT OR GRANT NO. N00024-72-C-5142 | 8b. ORIGINATOR'S REPORT NUMBER(S) SSC- 242 | | |
| d. PROJECT NO. | 9b. OTHER REPORT NO(S) (Any other numbers that may be assigned this report) | | |
| c. | | | |
| d. | | | |
| 10. DISTRIBUTION STATEMENT Distribution of this document is unlimited. | | | |
| 11. SUPPLEMENTARY NOTES | | 12. SPONSORING MILITARY ACTIVITY Naval Ship Systems Command | |
| 13. ABSTRACT This report presents findings of an Army Research Office supported study concerned with the response of high-strength steels to fast running cracks, and a separate Ship Structure Committee program dealing with unstable fractures in ship plates. Together, the results provide a new basis for measuring and characterizing the properties of structural alloys that control fast fracture and crack arrest. Measurements and calculations of unstable fracture and fracture arrest in 12.7 mm- and 25.4 mm-thick, high-strength SAE4340 steel and A517F steel plates are described. The unstable fractures which propagated at steady-state velocities in the range 185 ms ⁻¹ to 1180 ms ⁻¹ , were produced in wedge-loaded DCB- (double-cantilever-beam) test specimens. The study demonstrates a new concept: the "duplex" DCB-specimen. This consists of a high-strength/low-toughness 4340 steel "starter section" which is electron beam welded to the A517F test section. The fractures are initiated in the starter section, and this makes it possible to confront test materials with a fast moving crack under controlled conditions close to the transition temperature. A fully dynamic analysis of unstable crack propagation and arrest in the DCB-test piece is derived. The technique is based on the beam-on-elastic foundation model of the DCB specimen used previously but with the simple beam and foundation representations replaced by a Timoshenko beam and a generalized elastic foundation. Crack speeds, energy levels, and the crack length at arrest are calculated with this model using a finite-difference method and are compared with the measurements. The calculations and the measurements reveal that unstable propagation in the DCB-test piece proceed from the start with essentially constant, steady-state crack speeds that depend on specimen geometry and the starting conditions. The calculations also predict instances of discontinuous propagation at high speeds. The kinetic energy imparted to the test piece is recovered and contributes to the crack driving force. It follows from (Continued on back page) | | | |

DD FORM 1473

1 NOV 65

None

Security Classification

| 14. KEY WORDS | LINK A | | LINK B | | LINK C | |
|---|--------|----|--------|----|--------|----|
| | ROLE | WT | ROLE | WT | ROLE | WT |
| Unstable Fracture Propagation Fast Fracture Fracture Arrest Crack Speed Dynamic Fracture Energy Dynamic Fracture Toughness Arrest Toughness Double-Cantilever-Beam Test Specimen Wedge Loading SAE4340 Steel A517F Steel | | | | | | |
| Abstract (Continued) this that fracture arrest is controlled by the history of energy dissipation throughout the entire propagation event, rather than on K_a , a single static toughness value calculated at the arrest point. For the 4340 steel, increases in crack velocity up to 860 ms^{-1} at room temperature are accompanied by a 4-fold increase in the dynamic fracture energy (a 2-fold increase in the dynamic fracture toughness), and by increases in the size of the shear lip. Dynamic toughness values for the A517F grade at -78°C for crack speeds from 475 ms^{-1} to 780 ms^{-1} were also about 2 times the reported K_{IC} -value. | | | | | | |

SHIP RESEARCH COMMITTEE
Maritime Transportation Research Board
National Academy of Sciences-National Research Council

The Ship Research Committee has technical cognizance of the interagency Ship Structure Committee's research program:

- PROF. J. E. GOLDBERG, Chairman, *School of Civil Engineering, Purdue University*
DR. H. N. ABRAMSON, *Tech. Vice President, Dept. of Mech. Sciences, S.W. Res. Institut*
PROF. R. W. CLOUGH, *Prof. of Civil Engineering, University of California*
PROF. W. J. HALL, *Prof. of Civil Engineering, University of Illinois*
DR. S. R. HELLER, JR., *C'man, Civil & Mech. Eng. Dept., The Catholic Univ. of America*
MR. G. E. KAMPSCHAEFER, JR., *Manager, Technical Services, ARMCO Steel Corporation*
MR. R. C. STRASSER, *Director of Research, Newport News Shipbuilding & Dry Dock Company*
MR. H. S. TOWNSEND, *Vice President, U. S. Salvage Association, Inc.*
DR. S. YUKAWA, *Consulting Engineer, General Electric Company*

Advisory Group III, "Materials, Fabrication, and Inspection", prepared the project prospectus and evaluated the proposals for this project:

- PROF. W. J. HALL, Chairman, *Prof. of Civil Engineering, University of Illinois*
MR. P. E. JAQUITH, *Planning Supervisor, Bath Iron Works Corporation*
MR. G. E. KAMPSCHAEFER, JR., *Manager, Technical Services, ARMCO Steel Corporation*
PROF. A. W. PENSE, *Professor of Metallurgy, Lehigh University*
DR. W. F. SAVAGE, *Professor of Metallurgy, Rensselaer Polytechnic Institute*
DR. S. YUKAWA, *Consulting Engineer, General Electric Company*

The SR-201 Project Advisory Committee provided the liaison technical guidance, and reviewed the project reports with the investigator:

- MR. G. E. KAMPSCHAEFER, JR., Chairman, *Manager, Tech. Services, ARMCO Steel Corp.*
DR. J. M. KRAFFT, *Head, Ocean Materials Criteria Br., U. S. Naval Research Lab.*
PROF. H. W. LIU, *Prof. of Materials Science, Syracuse University*
PROF. H. C. ROGERS, *College of Engineering, Drexel University*
DR. W. K. WILSON, *Analytical Mechanics, Westinghouse Electric Corporation*

SHIP STRUCTURE COMMITTEE PUBLICATIONS

These documents are distributed by the National Technical Information Service, Springfield, Va. 22151. These documents have been announced in the Clearinghouse Journal U.S. Government Research & Development Reports (USGRDR) under the indicated AD numbers.

- SSC-230, *Program SCORES - Ship Structural Response in Waves* by A. I. Raff, 1972. AD 752468
- SSC-231, *Further Studies of Computer Simulation of Slamming and Other Wave-Induced Vibratory Structural Loadings on Ships in Waves* by P. Kaplan and T. P. Sargent. 1972. AD 752479
- SSC-232, *Study of the Factors Which Affect the Adequacy of High-Strength, Low Alloy Steel Weldments for Cargo Ship Hulls* by E. B. Norris, A. G. Pickett, and R. D. Wylie. 1972. AD 752480
- SSC-233, *Correlation of Model and Full-Scale Results in Predicting Wave Bending Moment Trends* by D. Hoffman, J. Williamson, and E. V. Lewis. 1972. AD 753223
- SSC-234, *Evaluation of Methods for Extrapolation of Ship Bending Stress Data* by D. Hoffman, R. van Hooff, and E. V. Lewis. 1972. AD 753224
- SSC-235, *Effect of Temperature and Strain Upon Ship Steels* by R. L. Rothman and R. E. Monroe. 1973. AD 768891
- SSC-236, *A Method for Digitizing, Preparing and Using Library Tapes of Ship Stress and Environment Data* by A. E. Johnson, Jr., J. A. Flaherty, and I. J. Walters. 1973. AD 767388
- SSC-237, *Computer Programs for the Digitizing and Using of Library Tapes of Ship Stress and Environment Data* by A. E. Johnson, Jr., J. A. Flaherty, and I. J. Walters. 1973. AD 768863
- SSC-238, *Design and Installation of a Ship Response Instrumentation System Aboard the SL-7 Class Containership S.S. SEA-LAND McLEAN* by R. A. Fain. 1973.
- SSC-239, *Wave Loads in a Model of the SL-7 Containership Running at Oblique Headings in Regular Waves* by J. F. Dalzell and M. J. Chiocco. 1973.
- SSC-240, *Load Criteria for Ship Structural Design* by E. V. Lewis, R. van Hooff, D. Hoffman, R. B. Zubaly, and W. M. Maclean. 1973. AD 767389
- SSC-241, *Thermoelastic Model Studies of Cryogenic Tanker Structures* by H. Becker and A. Colao. 1973.